POÇOS DE CALDAS PROJECT

NAGRA NTB 90-21
SKB TR 90-12
UK-DOE WR 90-043

Poços de Caldas Report No. 3

Mineralogy, petrology and geochemistry of the Poços de Caldas analogue study sites, Minas Gerais, Brazil.

II. Morro do Ferro

JANUARY 1991

An international project with the participation of Brazil, Sweden (SKB), Switzerland (NAGRA), United Kingdom (UK DOE) and USA (US DOE). The project is managed by SKB, Swedish Nuclear Fuel and Waste Management Co.

NAGRA NTB 90-21
SKB TR 90-12
UK-DOE WR 90-043

Poços de Caldas Report No. 3

Mineralogy, petrology and geochemistry of the Poços de Caldas analogue study sites, Minas Gerais, Brazil.

II. Morro do Ferro

JANUARY 1991

An international project with the participation of Brazil, Sweden (SKB), Switzerland (NAGRA), United Kingdom (UK DOE) and USA (US DOE). The project is managed by SKB, Swedish Nuclear Fuel and Waste Management Co.

Mineralogy, petrology and geochemistry of the Poços de Caldas analogue study sites, Minas Gerais, Brazil.

II. Morro do Ferro

N. WABER[1]

[1]Mineralogisch-Petrographisches Institut, Universität Bern, Baltzerstrasse 1, 3012 Bern, (Switzerland).

Abstract

The thorium - rare-earth element (Th-REE) deposit at Morro do Ferro is of supergene origin and was formed under lateritic weathering conditions. The ore body forms shallow NW-SE elongated argillaceous lenses that extend from the top of the hill downwards along its south-eastern slope. The deposit is capped by a stockwork of magnetite veins which have protected the underlying, highly weathered argillaceous host rock from excessive erosion. The surrounding country rocks comprise a sequence of subvolcanic phonolite intrusions that have been strongly altered by hydrothermal and supergene processes.

From petrological, mineralogical and geochemical studies and mass balance calculations, it is inferred that the highly weathered host rock was originally carbonatitic in composition and was initially enhanced in thorium and rare-earth elements compared to the surrounding silicate rocks. Intrusion of the carbonatite produced a fenitic alteration of the surrounding phonolites, consisting of an early potassic alteration followed by a vein-type Th-REE mineralization with associated fluorite, carbonate, pyrite and zircon. Subsequent lateritic weathering has completely destroyed the carbonatite, forming a residual supergene enrichment of Th and REEs.

Initial weathering of the carbonatite leading to solutions enriched in carbonate and phosphate may have appreciably restricted the dissolution of the primary Th-REE phases. Strongly oxidic weathering has resulted in a fractionation between cerium and the other light rare-earth elements (LREEs). Ce^{3+} is oxidized to Ce^{4+} and retained together with thorium by secondary mineral formation and adsorption on poorly crystalline iron- and aluminium-hydroxides. In contrast, the trivalent LREEs are retained to a lesser degree and are thus more available for secondary mineral formation and adsorption at greater depths down the weathering column. Seasonally controlled fluctuations of recharge waters into the weathering column may help to explain the observed repetition of Th-Ce enriched zones underlain by trivalent LREE enriched zones.

Zusammenfassung

Die Thorium-Seltene-Erden-Elemente(Th-SEE)-Lagerstätte von Morro do Ferro wurde durch eindringendes Oberflächenwasser unter lateritischen Verwitterungsbedingungen gebildet. Der Erzkörper bildet oberflächennahe, nach NW-SO gedehnte tonige Linsen, die sich von der Hügelkuppe dem S-O Hang entlang nach unten erstrecken. Die Lagerstätte ist von Magnetitgängen bedeckt, welche das darunterliegende, stark verwitterte, tonige Muttergestein vor starker Erosion schützte. Die umgebenden Gesteine sind eine Sequenz von subvulkanischen Phonolit-Intrusionen, die durch hydrothermale Prozesse und Einwirkung von Oberflächenwasser stark verändert wurden.

Aus petrologischen, mineralogischen und geologischen Untersuchungen sowie aus Massenbilanz-Rechnungen kann geschlossen werden, dass das stark verwitterte Muttergestein ursprünglich karbonatitische Zusammensetzung hatte und in bezug auf die umgebenden Silikatgesteinen an Thorium und Seltene-Erde-Elemente (SEE) angereichert war. Die Intrusion von Karbonatit führte zu einer fenitischen Veränderung der umgebenden Phonolite und zwar zunächst durch die Einwirkung von Kalium, gefolgt von einer gangartigen Th-SEE Vererzung in Begleitung von Fluorit, Karbonat, Pyrit und Zirkon. Die nachfolgende lateritische Verwitterung zerstörte den Karbonatit vollständig und führte zu der noch verbleibenden Anreicherung von Th und SEE.

Die anfängliche Verwitterung von Karbonatit könnte durch Bildung von karbonat- und phosphatreichen Lösungen wesentlich zur Verlangsamung der Auflösung der primären Th-SEE-Phase beigetragen haben. Stark oxidierende Verwitterung führte zu einer Trennung zwischen Cerium und den andern leichten Seltene-Erde-Elementen (LSEE). Ce^{3+} wurde zu Ce^{4+} oxidiert und zusammen mit Th^{4+} unter Bildung sekundärer Mineralien und durch Adsorption an Eisen- und Aluminium-Oxyhydroxiden zurückgehalten. Dagegen wurden die 3-wertigen LSEE's weniger stark fixiert und konnten so in grössere Tiefen gelangen. Die saisonalen Schwankungen des Infiltrationswassers in das Verwitterungsprofil könnten zum Verständnis der beobachteten Wiederholung der Schichtfolge von Th-Ce- und darunterliegender LSEE-Anreicherungszone beitragen.

Résumé

Le dépôt de thorium et terres rares (Th-TRs) de Morro do Ferro est d'origine secondaire; il a été formé sous des conditions d'altération latéritique. Le minerai forme un corps composé de lentilles argileuses peu profondes, allongées NW-SE, descendant du sommet de la colline le long de son versant SE. Le dépôt est coiffé d'un réseau de veines de magnétite qui a protégé d'une érosion excessive la roche d'acceuil argileuse et fortement altérée. La roche avoisinante est constituée d'une séquence d'intrusions de phonolite subvolcanique, fortement altérée par des processus de nature hydrothermale et secondaire.

Les analyses pétrographiques, minéralogiques et géochimiques, ainsi que les bilans de masse, indiquent que la roche d'acceuil fortement altérée était à l'origine une carbonatite, riche en Th-TRs par rapport aux roches silicatées voisines. L'intrusion de la carbonatite a produit à son contact une fénitisation des phonolites, à savoir une altération potassique suivie d'une minéralisation de Th-TRs en veines, accompagnés de fluorite, carbonates, pyrite et zircons. L'altération latéritique a ensuite complètement détruit la carbonatite, formant un enrichissement résiduel secondaire de Th-TRs.

La première altération de la carbonatite produisant des solutions enrichies en carbonates et phosphates a pu réduire notablement la dissolution des phases primaires de Th-TRs. Une altération très oxydante a conduit au fractionnement entre le cérium et les autres terres rares légères (TRLs); le Ce^{3+} est oxydé en Ce^{4+} et retenu avec Th dans la formation de minéraux secondaires et dans l'adsorption sur les hydroxydes de fer et d'aluminium mal cristallisés. En revanche, les TRLs trivalentes sont retenues à un moindre degré et donc plus disponibles pour la formation de minéraux secondaires et pour l'adsorption à des profondeurs plus grandes dans le profil d'altération. Des fluctuations saisonnières des eaux de recharge pourraient expliquer dans ce profil la répétition de zones enrichies en Th-Ce surmontant de zones enrichies en TRLs trivalentes.

Preface

The Poços de Caldas Project was designed to study processes occurring in a natural environment which contains many features of relevance for the safety assessment of radioactive waste disposal. The study area, in the State of Minas Gerais, Brazil, is a region of high natural radioactivity associated with volcanic rocks, geothermal springs and uranium ore deposits. It contains two sites of particular interest on which the project work was focussed: the Osamu Utsumi uranium mine and the Morro do Ferro thorium/rare-earth ore body. The first site is notable in particular for the prominent redox fronts contained in the rock, while Morro do Ferro was already well-known as one of the most naturally radioactive locations on the surface of the Earth, owing to the high thorium ore grade and the shallow, localised nature of the deposit.

The features displayed by these two sites presented the opportunity to study a number of issues of concern in repository performance assessment. The four objectives set after the first-year feasibility study were:

1. Testing of equilibrium thermodynamic codes and their associated databases used to evaluate rock/water interactions and solubility/speciation of elements.
2. Determining interactions of natural groundwater colloids with radionuclides and mineral surfaces, with emphasis on their role in radionuclide transport processes.
3. Producing a model of the evolution and movement of redox fronts, with the additional aim of understanding long-term, large-scale movements of trace elements and rare-earths over the front (including, if possible, natural Pu and Tc).
4. Modelling migration of rare-earths (REE) and U-Th series radionuclides during hydrothermal activity similar to that anticipated in the very near-field of some spent-fuel repositories.

The project ran for three and a half years from June 1986 until December 1989 under the joint sponsorship of SKB (Sweden), NAGRA (Switzerland), the Department of the Environment (UK) and the Department of Energy (USA), with considerable support from a number of organisations in Brazil, notably Nuclebrás (now Urânio do Brasil). The first-year feasibility study was followed by two and a half years of data collection and interpretation, focussed on the four objectives above.

This report is one of a series of 15, summarising the technical aspects of the work and presenting the background data. A complete list of reports is given below. Those in series A present data and interpretations of the sites, while those in series B present the results of modelling the data with performance assessment objectives in mind. The main findings of the project are presented in a separate summary (no. 15).

The work presented in this report is a detailed description of the clay mineralogy and rock geochemistry of Morro do Ferro, and forms the basis for many of the model calculations and interpretations, with direct input into objectives 1–3.

Poços de Caldas Project Report Series

Series A: Data, Descriptive, Interpretation

Report No.	Topic	Authors (Lead in Capitals)
1.	The regional geology, mineralogy and geochemistry of the Poços de Caldas alkaline caldera complex, Minas Gerais, Brazil.	SCHORSCHER, Shea.
2.	Mineralogy, petrology and geochemistry of the Poços de Caldas analogue study sites, Minas Gerais, Brazil. I: Osamu Utsumi uranium mine.	WABER, Schorscher, Peters.
3.	Mineralogy, petrology and geochemistry of the Poços de Caldas analogue study sites, Minas Gerais, Brazil. II: Morro do Ferro.	WABER.
4.	Isotopic geochemical characterization of selected nepheline syenites and phonolites from the Poços de Caldas alkaline complex, Minas Gerais, Brazil.	SHEA.
5.	Geomorphological and hydrogeological features of the Poços de Caldas caldera and the Osamu Utsumi mine and Morro do Ferro analogue study sites, Brazil.	HOLMES, Pitty, Noy.
6.	Chemical and isotopic composition of groundwaters and their seasonal variability at the Osamu Utsumi and Morro do Ferro analogue study sites, Poços de Caldas, Brazil.	NORDSTROM, Smellie, Wolf.
7.	Natural radionuclide and stable element studies of rock samples from the Osamu Utsumi mine and Morro do Ferro analogue study sites, Poços de Caldas, Brazil.	MacKENZIE, Scott, Linsalata, Miekeley, Osmond, Curtis.
8.	Natural series radionuclide and rare-earth element geochemistry of waters from the Osamu Utsumi mine and Morro do Ferro analogue study sites, Poços de Caldas, Brazil.	MIEKELEY, Coutinho de Jesus, Porto da Silveira, Linsalata, Morse, Osmond.

Report No.	Topic	Authors (Lead in Capitals)
9.	Chemical and physical characterisation of suspended particles and colloids in waters from the Osamu Utsumi mine and Morro do Ferro analogue study sites, Poços de Caldas, Brazil.	MIEKELEY, Coutinho de Jesus, Porto da Silveira, Degueldre.
10.	Microbiological analysis at the Osamu Utsumi mine and Morro do Ferro analogue study sites, Poços de Caldas, Brazil.	WEST, Vialta, McKinley.

Series B: Predictive Modelling and Performance Assessment

11.	Testing of geochemical models in the Poços de Caldas analogue study.	BRUNO, Cross, Eikenberg, McKinley, Read, Sandino, Sellin.
12.	Testing models of redox front migration and geochemistry at the Osamu Utsumi mine and Morro do Ferro analogue study sites, Poços de Caldas, Brazil.	Ed: McKINLEY, Cross, Haworth, Lichtner, MacKenzie, Moreno, Neretnieks, Nordstrom, Read, Romero, Scott, Sharland, Tweed.
13.	Near-field high-temperature transport: Evidence from the genesis of the Osamu Utsumi uranium mine, Poços de Caldas alkaline complex, Brazil.	CATHLES, Shea.
14.	Geochemical modelling of water-rock interactions at the Osamu Utsumi mine and Morro do Ferro analogue study sites, Poços de Caldas, Brazil.	NORDSTROM, Puigdomènech, McNutt.

Summary Report

15.	The Poços de Caldas Project: Summary and implications for radioactive waste management.	CHAPMAN, McKinley, Shea, Smellie.

Contents

1. Introduction

The thorium and rare-earth deposit (Th-REE deposit) at Morro do Ferro is located some 5 km to the north of the Osamu Utsumi uranium mine and about 10 km to the south of the city of Poços de Caldas in the state of Minas Gerais, Brazil (Fig. 1). It is closely related to a circular, internal structure within the larger ring structure of the Poços de Caldas alkaline complex (Almeida Filho and Paradella, 1977). This ring structure is of Mesozoic age and comprises a suite of alkaline volcanic, subvolcanic and plutonic rocks, generally containing normal background concentrations of uranium, thorium and rare-earth elements (REEs). Regional postmagmatic (deuteric) hydrothermal alteration of the complex has resulted in widespread pervasive argillation and zeolitization of the rocks (Schorscher and Shea, this report series; Rep. 1; Ulbrich, 1984). Some mobilization and concentration of U, Th and REEs probably also occurred at this stage. Subsequently, several different hydrothermal events of local extent, related to the emplacement of minor subvolcanic rocks and volcanic breccia pipes, have led to the formation of a number of radioactive anomalies of economic importance.

The Th-REE radioactive anomaly at Morro do Ferro was discovered in 1953. Weathering of the original host rock led to a supergene enrichment of Th and REEs in a shallow zone just below the surface. Estimates of ore reserves give values of 50,000 metric tons of ThO_2 and 300,000 metric tons of total REEs (Frayha, 1962) and 12,500 metric tons of ThO_2 and 35,000 metric tons of total REEs (Wedow, 1967), respectively, depending on the cut-off grade and depth of the ore considered. However, the ore was never exploited because of its very refractory nature with respect to conventional extraction methods, making recovery costly. The fact that Morro do Ferro is still largely unperturbed makes it extremely suitable for study in this present natural analogue context.

Within the scope of the Poços de Caldas Natural Analogue Project, current work at Morro do Ferro has entailed the drilling of four boreholes ranging in depth from 40–75 m. This present study has concentrated on the geological and geochemical background of the area based on material recovered from these boreholes, from surface sampling, and from an extensive literature review.

2. Previous work

Morro do Ferro initially drew the attention of mining prospectors due to the abundant occurrence of magnetite veins and dykes. In 1935 the Companhia Geral de Minas

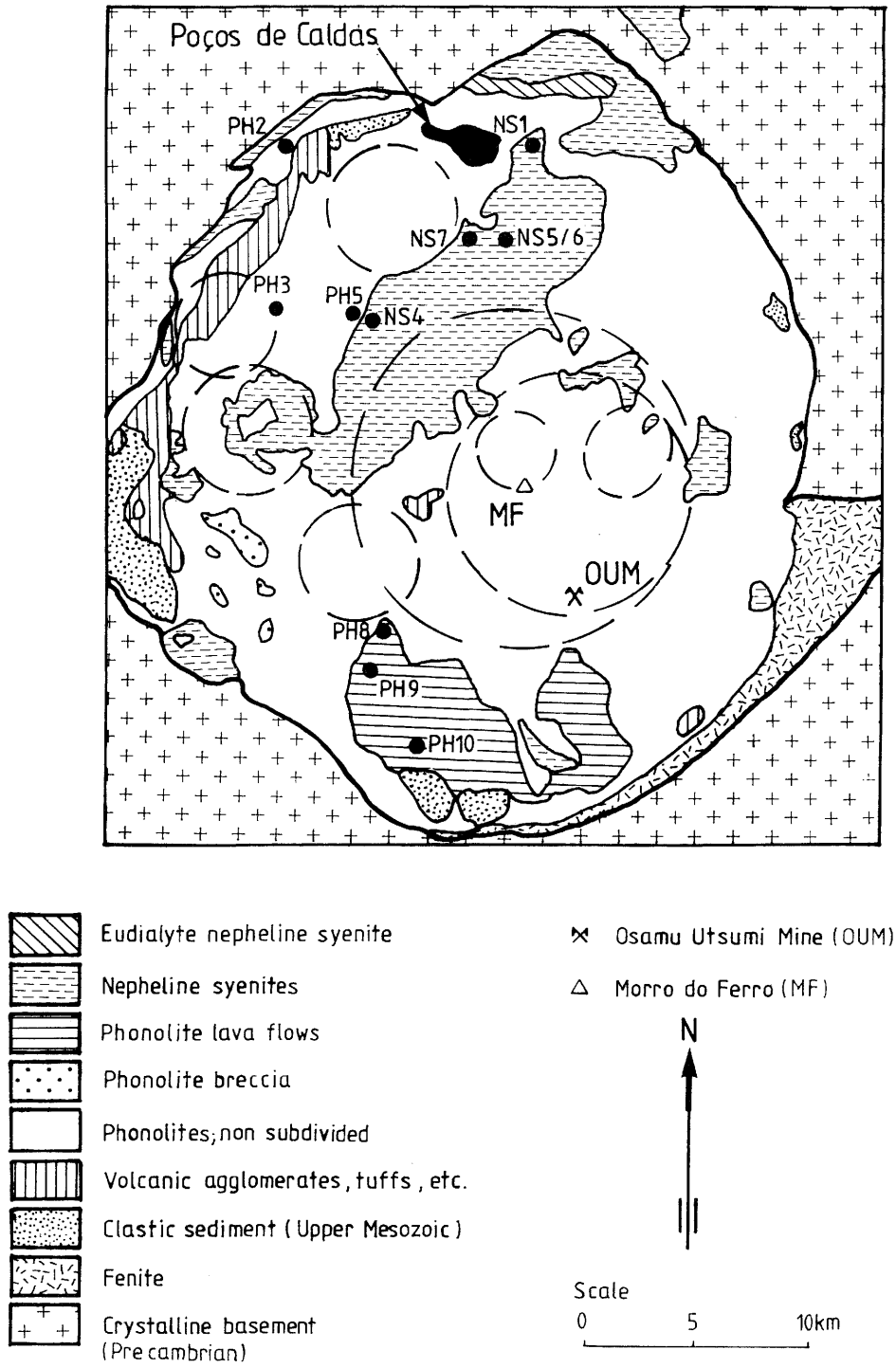

Figure 1. Geological map of the Poços de Caldas plateau modified after Ellert (1959) with the location of the Th-REE deposit at Morro do Ferro and the uranium deposit at Osamu Utsumi.

obtained the concession for the extraction of iron and associated minerals at Morro do Ferro; mining rights are still held by this company. It was not until 1953, however, that the strong radioactive anomaly of the deposit was recognized by aerial radiometric surveys carried out for the Conselho Nacional de Pesquisas (CNPq) on behalf of the U.S. Atomic Energy Commission (Tolbert, 1958a, b, 1966; IPT-Report, 1984). In the 1950s and early 1960s preliminary ground investigations of the Morro do Ferro area were carried out by the CNPq, the Comissão Nacional de Energia Nuclear (CNEN) and the Departemento Nacional da Produção Mineral (DNPM) in collaboration with the U.S. Geological Survey (USGS). These investigations revealed that this unique surface radioactive anomaly is almost entirely due to thorium and its daughter products, associated with rare-earth elements and minor uranium (Tolbert, 1958a, b, 1966; Frondel and Marvin, 1959; Frayha, 1962, 1966, 1967; Penna Franca *et al.*, 1965; Wedow, 1967). These early investigations included ground surveys, drilling, trenching, gallery construction, geochemical analysis and limited mineralogy studies, with a view to evaluating the potential of the ore body. By the mid 60s it had been verified that the near-surface ore body at Morro do Ferro did not contain any uranium mineralization of interest, that no prospect existed for the use of thorium in the near future, and that the REE ores were too refractory for conventional extraction methods, thus making recovery costly. However, the idea that some deeper-seated uranium deposit might exist at Morro do Ferro persisted until 1976 when the Empresas Nucleares Brasileiras SA (Nuclebrás, today Urânio do Brasil) drilled an inclined 463 m deep borehole from near the summit of the hill through the ore body in a south-west direction. Unfortunately, uranium contents were generally low and radioactivity decreased drastically below 40 m; only background values were measured below 200 m, intercalated by a few minor highly active zones. As a result, all exploration activity ceased.

New interest arose in the 1970s with the suggestion that the deposit could be used as a natural biosphere analogue for a radioactive waste repository. Activity in soils at Morro do Ferro is so high that natural foliage can easily be autoradiographed. This led to studies dealing with the exposure of plants and animals to Th and the uptake of ^{228}Ra by flora and fauna (Drew and Eisenbud, 1966). First investigations on the mobility of thorium and its daughter products were carried out mainly by the Institute of Biophysics, Federal University of Rio de Janeiro and the Institute of Environmental Medicine, New York University Medical Center, in collaboration with the Pontifical Catholic University of Rio de Janeiro and the CNEN. This work resulted in several reports and publications (Eisenbud, 1979, 1980; Eisenbud *et al.*, 1982; S. Fujimori, 1967; K. Fujimori, 1974, 1982,

1983; IPT-Report, 1984; Lei, 1984; Lei *et al.*, 1986; Miekeley *et al.*, 1982, 1985; Miekeley and Kuechler, 1987; and references cited therein).

3. Geological setting

Morro do Ferro is roughly elliptical in shape, trending north-east, and has a maximum diameter of about 1 km. With an altitude of 1541 m, Morro do Ferro marks one of the highest elevations within the Poços de Caldas plateau, rising some 140 m above the base. The hill is drained by two streams, one draining the northern side (north stream) and the other rising in the south (south stream) and curving around the south-eastern periphery (Fig. 2). The hill is devoid of vegetation except for grass and small bushes. A small densely wooded area lies along the south stream to about 0.75 km downstream, whereupon the stream drains into a swamp.

Morro do Ferro is situated in a geological environment very similar to that of the Osamu Utsumi uranium mine (Waber *et al.*, this report series; Rep. 2). The local geology of the Morro do Ferro area is characterized by hydrothermally altered (potassic) rocks overlain by a deep lateritic weathering cover. Although outcrops of fresh rock not affected by hydrothermal alteration and weathering are extremely rare in this area, several alkaline rock-types can be identified around Morro do Ferro, based on slight textural and mineralogical variations. Dominant types are phonolites, tinguaites and foyaites of the miaskitic and agpaitic suites (excess of aluminium and alkalies with respect to aluminium; Barretto and Fujimori, 1986). Mineralogically and geochemically, these rocks are comparable to the different alkaline rocks generally exposed all over the Poços de Caldas plateau (Ulbrich, 1984; Schorscher and Shea, this report series; Rep. 1).

In the near vicinity of Morro do Ferro, these alkaline rocks suffered intense hydrothermal alteration similar to that observed for the Osamu Utsumi uranium mine and several other locations within the plateau. The hydrothermally altered country rocks were termed "potassic rocks" to stress their main geochemical characteristic. A geological map of the Morro do Ferro area, derived from the rare outcrops of unweathered rock and the information obtained from drillcores, is shown in Figure 3. Superimposed on the geology are radiometric isocontour lines deduced from earlier surface surveys.

Intense weathering under semi-tropical conditions led to the formation of a 20-50 m-thick lateritic weathering zone on top of the different country rocks, which is

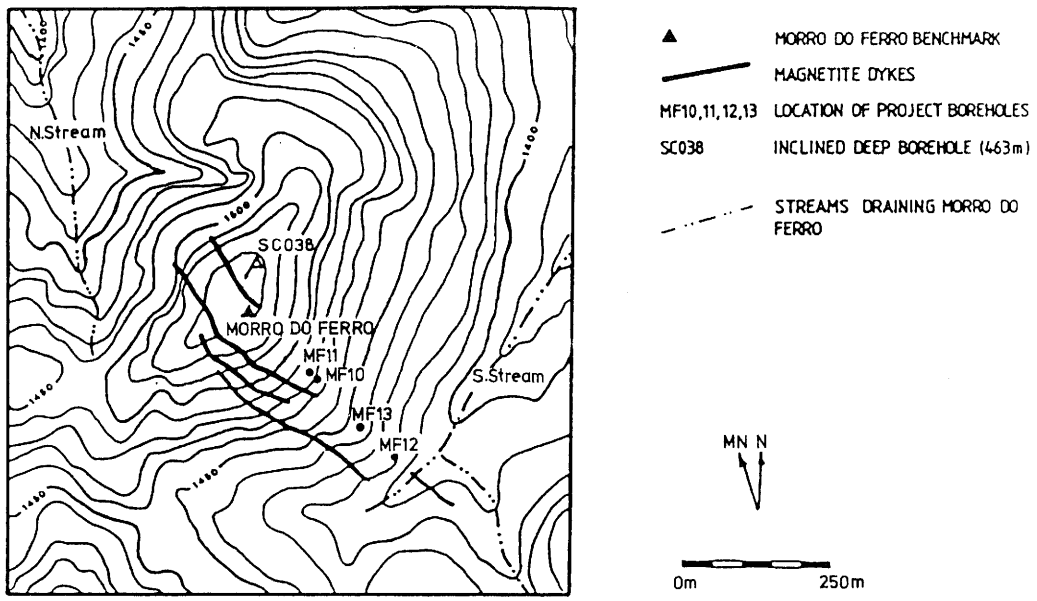

Figure 2. Topographic map of Morro do Ferro showing the location of boreholes MF10 to MF13, the position of the inclined 463 m-deep borehole drilled in 1976, and the approximate position of the magnetite dykes (modified from Barretto and Fujimori, 1986).

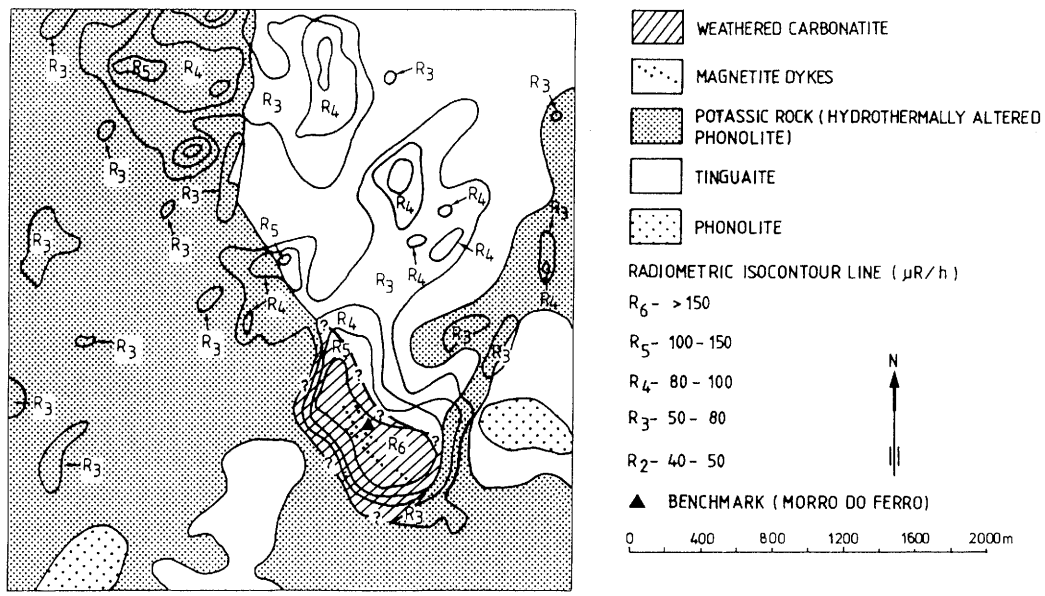

Figure 3. Interpretative geological map of the Morro do Ferro area with superimposed radiometric isocontour lines (modified from Barretto and Fujimori, 1986) and showing the approximate location of the weathered carbonatite.

mineralogically and geochemically comparable to that found at the Osamu Utsumi uranium mine.

Weathering of the host rock has taken place down to a depth of more than 100 m, and fresh host rock has never been recovered from any drillcore. The weathered material below the ore body differs markedly from the weathering zone on top of the surrounding hydrothermally altered phonolitic country rocks ("potassic rocks"). Based on mineralogical, geochemical and mass balance evidence, it is proposed that the original host rock was carbonatitic in type (see sections 6 and 7).

Rock fragments described as strongly hydrothermally altered, and brecciated potassic rocks, were only recovered at depths below 130 m in two vertical boreholes drilled at the periphery of the ore body (Frayha, 1962, 1966). These rock fragments indicate the lower extent of the original carbonatitic host rock. In both boreholes radioactivity decreased rapidly from moderate at the top to regional background values at depth.

In the inclined 463 m-deep borehole drilled by Nuclebrás in 1976, core recovery only started at a depth of 132 m where the drill encountered an 8 m-thick magnetite dyke. Down to 254 m, the recovered material is described macroscopically as oxidized, very fine-grained, homogeneous effusive rocks and tuffs, variably hydrothermally altered and brecciated with intercalated minor reduced zones (Camargo dos Santos, 1984). Thin magnetite veins are randomly distributed within this horizon. In this borehole the first occurrence of pyrite and fluorite are reported from a depth of 161 m in a reduced zone and the first K-feldspar phenocrysts are described at a depth of 208 m. From 254 m down to the bottom of the hole, the core consists of strongly hydrothermally altered and brecciated phaneric and aphanitic tinguaites. Fracture-related oxidized zones occur over several intervals. Microscopic investigations of samples from 380 m and 426 m revealed strongly brecciated and hydrothermally altered tinguaites, regionally known as potassic rocks, consisting of about 60% alkali-feldspars and 30% clay minerals, with additional pyrite, sphalerite, fluorite, cryptocrystalline REE-phases and gypsum, all occurring as fracture and pore infillings. It was concluded that these rocks had undergone a potassium-rich hydrothermal alteration and pyritization prior to their brecciation, the latter related to a second hydrothermal stage which also led to impregnation with cryptocrystalline REE- and Th-phases (IPT-Report, 1984).

The Th-REE ore body is a shallow zone of NW-SE elongated argillaceous lenses extending from the summit of the hill down along its south-eastern slope. Using a cut-off grade of 0.5% ThO_2, the ore body is 410 m long, 215 m wide and 10-35 m thick (Barretto and Fujimori, 1986). Within the ore body, the ThO_2 concentration ranges between 0.1–2.9%, in some cases reaching values as high as 5% ThO_2, and the total REE

concentration varies between 1.5–21%. Mineralized zones may be observed in the weathered host rock down to more than 100 m depth, although they are intercalated by thick barren zones (IPT-Report, 1984).

The magnetite veins are the dominant feature at the surface of Morro do Ferro, appearing to be concentrated in the uppermost 40 m of the hill. Isolated veins, however, occur down to a depth of at least 130 m below the summit. The thickness of these veins ranges from a few mm up to several metres. Major magnetite veins at the surface strike about N50° – 60°W and dip 50° – 85°NE. Minor veins strike N10° – 35°E with an inclination of 45° or more to the north-west or south-east (IPT-Report, 1984). The presence of this magnetite stockwork is generally believed to have preserved Morro do Ferro from excessive erosion so that the hill still marks one of the highest points within the Poços de Caldas plateau.

4. Analytical methods

Thin and polished sections were prepared from core samples for microscopic investigations, microprobe- and SEM-analysis. The remaining core material was then crushed and milled using agate. After milling, the rock powder was split into equal aliquots used for different analytical methods. Special care was taken during the preparation to avoid any trace element contamination of the samples.

X-ray diffraction was used for whole-rock mineral determination and the $<2\mu$ fraction for clay mineral identification. Whole-rock modal content analyses were carried out with a Philips PW1729 diffractometer on a random orientated powder sample using LiF as an internal standard. Using internal calibration curves allows the quantitative determination of quartz, alkali-feldspars, albite, calcite and dolomite with an accuracy of ± 3 wt.%. The internal calibration allows a mineral estimate of the wt.% compared to 100 wt.%. The difference between the two is thus the amount of accessories and sheet silicate minerals. Minerals not detected by this method (amounts of less than about 3 wt.%) were estimated from thin section and verified by point counting.

For clay mineralogical investigations, the $<2\mu$ clay fraction was separated by sedimentation of the crushed rock material in an Atterberg cylinder, the procedure being repeated three times. Reduction of the sedimentation time in the Atterberg cylinder also allowed the recovery of the silt fraction (divided into 2–6.3μ and 6.3–20μ fractions). Clay and silt fractions were treated with 2n HCl and saturated with Ca^{2+}. A suspension (clay or silt + solution) was then placed on a glass slide and allowed to evaporate to obtain

orientated samples. Three preparations were done on each sample: air-dried, glycolated and heated to 550°C. These preparations were analyzed on a Philips APD-system (PW1710) with monochromatic CuKα-radiation. Clay mineral abundance was estimated using the intensity ratios of the corresponding basal reflections. This method allows only a semi-quantitative determination of the clay mineral content due to variations in crystallinity and mineral chemistry. Illite crystallinity was determined to estimate the temperature of formation according to the method of Kubler (1968) and, for a smaller set of samples, corrected according to the methods proposed by Środoń (1980, 1984). Trace mineral identification was performed using a Guinier camera with FeKα-radiation.

Mineral chemical analysis was performed on an ARL-SEMQ microprobe equipped with 6 crystal spectrometers and an energy-dispersive system (EDS). Raw data were corrected for beam current drift, dead-time and background (COMIC-ED; Sommerauer, 1981). Final data reduction was performed using a ZAF-correction (EMMA-5/1-86).

Bulk chemical composition was determined by automated X-ray fluorescence (XRF) spectrometry on a Philips PW1400 system. Major elements were corrected on-line and trace elements were corrected according to the method of Nisbet *et al.* (1979), modified by Reusser (1986; XRF-System V-86). Glass pellets of fused rock powder mixed with $Li_2B_4O_7$ in the ratio 5:1 were used to determine major elements, and pressed rock powder pills were used for trace elements. Several samples were analyzed for U and Th using a manual XRF-system (Philips PW1410) with internal calibration based on international standards. The advantage of this method compared to the routine analytical XRF-method is the lower detection limit (1 ppm) for U and Th, coupled with better accuracy in low concentrations.

Sulphur and CO_2 were determined by coulometric methods (Coulomat 702). REE analyses were performed with Inductively Coupled Plasma Source Optical Emission Spectroscopy (ICPOES) and neutron activation, and radiochemical separation and alpha-spectrometry were used for Th and U.

Scanning electron microscope (SEM) investigations were performed on a CamScan S4 microscope equipped with a energy-dispersive system Tracor Norton TN 5600. Both secondary and backscatter electron methods were used.

Cathodoluminescence investigations were carried out with a hot cathode instrument with directly heated tungsten filament (Ramseyer *et al.*, 1989). Working conditions were 70 keV and 30 Amps with exposure times varying from 30 to 240 seconds.

Bulk density (ρ) measurements were also carried out. The samples were dried, weighed and then coated with molten paraffin wax, which was then followed by immersion in mercury to measure their displaced volume. This method produces errors in the range of 2%. Average grain density (ρg) was determined using He-gas in a Multipycnometer. Total porosity (P) was calculated from grain density and bulk density according to the formula $P=(1-\rho/\rho g)\cdot 100$.

5. Borehole description and sampling

Boreholes MF10, MF11 and MF13 were all drilled along the south-eastern slope of Morro do Ferro, whereas MF12 was drilled at the bottom of the slope near the south stream. The location of the boreholes in relation to the mineralization and the dry season water table is shown in Figures 4 and 5. Owing to the heavily weathered nature of the bedrock and the resulting rock friability during drilling, standard drilling techniques would only have served to wash out portions of the borehole. This difficulty was overcome by using a simple dry-pushing method with a short barrel (75 mm in diameter), which allowed core recovery of more than 90%. This method was employed for MF10 to 60 m, for MF11, and for MF13 to 40 m; thereafter water-flush rotary coring was used to complete MF10, MF13 and most of MF12. For MF12 the upper 38.86 m were drilled using mud-flushing to ensure greater bedrock stability through the weathered zone. MF10 to MF12 have been logged and cased using PVC tubing, but only MF12 penetrated rock which was stable enough to allow adequate hydraulic testing (Holmes *et al.*, this report series; Rep. 5). Both MF10 and MF12 have been completed using mechanical packer systems. As the objective of MF11 was to provide access to the top of the saturated zone, completion using packers has not been necessary. For MF13 the rock was too friable to install a packer system and groundwater enters through the perforated bottom of the PVC casing.

Borehole MF10 was drilled at 1480 m above sea-level on the south-eastern slope of Morro do Ferro (Fig. 5). The borehole penetrated through the Th-REE ore body and terminated at a depth of 74 m in the completely decomposed host rock. The highest activity was recorded in the first 11 m of the hole; a less active zone, about one third of the activity, was traversed between 11–22 m. From there to the bottom of the hole, activity values represent background levels. The recovered clay/silt material is predominantly a dark-red/brown colour in the ore body when intercepted by small

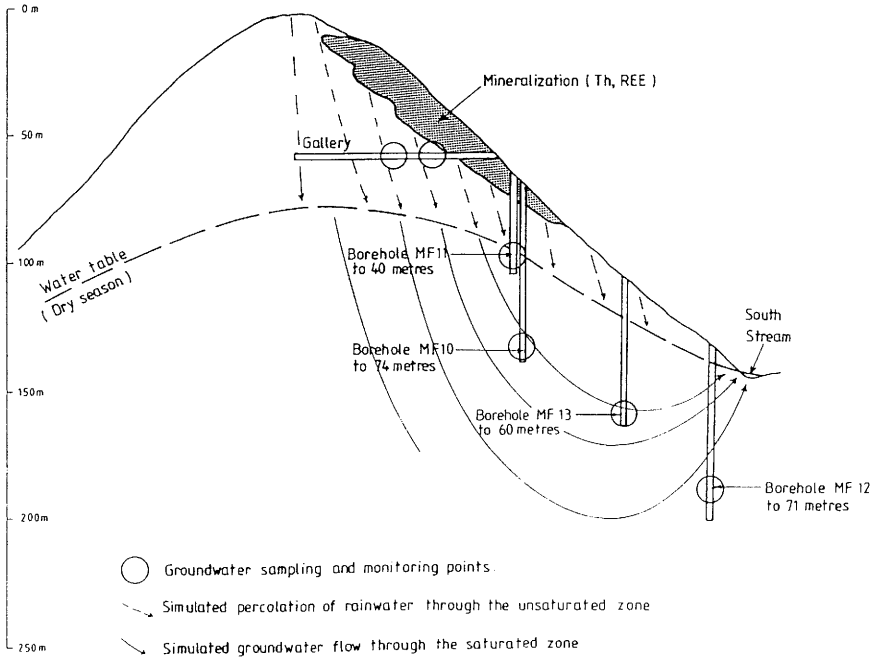

Figure 4. Location of boreholes MF10 to MF13 at Morro do Ferro in relation to the mineralization and the dry season water table.

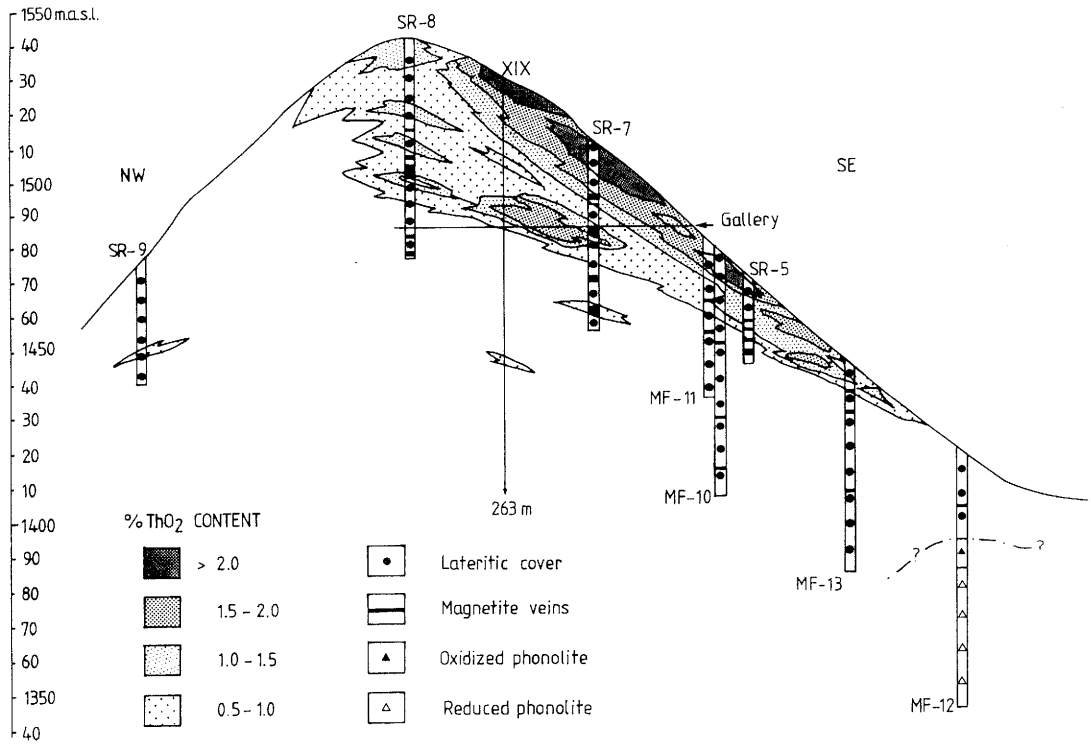

Figure 5. Profile across Morro do Ferro showing the distribution of thorium. Borehole XIX and those prefixed with SR were drilled during exploratory studies extending back to the 1950s. The construction of the gallery dates from the same period.

magnetite veins; a few thin white layers are also present. Below the ore body, from 22–75 m, the clay/silt material is much brighter in colour, varying from yellowish-white to reddish-white and intercepted by thin dark-red/brown and black zones. Magnetite veins are much less abundant in this completely weathered host rock.

Borehole MF11, located a few metres further uphill from borehole MF10, was drilled at 1483 m above sea-level down to a depth of 40 m. Highly active material was recovered in the first 10 m of the hole. Down to 20 m the activity decreases to moderate values and, from there to the bottom of the hole, it displays background values. The recovered material from the ore body and the completely weathered host rock below are similar to the material recovered from the MF10 borehole.

Borehole MF12, drilled at the bottom of the south-eastern slope at 1420 m above sea-level (Fig. 5), penetrated through a lateritic weathering zone down to 27.52 m, including an initial 0.7 m-thick soil horizon rich in organic material. After the laterite, the borehole encountered oxidized country rock, and later a diffuse redox front was encountered at 35.7 m. From there on, reduced country rock was recovered down to the bottom of the hole at 71 m. All the country rocks recovered were phonolites that had undergone intense hydrothermal alteration ("potassic rocks") and, in restricted zones, brecciation. Two zones of volcanic breccia, both highly conductive, were encountered between 54.40–56.50 m and 68.97–69.94 m depth. Throughout the length drilled, the country rocks were intruded by several small-sized leucocratic dykes.

Borehole MF13 was drilled midway between boreholes MF10 and MF12 at 1445 m above sea-level down to a depth of 60 m. As the main emphasis of drilling was to sample groundwater, no detailed logging or core mapping was carried out. Moderate activity was recorded in the uppermost 5 m of the borehole, before decreasing to background values.

Drillcore mapping and sampling of boreholes MF10, MF11 and MF12 were carried out immediately after recovery. Lithological logs of MF10 and MF12 are given in Appendices 1 and 2 together with the geophysical logs for MF12. No geophysical logging could be performed in boreholes MF10, MF11 and MF13 due to the friability of the strongly weathered material, which necessitated casing the holes during drilling.

From the boreholes drilled, one-third of the core was kept as reference material for the owner company of Morro do Ferro (Minegral). The remaining two-thirds were used for mineralogical, geochemical and isotope analyses. The ore material and the highly weathered host rock were split using a plastic knife and dry sawing was used for the massive country rock to avoid any possible contamination.

6. Country rock

The country rocks encountered in borehole MF12 are strongly altered leucocratic phonolites of subvolcanic origin. All the recovered phonolites are characterized by intense hydrothermal and metasomatic alteration which have led to a very potassium-rich composition ("potassic rocks"). This type of alteration is comparable to the fenitic alteration found in potassium fenites around certain carbonatite intrusions, as for instance at Songwe, Tansania (Brown, 1964), at Kaiserstuhl, Germany (Sutherland, 1967) and in Zambia (Bailey, 1966) among others. Following hydrothermal activity, oxidation and lateritization of the altered phonolites began, processes that are still taking place at the present time, resulting in today's vertical profile. Assuming that the hydrothermally unaffected lamprophyric dykes exposed in the Osamu Utsumi uranium mine represent the final state of magmatic and hydrothermal activity in the area, i.e. 76 ± 1 Ma ago according to Shea (this report series; Rep. 4), meteoric weathering should therefore have lasted over a similar period of time.

6.1. Phonolites

Genetically, the recovered phonolites are closely related and represent different phases of emplacement during the magmatic activity in the Poços de Caldas alkaline complex. Contact phenomena are lacking, or only poorly developed, between the single phonolite stocks, but otherwise may be observed around some of the small-sized hololeucocratic dykes that intrude the different phonolites. Such dykes certainly represent the latest phonolite-magmatic activity in the recovered profile.

Despite their intense hydrothermal overprint, the recovered subvolcanic phonolitic country rocks may be subdivided into three major groups according to differences in textural features and their modal and chemical composition :

- leucocratic phonolite
- leucocratic tephri-phonolite
- hololeucocratic phonolitic dykes

All the phonolites are quartz undersaturated. By analogy with the less altered phonolites of the Osamu Utsumi mine and the unaltered regional phonolites, euhedral

aggregates of illite and kaolinite were interpreted as pseudomorphically replaced nepheline, which was the most important foidic mineral in these phonolites.

6.1.1. Petrography

Reduced leucocratic phonolite was encountered in the MF12 borehole from 68.17–71 m. This bright grey-coloured phonolite is porphyritic in texture with a fine-grained matrix (0.05–0.1 mm) containing alkali-feldspar phenocrysts (0.5–1 cm), nepheline (0.3–1 cm) and rare pseudoleucite (0.5–4 cm). The fine-grained matrix ranges between 50-60 vol.% of the bulk composition. Alkali-feldspars are the predominant matrix minerals, followed by pseudomorphically replaced nepheline and replaced mafic components. In a few cases relict pyroxene occurs as inclusions in alkali-feldspars. Primary magmatic accessories are rare; only in a few cases do apatite, sphene and zircon occur embedded in the matrix or as inclusions in alkali-feldspars. Although monazite is locally rather abundant, it mainly occurs along fissures and was never observed as inclusions; it therefore reflects a hydrothermal rather than a magmatic origin.

Xenoliths of both fine-grained phonolites and coarse-grained nepheline syenites, together with amygdaloidal structures comprising alkali-feldspars and clay minerals, frequently occur in the leucocratic phonolite. The xenoliths range between 0.5 and 2 cm in diameter and display the same alteration features as the phonolite.

The reduced leucocratic phonolite is commonly impregnated with fine-grained disseminated pyrite. The degree of impregnation is somewhat dependent on the degree of argillic alteration, in that zones very rich in clay minerals are only weakly impregnated with pyrite. Besides pyrite, there occur fluorite, very fine-grained to cryptocrystalline REE-phases, Zr-phases and U-Th-phases, with subordinate carbonates as hydrothermal mineralization products. All these minerals are commonly concentrated along fractures and penetrate along grain boundaries into the rock matrix.

Reduced tephri-phonolite was intercepted by the MF12 borehole between 37 and 68.17 m. The grey-coloured tephri-phonolite is porphyritic in texture with an aphanitic matrix (0.01–0.05 mm) containing phenocrysts of subordinate alkali-feldspars (1–10 mm) and replaced nepheline (0.5–5 mm). Pseudoleucite is absent as phenocrysts as well as in the matrix. The aphanitic matrix comprises about 70–80 vol.% of the tephri-phonolite. As in the leucocratic phonolite, alkali-feldspars are by far the predominant minerals in the matrix, followed by pseudomorphically replaced nepheline and mafic components. In contrast to the leucocratic phonolite, however, alkali-feldspars in the tephri-phonolite

always display microperthitic exsolution in the matrix as well as in the phenocrysts. Pseudomorphically replaced primary mafic minerals are more abundant than in the leucocratic phonolite. Primary magmatic accessories are rare and include apatite and zircon.

Randomly distributed xenoliths of phonolitic and nepheline-syenitic composition occur throughout the tephri-phonolite, as do amygdaloidal structures comprising alkali-feldspars and clay minerals.

Fine-grained disseminated pyrite occurs throughout the tephri-phonolite. An interesting feature is that the tephri-phonolite core changes its colour from grey to black within a few hours after extraction due to the surficial oxidation of the fine-grained pyrite. Such a reaction was not observed in the leucocratic phonolite or in the phonolites of the Osamu Utsumi mine; whenever it was observed, the reaction took place several months after extraction of the cores.

Fluorite, carbonate and, less abundantly, very fine-grained to cryptocrystalline U-Th-REE-phases and Zr-minerals occur together with pyrite and clay minerals along fractures and grain boundaries.

Hololeucocratic dykes occur within both phonolites. The dykes consist mainly of randomly orientated alkali-feldspars with subordinate hydrothermally replaced nepheline; mafic minerals and magmatic accessories are rare. The dykes are equigranular to porphyritic in texture and vary in grain size from very fine-grained to coarse-grained. Some of the dykes display chilled margins against the surrounding phonolite, and the contacts have often been subjected to strong argillic alteration. In some of the investigated dykes, alkali-feldspars show microperthitic exsolution similar to the alkali-feldspars in tephri-phonolite, whilst in others it resembles more the alkali-feldspars of the leucocratic phonolite. All the dykes are pyrite-impregnated and have the same hydrothermally induced mineral assemblages (fluorite, U-Th-REE-phases, carbonate) along fissures similar to the surrounding phonolites, indicating emplacement before the main mineralization phase. Compared to the phonolites they are not decidedly richer in such minerals.

Volcanic breccia veins, which occur between 54.40 – 56.50 m and 68.97 – 69.94 m in the MF12 borehole, have a very fine-grained matrix composed of clay minerals, pyrite, fluorite and very fine-grained to cryptocrystalline U-Th-REE phases. K-feldspars are also present but much less abundantly than in the phonolites. The xenoliths in these veins, although exclusively of phonolitic origin, are, however, distinct in texture and content of replaced mafic minerals. All the xenoliths are hydrothermally altered in the same way as the phonolites and display pyrite impregnation to various degrees.

6.1.1.1. Oxidized zone

A similar rock to the leucocratic phonolite was encountered from 27.52 m to 37 m. At this depth the phonolite is in its oxidized state, seen as a distinct colour change from bright grey to orange-brown. This colour change is mainly attributed to ferrous to ferric oxidation and the formation of clay phases due to the downward diffusion of oxygen in groundwaters during weathering. The encountered redox front is much more disperse (about 1 m in thickness) than the redox fronts observed in the Osamu Utsumi mine (Waber *et al.*, this report series; Rep. 2), which may be due to a lateral input of oxygenated groundwaters. The overall strong iron staining and manganese-oxyhydroxide content make microscopic investigations difficult. Yet, the only obvious difference in the leucocratic phonolite when in its reduced state concerns the amount of pseudoleucite, which is more abundant in the oxidized phonolite.

6.1.1.2. Modal composition

A qualitative compilation of the mineralogical compositions derived from microscopic and X-ray diffractometric (XRD) investigation of the different phonolitic rocks is given in Table I. A compilation of the mode and the relative abundance of the clay minerals in the $<2\mu$ fraction determined by XRD is provided in Table II.

The most striking differences between the leucocratic phonolite and the tephri-phonolite include the higher abundance of alkali-feldspars, the lower contents of replaced mafic minerals, the lack of plagioclase, and a clay fraction dominated by illite and kaolinite in the leucocratic phonolite as compared to the tephri-phonolite. In addition, the tephri-phonolite exhibits a slightly higher abundance of hydrothermally produced minerals (see below), especially fluorite. In the oxidized zone, alkali-feldspars display intermediate values and the clay fraction is dominated by kaolinite. Figure 6 shows the mineralogical variation with depth in the MF12 borehole.

6.1.1.3. Rock physical properties

The variation of porosity, bulk and grain density with depth in the MF12 borehole is shown in Figure 7. In the reduced rocks, porosity averages around 5%, displaying only minor variations over the whole profile, with the exception of strongly brecciated zones (up to 12%) and the two breccia veins (up to 20%). Such zones always proved to be

TABLE I

Borehole MF12: qualitative mineralogical composition of the hydrothermally altered phonolites and the lateritic weathering zone.

	Hydrothermal mineral assemblage												**Mineralization and gangue mineral**								**Weathering**			
Hydrothermally altered rocks	Kf	Ne	Psl	Cpx	Ab	Sphe	Ap	Zir	Ill	Kaol	Chl	Sm	Py	Spha	Flu	Carb	Mon	Bae	Zr-P	other	Cran	FeOx	MnOx	Gib
Reduced zone																								
leucocratic phonolite	M	M*	tr	0-tr	0-tr	–	0-tr	0-tr	M	M	tr	tr	m	0-tr	m	tr	tr	tr	tr	tr	tr	–	–	–
tephri-phonolite	M	M*	0-tr	M*	m	tr*	0-tr	0-tr	M	m	m	m	m	0-tr	m	tr-m	tr	tr	tr	tr	tr	–	–	–
phonolitic dyke	M	m*	0-tr	0-tr	m	–	0-tr	0-tr	M	M	m	m	m	0-tr	tr	tr	–	–	–	tr	tr	–	–	–
Oxidized zone																								
leucocratic phonolite	M	M*	0-tr	0-tr	0-tr	–	0-tr	0-tr	M	M	–	–	–	–	–	–	0-tr	0-tr	tr	tr	tr-m	m	m	tr
Weathering zone																								
laterite	0-m	–	–	–	–	–	–	tr	M	M	–	–	–	–	–	–	0-m	0-m	0-tr	tr-m	tr-m	m-M	tr-m	m-M

Components:

M – Major, > 10 vol.%
m – minor, 1-10 vol.%
tr – trace, < 1 vol.%

Kf – alkali-feldspars
Ne – nepheline, *replaced
Psl – pseudoleucite
Cpx – clinopyroxene, *replaced
Ab – albite
Sphe – sphene, *replaced
Ap – apatite
Ill – illite and sericite
Kaol – kaolinite
Chl – chlorite
Sm – smectite
Py – pyrite
Spha – sphalerite
Flu – fluorite
Carb – carbonate
Mon – monazite group minerals
Bae – bastnaesite
Zr-P – zircon, incl. cryptocryst. Zr-REE phases
Other – alunite, jarosite etc.
Cran – florencite, goyazite gorceixite
FeOx – hematite, goethite, amorph. Fe-hydroxide
MnOx – Mn-oxyhydroxides
Gib – gibbsite

Table II

Borehole MF12: average modal content of the hydrothermally altered phonolites and the lateritic weathering zone.

Whole-rock (wt.%)

Rock / Mineral	Reduced leucocratic phonolite	Reduced tephri-phonolite	Reduced phonolitic dyke	Oxidized leucocratic phonolite	Oxidized weathered zone
alkali-feldspars	85	50	74	65	0 – 28
albite	–	10	4	–	–
clinopyroxene (replaced)	2	10	–	–	–
others*	3	5	10	7	5 – 22
gibbsite	–	–	–	–	1 – 12
total clay fraction (<2μ)	10	25	12	28	65 – 90

* others: pyrite, fluorite, zircon, REE-minerals and magmatic accessories in the reduced zone; Fe- and Mn-oxyhydroxides, alunite, jarosite and crandallite group minerals in the oxidized zone.

Relative abundance in the clay fraction in %

illite	70	55	60	40	10 – 38
kaolinite	27	12	15	56	60 – 90
smectite	tr	21	15	–	–
chlorite	tr	10	7	–	–
mixed-layer	–	tr	tr	tr	–
others**	tr	tr	tr	minor	minor

** others: florencite, goyazite, gorceixite, alunite, jarosite and hydrous ferric oxides.

conductive. A strong increase in porosity occurs in the oxidized phonolite towards the weathered cover. The deepest investigated oxidized phonolite sample (MF12-35-1A) has a porosity of 10%, and the sample adjacent to the laterite junction has a porosity of 33%.

The observed porosity changes are a product of hydrothermal alteration and superimposed weathering processes. During heavy rainfall, clay minerals are washed out from such highly argillically altered zones and the porosity increases. In the oxidized phonolite, the dissolution of the no longer stable minerals (pyrite, fluorite, carbonate, K-feldspar, etc.) additionally increases the porosity.

Bulk and grain density only show a small variation in the reduced rocks. The leucocratic phonolite has a slightly lower average grain density compared to the tephri-phonolite, consistent with its lower content of replaced mafic minerals and weaker

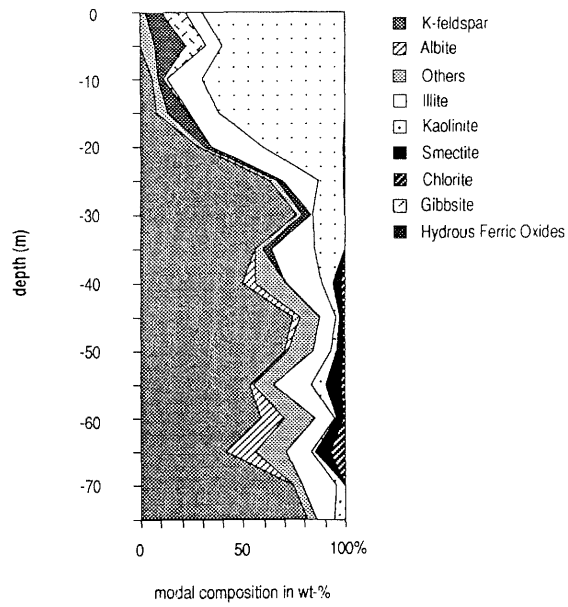

Figure 6. Borehole MF12: mineralogical variation with depth.

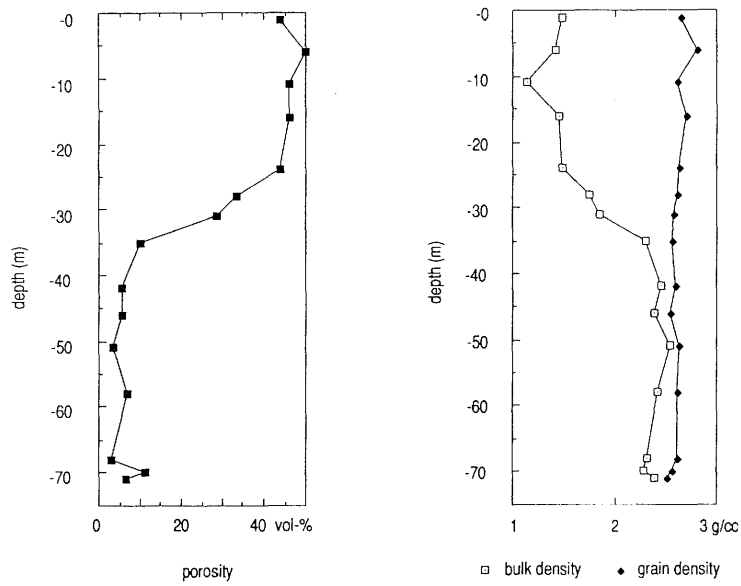

Figure 7. Borehole MF12: variation of porosity, bulk and grain density with depth.

pyrite impregnations. In the oxidized phonolite, bulk density decreases due to the alteration of alkali-feldspars to sparry clay aggregates and the dissolution of unstable minerals, leaving open pores behind.

6.1.2. Mineralogy

The hydrothermal alteration has produced a very similar general mineral composition in the different phonolites. The specific mineral descriptions are therefore valid for all phonolites unless specified otherwise (e.g. alkali-feldspars, plagioclase etc.). The mineralogical composition of the phonolites may be subdivided into three assemblages: the hydrothermal alteration assemblage, the hydrothermally induced mineralization assemblage and the mineral assemblage of the oxidized zone, which is superimposed on the two earlier assemblages.

The hydrothermal alteration assemblage includes all the primary magmatic minerals, together with their exchange and alteration products. The hydrothermally induced mineralization assemblage includes all the minerals newly formed during the hydrothermal overprint (pyrite, fluorite, U-Th-REE phases, newly precipitated K-feldspar, etc.), while the assemblage of the oxidized zone includes minerals formed under oxidizing weathering conditions.

Clay minerals were/are formed and/or decomposed during all three major processes and are described separately in section 6.1.3.

6.1.2.1. Hydrothermal alteration assemblage

Minerals of this assemblage include alkali-feldspars, nepheline, pseudoleucite, plagioclase, clinopyroxene and magmatic accessories comprising sphene, zircon and apatite.

Alkali-feldspars

Alkali-feldspars are the only minerals that show distinct differences between the leucocratic phonolite and the tephri-phonolite. In both phonolites alkali-feldspars occur mainly in four textural variations: sanidine-shaped euhedral laths and prisms in the matrix, lathy to tabular phenocrysts, subordinate euhedral tabular alkali-feldspars in amygdaloidal structures and xenomorphic to euhedral K-feldspar that occurs

interstitially and as infillings in voids and fractures, the latter belonging to the mineralization assemblage. In the leucocratic phonolite, both the matrix alkali-feldspars and phenocrysts suffered almost complete alkali-exchange, yielding an X-ray pattern for single grains of intermediate microcline with a nearly pure orthoclase composition. Only in a few phenocrysts are microperthitic exsolution structures preserved in the very centre; X-ray patterns of such phenocrysts are easily discernable from the bulk. The intermediate microcline normally shows zoning from a core rich in minute hematite and fluid inclusions to a clear growth rim free of hematite. All the intermediate microclines show slight sericitization in their core but not in the growth rim.

In the tephri-phonolite, microperthitic exsolution in matrix microclines and in the phenocrysts is much more abundant. Alkali-exchange did not reach completion as observed with the leucocratic phonolite, and the X-ray pattern is clearly distinct from those intermediate microclines, displaying a low to moderate albite component. Sericitization and zoning are the same as in the leucocratic phonolite. Hematite inclusions in the centre, however, seem to be less abundant.

The alkali-feldspars of the phonolitic dykes generally display the same features as their counterparts in the leucocratic phonolite. In one dyke cutting the tephri-phonolite, however, the alkali-feldspars are completely free of hematite and display no microperthitic exsolution.

In the amygdaloidal structures the alkali-feldspars occur as radially arranged euhedral crystals free of hematite inclusions. The slightly argillically altered crystals have a grain size intermediate between the matrix and phenocrysts and do not exhibit microperthitic exsolution structures.

Under cathodoluminescence, the bulk of alkali-feldspars in the leucocratic phonolite show an irregular patchy orange-red coloured luminescence in the centre, changing from a light lilac colour to a nearly non-luminescent rim. The same colour zoning occurs in the feldspars of the amygdaloidal structures. In addition, the tephri-phonolite alkali-feldspars exhibit a dark-blue coloured core which yielded a high-sanidine XRD pattern. This blue luminescence colour is characteristic for these magmatic alkali-feldspars (Marshall, 1988). Red luminescence colours in alkali-feldspars are due to lattice impurities such as Fe^{3+}. Such colours are, among others, characteristic of rocks that have undergone fenitization (Marshall, op. cit.). The weakly luminescent dull yellow-brown colour of the growth rims is a characteristic feature of the alteration of short-lived luminescence, caused by prolonged electron bombardment, typical for K-feldspar precipitated from low-temperature solutions (Ramseyer *et al.*, 1989).

Nepheline

Nepheline is always completely pseudomorphed by illite and kaolinite, both in the matrix and the phenocrysts. The pseudomorphs frequently display a zoned arrangement from a kaolinite-rich core to an illite-rich border zone. Fine-grained pyrite and fluorite sporadically occur as inclusions intimately intergrown with illite/sericite and kaolinite. In the illite-rich border zone, textural evidence indicates a substitution of kaolinite by a somewhat coarser-grained illite/sericite.

Pseudoleucite

Pseudoleucite mainly occurs as phenocrysts; in some cases, possible pseudoleucite was also observed in the matrix. However, its identification in the latter case is problematic due to the fine grain size of the matrix and the degree of argillic alteration.

Pseudoleucite phenocrysts comprise orientated intergrowths of alkali-feldspars and pseudomorphically replaced nepheline. The former has a red-orange luminescence colour.

Plagioclase

Plagioclase occurs in tephri-phonolite and in the hololeucocratic phonolitic dyke, but not in the leucocratic phonolite. It is of nearly pure albite composition and is exclusively found in the matrix, occurring interstitially between the alkali-feldspars or as microperthitic exsolutions in alkali-feldspars.

Clinopyroxene

Hypidiomorphic to idiomorphic aggregates of iron- and titanium-oxides, together with silicate phases, are interpreted, by analogy with the phonolites of the Osamu Utsumi mine, as being pseudomorphically replaced clinopyroxenes. This interpretation is supported by the occurrence of green coloured clinopyroxene as inclusions in some alkali-feldspar phenocrysts. The silicate phases of such pseudomorphs are mainly chlorite and smectite.

Magmatic accessories

Magmatic accessories are rare in all the phonolitic rocks of the MF12 borehole. Sphene and apatite are the most abundant besides zircon and a few opaque phases; sphene is always completely pseudomorphically replaced by leucoxene and calcite. Such pseudomorphs are randomly distributed throughout the matrix and are somewhat more abundant in the tephri-phonolite. Apatite and zircon occur as hypidiomorphic to idiomorphic single needles and prisms, and in several cases may be observed as inclusions in alkali-feldspars and replaced nepheline.

6.1.2.2. Hydrothermal mineralization assemblage

Minerals that belong to this assemblage include pyrite, fluorite, carbonates, U-Th-minerals, REE-minerals, zircon and Zr-minerals, and sphalerite. In addition, the newly precipitated K-feldspar and clay minerals belong to this assemblage.

K-feldspar

Xenomorphic to euhedral alkali-feldspars that occur interstitially in void and fracture infillings are normally free of hematite inclusions; fluid inclusions are also rare. Macroscopically, these alkali-feldspars often have a light bluish colour and the X-ray patterns indicate a fully ordered, triclinic low microcline, clearly discernable from the patterns of all other alkali-feldspars. Such low microcline has a characteristically dull yellow-brownish luminescence, similar to the thin growth rims around the alkali-feldspars of the phonolites, both matrix and phenocryst varieties. This characteristic luminescence is typical for K-feldspars precipitated from low-temperature solutions (Ramseyer *et al.*, 1989).

Pyrite

Pyrite is by far the main ore mineral present in the hydrothermally altered phonolites, occurring mostly as fine disseminations. Such pyrites are very fine-grained (0.005 – 0.5 mm) and exhibit a euhedral cubic shape. Somewhat coarser-grained pyrites occur in void infillings and on fracture planes (0.1 – 2 mm), where they commonly form intimately intergrown aggregates with all the other assemblage minerals.

Pyrite is slightly more abundant in the tephri-phonolite than in the leucocratic phonolite or the phonolitic dykes. An average content of pyrite is difficult to estimate due to its irregular distribution, but it may lie between 1 to 3 vol.% in the leucocratic phonolite and 3 to 4 vol.% in the tephri-phonolite.

Fluorite

Fluorite mainly occurs in interstices, as void and vein infillings, and on fracture planes; idiomorphic fluorite is only present in open cavities. The grain size of the fluorite ranges between 0.5 – 30 mm, the largest fluorites occurring as poorly defined aggregates on fractures. The majority of fluorites are violet coloured, often display radiation damage, and contain tiny opaque inclusions. In several zones colourless or greenish varieties of fluorite occur as isolated grains, not intimately associated with the other minerals of this assemblage. All fluorites contain abundant fluid inclusions of different generations and inclusions and/or intergrowths with carbonate are frequent.

Carbonate

Sideritic carbonate is frequently observed in interstices and void infillings in close association with pyrite and fluorite. Carbonate is often observed penetrating from veins into the rock matrix and partly replacing some of the minerals. In conductive fractures carbonate is lacking due to dissolution, supported by the partial removal of the carbonate impregnations adjacent to such fractures. The modal abundance of carbonate rarely reaches 2 vol.%.

REE-minerals

Besides the potential REE-bearing minerals of magmatic origin (clinopyroxene, apatite, zircon, sphene), monazite is the most abundant REE-mineral present in the phonolitic rocks. It occurs as very fine-grained euhedral crystals (10 to 150μ) finely disseminated throughout the rocks. Coarser-grained monazite is restricted to void and vein fillings, where in rare cases it may reach millimetric dimensions.

Further identified by X-ray and SEM investigations were cheralite and bastnaesite. Both these minerals could only be detected in vein fillings, spreading from there along grain boundaries into the rock matrix. The REE-minerals are commonly associated with pyrite and, in parts, with fluorite and Ti-oxides.

Zircon and Zr-minerals

Zircon is more abundant in the leucocratic phonolite than in the tephri-phonolite. It is only rarely found in crystals exceeding 1 mm in size and mostly occurs as vein infillings together with the REE phases, fluorite and pyrite. In several cases it forms intimate intergrowths with another Zr-mineral, most probably baddeleyite.

Sphalerite

Sphalerite was detected only in a few samples, where it occurs intimately intergrown with pyrite on fracture planes and in void infillings.

6.1.2.3. Oxidized zone

The oxidized phonolite is characterized by the absence of pyrite, fluorite, sphalerite and reduced U-Th-REE and manganese phases. In addition, K-feldspars have decomposed to kaolinite and subordinate illite. This transformation becomes more complete further up the vertical profile in the lateritic weathering cover (Fig. 6; section 6.2). Minerals formed in the oxidized zone include:

- Fe-hydroxides (mainly goethite and ferrihydrite),
- kaolinite,
- illite,
- Mn-hydroxides/oxides (cryptomelane, nsutite, pyrolusite, manganite?),
- crandallite group minerals (gorceixite, goyazite, florencite),
- alunite-jarosite group minerals.

Fe-oxides and hydroxides

Amorphous to low crystalline hydrous ferric oxides and goethite (α-FeOOH) are most abundant among the newly formed iron phases; hematite occurs in trace amounts. All these iron phases are products of pyrite oxidation. The oxidation of pyrite is complete 2 to 3 cm from the redox front within the oxidized zone, and only strongly corroded relict pyrite may still be present in the centre of hydrous ferric oxide clay aggregates within that narrow zone. The general coating of all the minerals with hydrous ferric oxides makes optical investigations extremely difficult.

Rhythmic layering of hydrous ferric oxides in fractures and pores, often separated by thin Mn-hydroxide layers, suggests formation of the iron and manganese phases in several stages.

Mn-hydroxides

Mn-hydroxides, always in close association with Fe-hydroxides, are especially abundant on the oxidized side of the redox front where they occur as fracture fillings migrating dendritically into the rock matrix. Some of the Mn-hydroxides in such fractures clearly display replacement by other Mn-hydroxides and -oxides (e.g. nsutite → pyrolusite).

Crandallite group minerals

Gorceixite and goyazite occur as thin coatings in fractures and in pore spaces. Florencite is observed in close association with bastnaesite and other cryptocrystalline, highly birefringent phases. All the crandallite group minerals are most probably of secondary weathering origin.

Alunite-jarosite group minerals

Alunite and jarosite are mainly found in fractures and in zones together with abundant Fe-hydroxides. Their association with Fe-hydroxides pseudomorphically replacing pyrite indicates their formation through the oxidation of pyrite.

6.1.3. Clay mineralogy

The clay mineral composition is very distinct between the leucocratic phonolite and the tephri-phonolite (Fig. 8). The leucocratic phonolite has a comparatively low abundance of total clay minerals (approx. 10% of the whole rock; see Table II), and the predominant clay minerals are illite (average 70%) and kaolinite (27%); chlorite and smectite are rare and sporadically occur as traces. Only trace amounts of other minerals such as halloysite and alunite were detected in the $<2\mu$ fraction.

In contrast, the $<2\mu$ fraction constitutes on average about 25% of the bulk composition of the tephri-phonolite. Illite is again the most abundant clay mineral

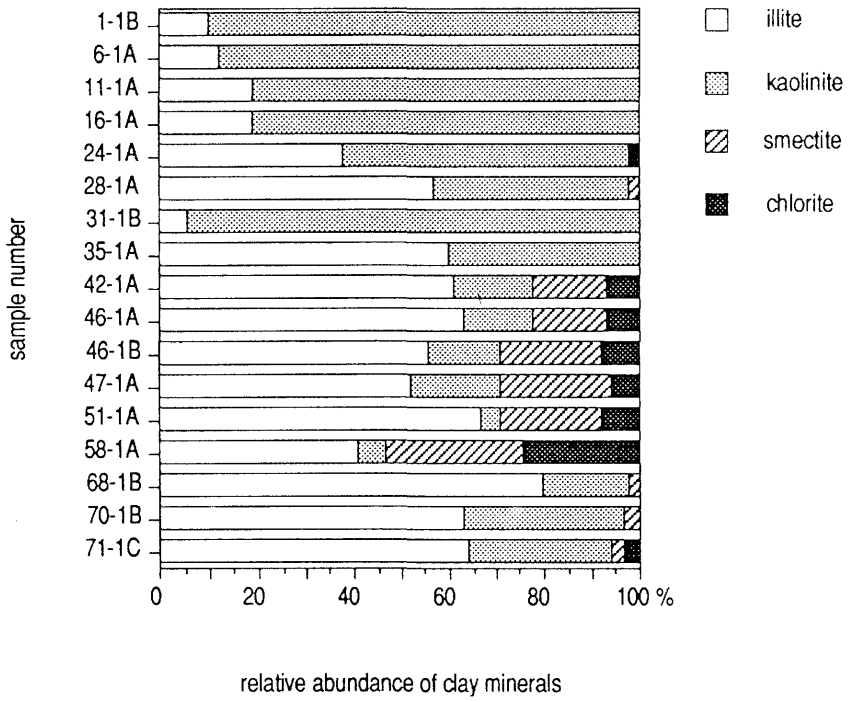

Figure 8. Borehole MF12: clay mineralogical composition; sample numbers refer to the depth of sampling.

Laterite: samples 1-1B to 24-1A,
Oxidized leucocratic phonolite: samples 28-1A to 35-1A,
Reduced tephri-phonolite: samples 42-1A, 46-1B to 58-1A,
Phonolitic dyke: sample 46-1A,
Reduced leucocratic phonolite: samples 68-1B to 71-1C.

(average 55%) but is now followed by smectite (22%), kaolinite (12%) and chlorite (10%). Besides halloysite, alunite and the crandallite group minerals occur as traces in the $<2\mu$ fraction.

Indications of mixed-layers are completely lacking in the leucocratic phonolite, but were found in a few samples from the tephri-phonolite. However, the smectite content of these illite-smectite mixed-layers does not exceed 5%.

In the oxidized zone the $<2\mu$ fraction constitutes on average about 28% of the bulk rock. Here, kaolinite is the most abundant clay mineral (average 56%), followed by illite (40%); chlorite is absent and smectite sporadically occurs as traces. Alunite-jarosite group minerals and crandallite group minerals are always present in trace amounts in the $<2\mu$ fraction.

Illite/sericite

The term sericite here applies to a fine-grained ($2–60\mu$) variety of flaky white mica that is larger than the illite of the clay fraction. Illite occurs as an alteration product mainly from nepheline, but also from alkali-feldspars, and as a hydrothermal precipitate. The coarser sericite variety occurs as a hydrothermal formation within the matrix, and as a substitute for kaolinite in the nepheline pseudomorphs. It normally has a pale green pleochroism indicating a moderate iron content.

Illite crystallinity measurements after Kubler (1968) give values for the leucocratic phonolite of less than 0.25, and for all the tephri-phonolite samples values higher than 0.25. According to the Kubler scale this would indicate a lower temperature of formation for the tephri-phonolite (anchizonal) than for the leucocratic phonolite (epizonal). This seems to be rather unreasonable for the Morro do Ferro country rocks where the difference in the illite crystallinity is much more due to a moderate K^+-activity in the tephri-phonolite compared to a high K^+-activity in the leucocratic phonolite during illite formation. This coincides very well with the fact that the alkali-feldspars are completely replaced in the leucocratic phonolite but not in the tephri-phonolite (compare section 6.1.2.).

Kaolinite

In the reduced phonolites, kaolinite occurs almost exclusively as a replacement product of magmatic nepheline. In strongly brecciated zones, kaolinite occurs as infillings in open cavities and fractures. All the texturally distinct kaolinites display X-ray patterns with well-defined peaks.

In the reduced samples selected only a few millimetres from the redox front, and in the oxidized phonolite itself, secondary kaolinite is formed by the decomposition of K-feldspars. Additionally, kaolinite is, at least in part, believed to be of secondary origin on fracture planes known to be active conductive zones. In such cases kaolinite displays less well-defined X-ray patterns.

Smectite

Dioctahedral smectite is found mainly in pseudomorphs after primary mafic components in the tephri-phonolite together with small amounts of chlorite (Fig. 8). No indications are found in the rock matrix for an illite to smectite transformation.

Smectite also occurs as fracture infillings, whereupon mixed-layering was observed more frequently. The mixed-layers seem to be restricted to a zone between a depth of about 58 m and 70 m, which corresponds to the most highly conductive zone in the MF12 borehole. The illite to smectite ratio of these mixed-layers is about 9 : 1.

6.1.4. Geochemistry

The preceding geological and petrographical studies have shown that the phonolites recovered from the MF12 borehole resemble the hydrothermally altered phonolites of the Osamu Utsumi mine in many of their features. There also exists a strong relationship in the general chemistry, which is more pronounced between the leucocratic phonolite and the Osamu Utsumi mine phonolites. In general, the country rocks of Morro do Ferro underwent similar geochemical processes after magmatic emplacement as did the rocks of the Osamu Utsumi mine. These processes include deuteric alteration (Schorscher and Shea, this report series; Rep. 1), hydrothermal (potassic) alteration, infiltration of oxidizing groundwaters, and surface weathering coupled with soil formation.

In order to study the geochemical changes that took place during hydrothermal alteration, the country rocks are compared to the regional phonolite samples as discussed in Schorscher and Shea (op. cit.) and to the unaltered and altered, but non-mineralized

phonolitic rocks of the Osamu Utsumi mine (Waber *et al.*, this report series; Rep. 2). Despite the miaskitic to intermediate affinity of the regional rocks (K_2O+Na_2O/Al_2O_3 = 0.89 – 1.12), these comparisons seem to be reasonable due to the mineralogical similarity of the regional rocks to the unaltered samples of the Osamu Utsumi mine (K_2O+Na_2O $/Al_2O_3$ = 0.69 – 0.88), and of the hydrothermally altered country rocks at Morro do Ferro (K_2O+Na_2O/Al_2O_3 = 0.56 – 0.71) to the altered phonolitic rocks in the Osamu Utsumi mine ($K_2O+Na_2O/+Al_2O_3$ = 0.37 – 0.90). No minerals or relicts of minerals typical for the peralkaline (agpaitic) suite of alkaline rocks could be detected in these rock groups as they are described by Ulbrich (1984), for example phonolites and nepheline syenites from different localities in the Poços de Caldas plateau.

The country rocks recovered from the MF12 borehole exhibit particular differences in major and trace element composition, reflecting their mineralogical dissimilarities. Differences are most pronounced between the leucocratic phonolite and the tephri-phonolite. The investigated phonolitic dyke displays a composition comparable to the leucocratic phonolite. Mean values for the different phonolitic country rocks encountered with depth are given in Table III. For comparison, the mean values for the hydrothermally altered, reduced leucocratic phonolites from the Osamu Utsumi mine (Waber *et al.*, op. cit.) and the unaltered regional samples (Schorscher and Shea, op. cit.) are also listed. The geochemical analyses for single samples and the elemental variation with depth in the MF12 borehole are given in Appendix 2.

6.1.4.1. Major elements

The leucocratic phonolite is characterized by its extremely elevated K_2O content (average of 13.33 wt.%), reflecting the potassium-rich hydrothermal alteration. In contrast, Fe_{tot}, Na_2O, MgO, CaO and MnO are more or less completely depleted in this rock, compared to the unaltered regional rocks (Fig. 9). The major element composition is comparable to the mean composition of the leucocratic phonolite from the Osamu Utsumi mine. In Figure 10, the average value for the leucocratic phonolite is normalized to the mean value for the leucocratic phonolite of the Osamu Utsumi mine. As can be seen from this figure, minor differences between the two phonolites include slightly higher contents of TiO_2, Na_2O, MgO and P_2O_5, and lower values for Fe_{tot}, MnO, CaO and crystalline water.

The tephri-phonolite is characterized by having less SiO_2 (51.3 wt.%) and K_2O (8.69 wt.%) compared to the leucocratic phonolite. In contrast, Fe_{tot}, MnO, CaO, Na_2O,

TABLE III

Geochemical mean values for hydrothermally altered phonolites, weathered carbonatitic host rock and ore body, together with the mean values for hydrothermally altered phonolites of the Osamu Utsumi mine (data from Waber *et al.*, this report series; Rep. 2) and the unaltered regional samples (data from Schorscher and Shea, this report series; Rep. 1). Mean values for the ore body, weathered host rock and laterite are statistically irrelevant due to the large scatter of analytical data with respect to the number of samples.

		MORRO DO FERRO						OSAMU UTSUMI MINE*						REGIONAL SAMPLES**	
		Borehole MF10				**Borehole MF12**									
		Ore body		Weathered host rock (carbonatite)		Laterite		Leucocratic phonolite oxidized	Tephri-phonolite reduced	Leucocratic phonolite reduced	Leucocratic phonolite oxidized	Leucocratic phonolite reduced	Plc-Cpx phonolite reduced	Subvolcanic phonolite fresh	Volcanic phonolite fresh
		Average n = 12	Range	Average n = 8	Range	Average n = 5	Range	n = 3	n = 5	n = 3	n = 6	n = 21	n = 9	n = 2	n = 4
SiO_2	wt.%	20.59	(6.01-39.41)	33.52	(26.73-40.64)	38.49	(28.1-48.16)	54.17	51.31	57.87	55.74	56.89	55.87	52.87	53.11
TiO_2		2.05	(0.97-3.12)	1.93	(1.09-5.42)	1.02	(0.77-1.41)	0.71	0.57	0.62	0.53	0.44	0.41	0.66	0.56
Al_2O_3		25.95	(14.11-38.06)	27.36	(22.07-32.84)	32.60	(28.4-38.84)	23.00	20.55	21.61	23.28	21.80	22.20	19.57	19.64
Fe tot		18.95	(6.49-36.21)	15.71	(4.5-29.44)	6.85	2.11-12.94	3.67	6.27	1.62	3.04	2.53	2.35	4.14	3.73
MnO		2.69	(0.09-10.63)	2.05	(0-6.91)	1.03	(0-4.11)	0.00	1.30	0.00	0.00	0.04	0.00	0.00	0.00
MgO		0.23	(0.1-0.51)	0.13	(0.07-0.22)	0.08	(0.04-0.12)	0.07	0.27	0.10	0.03	0.05	0.15	0.31	0.22
CaO		0.03	(0-0.04)	0.02	(0.01-0.04)	0.03	(0.01-0.05)	0.03	1.43	0.08	0.00	0.19	0.06	1.85	1.55
Na_2O		0.30	(0.2-0.55)	0.16	(0.08-0.27)	0.26	(0.18-0.37)	0.37	1.25	0.51	0.29	0.36	0.99	7.55	7.63
K_2O		2.93	(1.3-4.77)	2.91	(2.7-3.34)	3.92	(2.1-7.93)	11.35	8.69	13.33	12.96	13.72	13.44	8.26	8.26
P_2O_5		0.77	(0.18-1.19)	0.15	(0.06-0.32)	0.33	(0.14-0.79)	0.12	0.09	0.11	0.07	0.06	0.10	0.10	0.06
LOI		13.25	(9.15-20.43)	11.30	(9.66-12.7	11.90	(7.51-15.19)	2.57	3.95	2.28	3.27	3.08	2.64	1.44	1.35
CO_2		n.a.	n.a.	n.a.	n.a.	0.62	(0.4-1.0)	1.65	2.46	0.27	n.a.	n.a.	0.24	n.a.	n.a

(contd.).

TABLE III (contd.).

		MORRO DO FERRO									OSAMU UTSUMI MINE*			REGIONAL SAMPLES**	
		Borehole MF10				**Borehole MF12**									
		Ore body		Weathered host rock (carbonatite)		Laterite		Leucocratic phonolite oxidized	Tephri-phonolite reduced	Leucocratic phonolite reduced	Leucocratic phonolite oxidized	Leucocratic phonolite reduced	Plc-Cpx phonolite reduced	Subvolcanic phonolite fresh	Volcanic phonolite fresh
		Average n = 12	Range	Average n = 8	Range	Average n = 5	Range	n = 3	n = 5	n = 3	n = 6	n = 21	n = 9	n = 2	n = 4
F	ppm	1708	(612-2585)	693	(242-1144)	1134	(599-1777)	1734	5936	1706	1218	2085	1466	1983	1561
Ba		155	(10-529)	95	(13-187)	192	(36-360)	147	150	158	583	677	913	425	50
Rb		113	(40-169)	101	(74-136)	126	(93-220)	339	208	328	315	309	294	160	154
Sr		698	(146-1359)	85	(42-175)	891	(51-3189)	211	681	278	188	198	575	2327	1421
Pb		136	(65-253)	55	(9-95)	249	(43-822)	29	31	28	30	4	51	5	2
Th		8767	(1404-14843)	408	(165-849)	219	(103-554)	77	52	40	46	30	47	8	5
U		27	(<5-64)	7	(<5-45)	92	(45-173)	33	25	19	185	20	46	b.d.	b.d.
Nb		1084	(731-2206)	1117	(504-3144)	543	(368-751)	355	274	291	225	188	219	212	261
La		4154	(1286-11100)	4314	(1239-8573)	1882	(1405-8649)	2148	928	615	309	268	403	250	279
Ce		7628	(1516-13962)	1620	(842-2632)	1795	(1470-2406)	1254	1106	667	673	311	401	316	379
Nd		2011	(701-5142)	2058	(638-3758)	1410	(387-4723)	489	244	168	83	61	82	82	100
Y		404	(200-416)	297	(163-581)	228	(136-378)	118	97	85	73	54	111	36	41
Zr		2318	(1469-3619)	2445	(1473-5253)	2133	(1304-2669)	1402	933	1148	1360	1009	1344	880	885
V		597	(95-1156)	630	(306-1259)	220	(110-347)	136	97	187	239	236	218	72	72
Cr		54	(17-99)	34	(27-44)	19	(6-25)	5	8	b.d.	7	6	b.d.	b.d.	b.d.
Ni		22	(7-40)	7	(<5-18)	8	(<5-19)	b.d.	b.d.	b.d.	5	b.d.	b.d.	b.d.	b.d.
Co		17	(<5-58)	17	(<5-34)	15	(<5-40)	9	14	5	6	5	4	10	19
Cu		25	(<5-44)	b.d.	b.d.	7	(<5-18)	b.d.	b.d.	b.d.	b.d.	b.d.	b.d.	b.d.	b.d.
Zn		724	(135-1039)	675	(125-1836)	196	(60-363)	78	562	163	24	222	220	153	165
Hf		62	(28-78)	41	(21-91)	39	(20-51)	20	11	12	12	10	16	12	10
Sc		3	(<2-7)	b.d.	b.d.	3	(<3-4)	5	3	6	3	3	6	b.d.	b.d.
S		448	(84-1649)	379	(119-1044)	134	(72-245)	139	3459	3140	27	8237	5925	8153	6229

b.d. = below detection limit, n.a. = not analyzed, LOI = Lost On Ignition

* Data from Waber et al., this report series; Rep. 2.

** Data from Schorscher and Shea, this report series; Rep. 1.

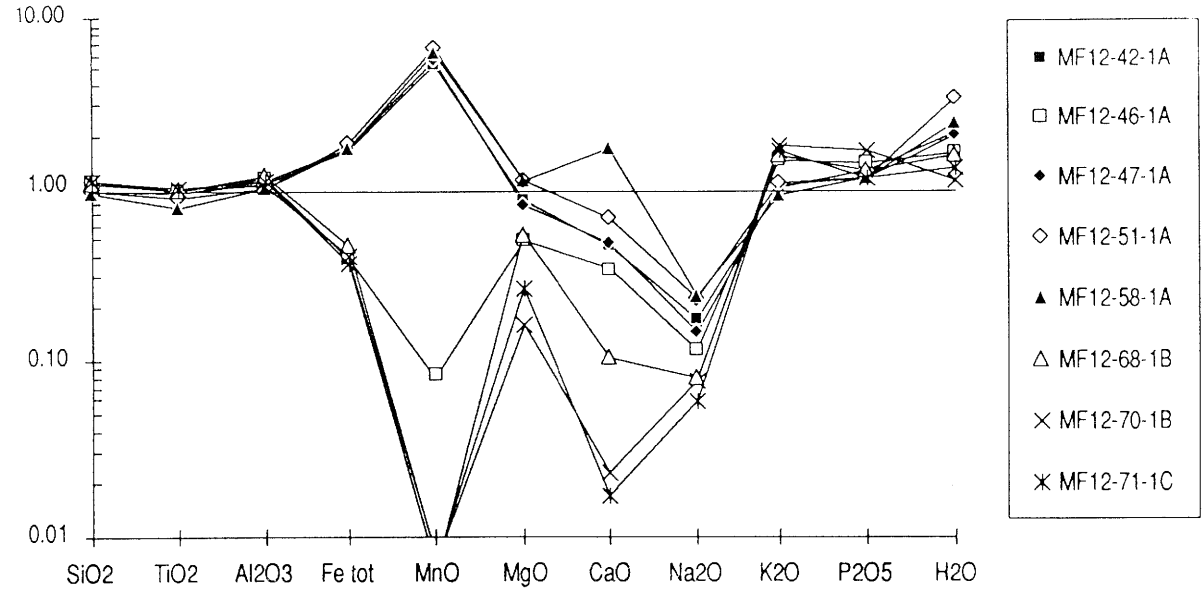

Figure 9. Borehole MF12: major elements for the reduced hydrothermally altered phonolites normalized to the average for regional phonolites (data from Schorscher and Shea, this report series; Rep. 1).

Tephri-phonolite: samples 42-1A, 47-1A, 51-1A and 58-1A,
Leucocratic phonolite: samples 68-1B, 70-1B, 71-1C,
Phonolitic dyke: sample 46-1A.

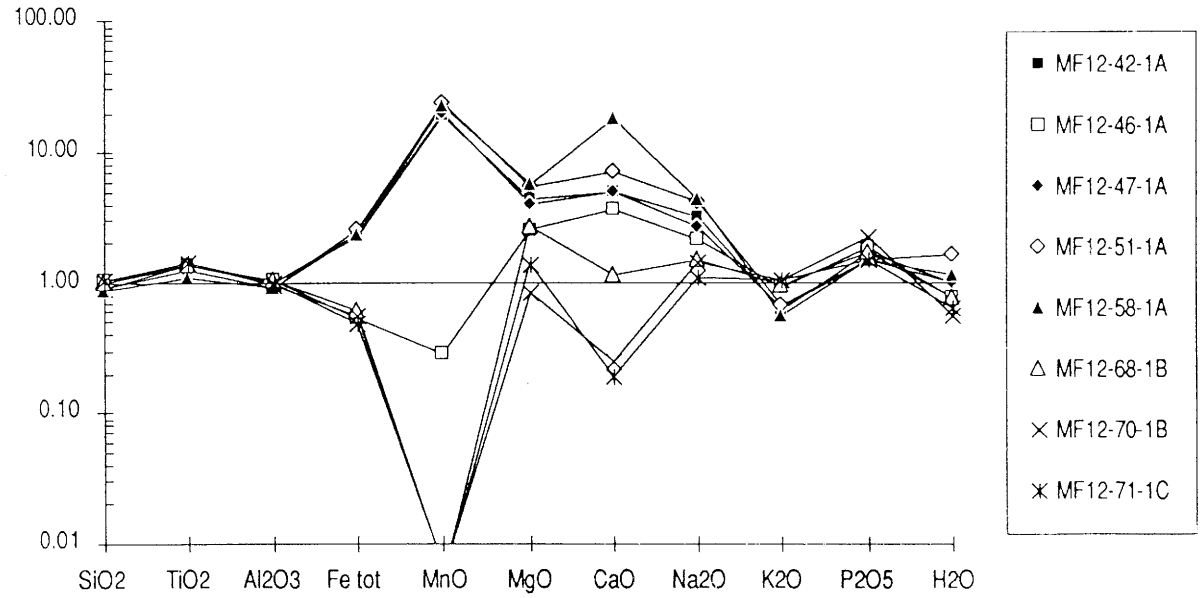

Figure 10. Borehole MF12: major elements for the reduced hydrothermally altered phonolites normalized to the average for reduced hydrothermally altered phonolites of the Osamu Utsumi mine (data from Waber et al., this report series; Rep. 2).

Tephri-phonolite: samples 42-1A, 47-1A, 51-1A and 58-1A,
Leucocratic phonolite: samples 68-1B, 70-1B, 71-1C,
Phonolitic dyke: sample 46-1A.

crystalline water and CO_2 are moderately to strongly increased (Table III). Mineralogically, these differences are reflected in a lower abundance of modal alkali-feldspars which did not suffer complete alkali-exchange in the tephri-phonolite, a higher abundance of relict primary mafic minerals, and a stronger impregnation with pyrite and carbonates compared to the leucocratic phonolite. In comparison with the hydrothermally unaltered regional rocks, the tephri-phonolite has increased contents of Fe_{tot}, MnO, CO_2, crystalline water and, in one sample (MF12-58-1A), also of CaO (Fig. 9). SiO_2, Na_2O and, in the majority of the samples, CaO are lower than in the regional rocks. K_2O, although slightly increased in some samples, displays very similar concentrations to that in the regional rocks.

When comparing the tephri-phonolite with the hydrothermally altered leucocratic phonolite of the Osamu Utsumi mine, the higher contents of Fe_{tot}, MnO, MgO, CaO, Na_2O, P_2O_5, crystalline water and CO_2 (not averaged in Table III; a small set of samples from the mine leucocratic phonolites yield CO_2 concentrations between 0.05 and 0.44 wt.%), together with the much lower K_2O and SiO_2 concentrations, are most obvious. The same general pattern arises when the tephri-phonolite is compared to the hydrothermally altered clinopyroxene-bearing phonolite of the Osamu Utsumi mine (Table III).

The leucocratic dyke (sample MF12-46-1A) displays, in its major element composition, a strong affinity to the leucocratic phonolite. Differences include a slightly lower K_2O content and higher values of MnO, CaO and Na_2O, intermediate between tephri-phonolite and leucocratic phonolite (Table III; Figs. 9 and 10).

Interelement correlations are not obvious among the major elements. In both the tephri-phonolite and the leucocratic phonolite, SiO_2 and K_2O are positively correlated. In the tephri-phonolite Fe_{tot} displays a very good correlation with MnO ($r = 0.99$; $n = 5$). The better correlation in both phonolites between CaO and F ($r = 0.99$; $n = 8$) than between CaO and CO_2 ($r = 0.64$; $n=8$) sustains the mineralogical observations that fluorite is the major fluorine and calcium-bearer, whereas CO_2 is preferentially present in carbonates other than calcite, for example siderite ($r_{Fe\text{-}CO_2} = 0.75$, $r_{Mn\text{-}CO_2} = 0.73$; $n = 8$) and REE carbonates (e.g. bastnaesite: $r_{Ce\text{-}CO_2} = 0.82$; $n = 8$).

6.1.4.2. Trace elements

The most striking differences in the trace element composition between the two phonolitic rocks include the higher mean values for the tephri-phonolite (factor 3.5), Zn

(factor 3), Co (factor 2.8), Sr (factor 2.4), total LREE (factor 1.6, XRF data), U and Th (both by a factor 1.3) and Cr, which is below detection in the leucocratic phonolite. In contrast, Rb (factor 1.6), V (factor 1.9) and Sc (factor 2) are enriched in the leucocratic phonolite. Rb, V and Sc are mainly incorporated in alkali-feldspars and the enrichment factors reflect exactly the difference in modal abundance of alkali-feldspars in the two phonolites.

All these elements, with the partial exception of Sr, occur in mineral phases of the hydrothermal mineralization assemblage and corroborate the mineralogical observations. By analogy with the unaltered regional rocks, where Sr is also incorporated into alkali-feldspars (M. Ulbrich, 1983), Sr might still be partly present in the residual alkali-feldspars of the tephri-phonolite. In addition, the tephri-phonolite has a fair amount of smectite in its clay fraction (see section 6.1.3) which has a high capacity to incorporate Sr.

For most trace elements, the phonolitic dyke (MF12-46-1A) displays an intermediate composition between the leucocratic phonolite and the tephri-phonolite. The dyke is, however, lower in U, Th and Pb than both phonolites. For F, Sr and Zn, the dyke displays a closer affinity to the tephri-phonolite, whereas the Rb and Co behaviour is more comparable to the leucocratic dyke. Sulphur is lowest in the dyke when compared to all the other samples (Table III).

In comparison with the unaltered regional rocks, the strong enrichment of U, Th, LREEs, Y and Pb and depletion of Ba and Sr are the most obvious features in both phonolites (Fig. 11). F, Cr, Co and Zn are enriched in the tephri-phonolite, whereas they are slightly to strongly depleted in the leucocratic phonolite. Rb, V and Sc exhibit greater values in the leucocratic phonolite but more or less equal values to the tephri-phonolite compared to the regional samples. Nb, Zr and Hf display similar values to the regional rocks. Sulphur is enriched in both phonolites, with the exception of two strongly argillically altered samples (MF12-47-1A, MF12-68-1A) and the phonolitic dyke.

In Figure 12 the mean values of the Morro do Ferro phonolites are normalized to the mean value of the reduced, hydrothermally altered rocks of the Osamu Utsumi mine. Here too, the country rocks are enriched in LREEs, Y, Th and Pb and depleted in Ba. Compared to the Osamu Utsumi mine phonolites, however, all the country phonolites of Morro do Ferro are depleted in U (with the exception of sample MF12-58-1A) and V. Zr, F, Co and Zn are increased in the tephri-phonolite but decreased in the leucocratic phonolite; on the other hand, S occurs in much lower amounts in both if compared to the Osamu Utsumi mine phonolites.

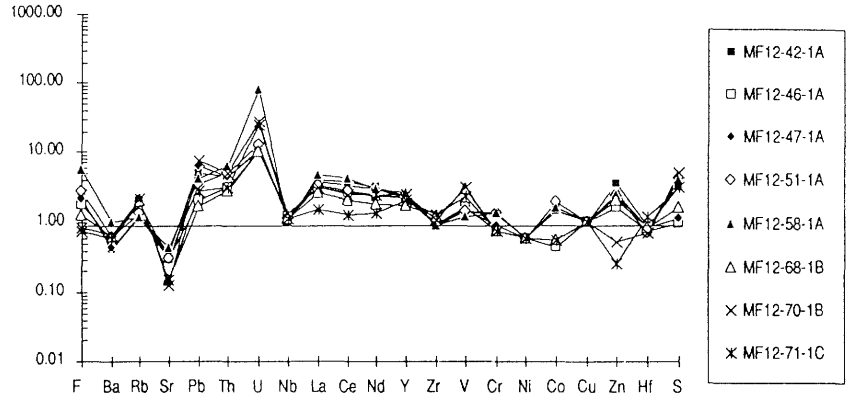

Figure 11. Borehole MF12: trace elements for the reduced hydrothermally altered phonolites normalized to the average for regional phonolites (data from Schorscher and Shea; this report series; Rep. 1).

Tephri-phonolite: samples 42-1A, 47-1A, 51-1A and 58-1A,
Leucocratic phonolite: samples 68-1B, 70-1B, 71-1C,
Phonolitic dyke: sample 46-1A.

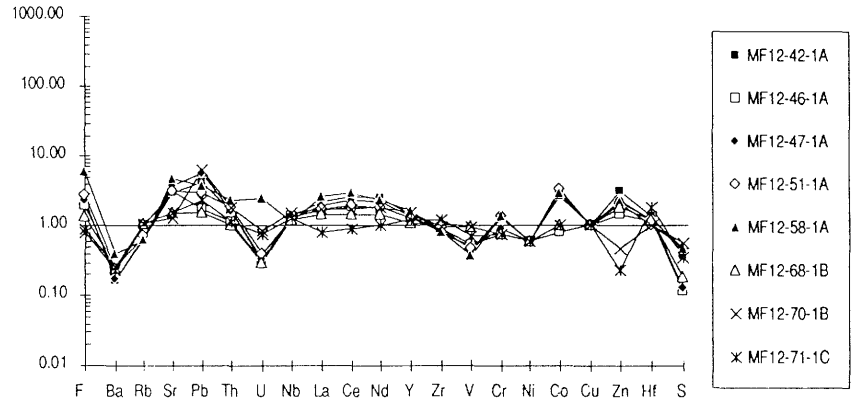

Figure 12. Borehole MF12: trace elements for the reduced hydrothermally altered phonolites normalized to the average for reduced hydrothermally altered phonolites of the Osamu Utsumi mine (data from Waber et al., this report series; Rep. 2).

Tephri-phonolite: samples 42-1A, 47-1A, 51-1A and 58-1A,
Leucocratic phonolite: samples 68-1B, 70-1B, 71-1C,
Phonolitic dyke: sample 46-1A.

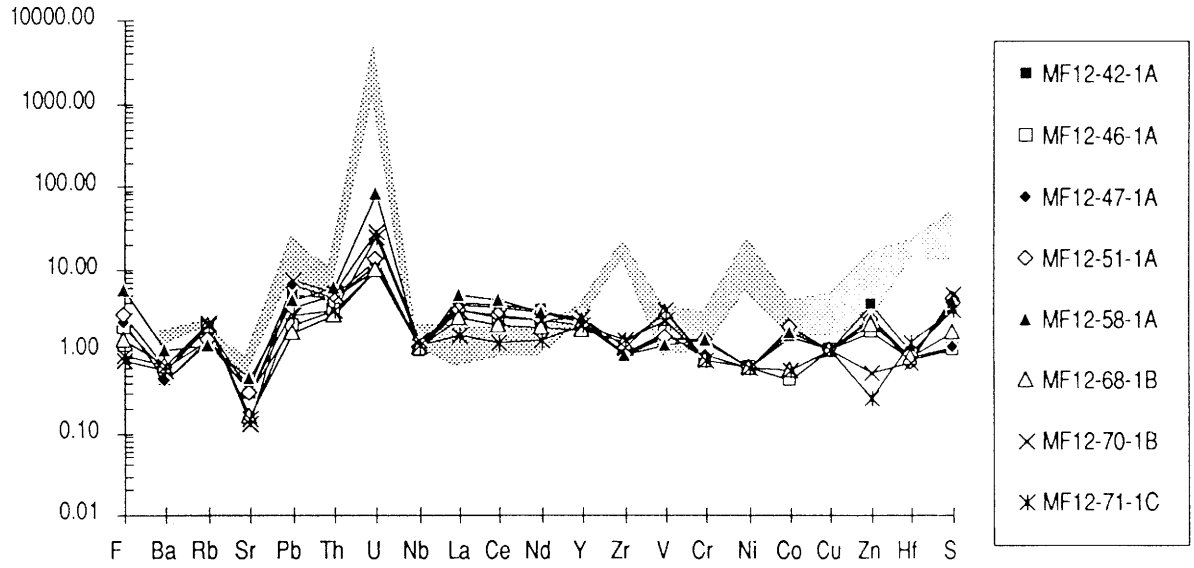

Figure 13. Borehole MF12: trace element content of the reduced hydrothermally altered phonolites in comparison with highly mineralized breccia samples from the Osamu Utsumi mine (shaded area, borehole F4, sample series 243; data from Waber et al., this report series; Rep. 2) normalized to the average of regional phonolites (data from Schorscher and Shea, this report series; Rep. 1).

Tephri-phonolite: samples 42-1A, 47-1A, 51-1A and 58-1A,
Leucocratic phonolite: samples 68-1B, 70-1B, 71-1C,
Phonolitic dyke: sample 46-1A.

In comparison with the highly mineralized volcanic breccia samples of the Osamu Utsumi mine, the Morro do Ferro country rocks are much poorer in U, Th, Pb, Nb, Zn, Ba and particularly in Y, Zr, Hf and S. When normalized to the unaltered regional rocks, however, the general distribution pattern is very similar, with the exception of higher LREEs but lower Y, Zr, Hf and S in the Morro do Ferro rocks (Fig. 13).

6.1.4.3. Oxidized zone

In the oxidized leucocratic phonolite the increase in the Al_2O_3 content and the decrease in the SiO_2 and K_2O contents, when compared to its reduced counterpart, reflect the decomposition of K-feldspars to clay minerals. MgO, CaO and Na_2O are also lower, whereas Fe_{tot}, crystalline water and CO_2 show increased values.

The mineralogical investigations have shown that the oxidized leucocratic phonolite is more strongly impregnated with highly birefringent cryptocrystalline phases than its reduced counterpart. It was assumed that the present oxidized phonolite was primarily more strongly mineralized than the leucocratic phonolite recovered from the bottom of the borehole. This is also reflected in the chemical trace element composition of the oxidized zone; for example, the LREEs show much higher absolute contents in the oxidized phonolite than in the reduced part (Table III). Similarly, F displays equal values in the oxidized and reduced leucocratic phonolites, although fluorite is no longer present in the oxidized part. This supports the above observation that fluorite is not the only F-bearing mineral, but that primary fluoro-carbonates must also be present. Furthermore, F might be retained by secondary minerals formed under oxidizing conditions.

Zn and S are the only elements that show the same drastic depletion due to the overall dissolution of the sulphides, as observed in the Osamu Utsumi mine. Sr, although depleted, is still fairly high in the oxidized phonolite and is partly retained in secondary mineral phases (goyazite). Both U and Th are more abundant in the oxidized phonolite than in both reduced phonolites. Again, this has to be explained by higher primary contents and additionally, for U, by the retention through absorption onto iron-oxyhydroxides. That multiple processes govern the distribution of U and Th in the oxidized phonolite is also supported by the natural decay series (see MacKenzie *et al.*, this report series; Rep. 7).

In comparison with the mean value for the oxidized leucocratic phonolites of the Osamu Utsumi mine, the oxidized phonolite of the MF12 borehole shows similar

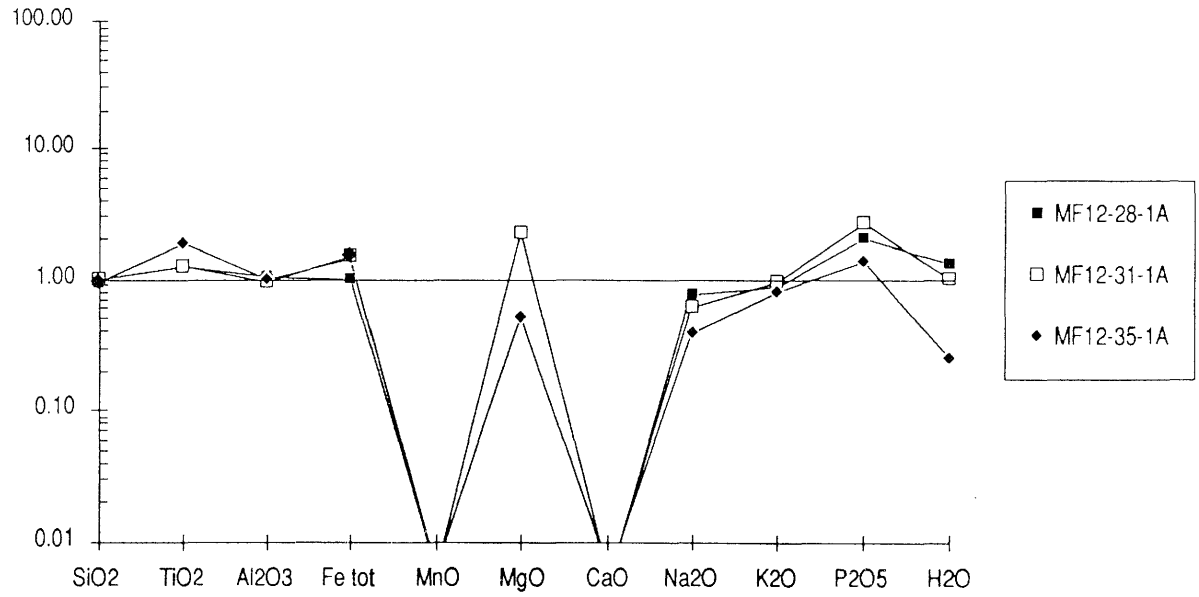

Figure 14. Borehole MF12: major element contents of the oxidized hydrothermally altered phonolites normalized to the average of the oxidized hydrothermally altered phonolites from the Osamu Utsumi mine (data from Waber et al., this report series; Rep. 2).

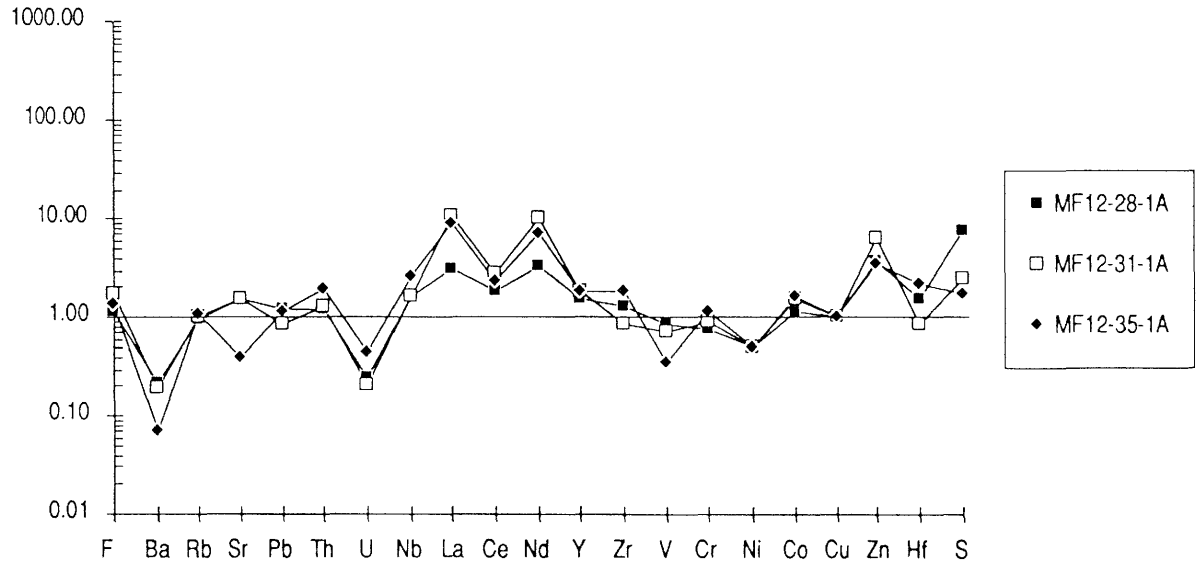

Figure 15. Borehole MF12: trace element contents of the oxidized hydrothermally altered phonolites normalized to the average of the oxidized hydrothermally altered phonolites from the Osamu Utsumi mine (data from Waber et al., this report series; Rep. 2).

abundances in the major elements, with the exception of Na_2O which is depleted and P_2O_5 which shows higher values (Fig. 14). The trace element composition exhibits similar trends as for the reduced rocks (Fig. 15); the LREEs, Y, Th, F, La and Zn are enriched in the leucocratic phonolite of Morro do Ferro compared to its counterpart from the Osamu Utsumi mine, whereas Ba, U and V display lower contents. During normalization, Ce depletion becomes evident in all the samples.

6.1.4.4. Rare-earth elements

Because the charge density ratios of light REEs closely resemble those of the trivalent transuranic elements Am and Cm, which by virtue of their relatively long radioactive half-lives and the decay characteristics of many of their isotopes are considered important for high-level waste safety assessments, mainly the light rare-earths (which include La, Ce, Pr, Nd and Sm) were studied. One sample from each reduced phonolite, two samples from the oxidized leucocratic phonolite, one sample from the transition zone of saprolite-oxidized phonolite and one laterite sample were analyzed for REEs by ICPOES. The results of this work are presented in McKenzie *et al.* (this report series; Rep. 7) and will be only briefly summarized here. The analyses of these samples are shown in Table IV and Figure 16 shows the LREE pattern normalized to ordinary

TABLE IV

Borehole MF12: LREE analyses (ppm) and chondrite normalized values of the different rock units.

Borehole	Rock-type	La	Ce	Pr	Nd	Sm
MF12-16-1A	laterite	7353	1878	1414	4551	1414
MF12-28-1A	oxid. leuc. phonolite	654	1040	76	258	76
MF12-31-1B	oxid. leuc. phonolite	2630	1453	261	736	261
MF12-35-1A	oxid. leuc. phonolite	2090	1318	168	495	158
MF12-37-1B	red. leuc. phonolite	1362	1639	118	328	118
MF12-58-1A	red. tephri-phonolite	987	1275	93	257	93
Chondrite normalized values		0.2974	0.7643	0.1129	0.5732	0.1864
MF12-16-1A	laterite	24724	2457	12524	7940	7586
MF12-28-1A	oxid. leuc. phonolite	2199	1361	673	450	408
MF12-31-1B	oxid. leuc. phonolite	8843	1901	2312	1284	1400
MF12-35-1A	oxid. leuc. phonolite	7028	1724	1488	864	848
MF12-37-1B	red. leuc. phonolite	4580	2144	1045	572	633
MF12-58-1A	red. tephri-phonolite	3319	1668	824	448	499

Analysis by ICPOES at New York University Medical Center, New York.

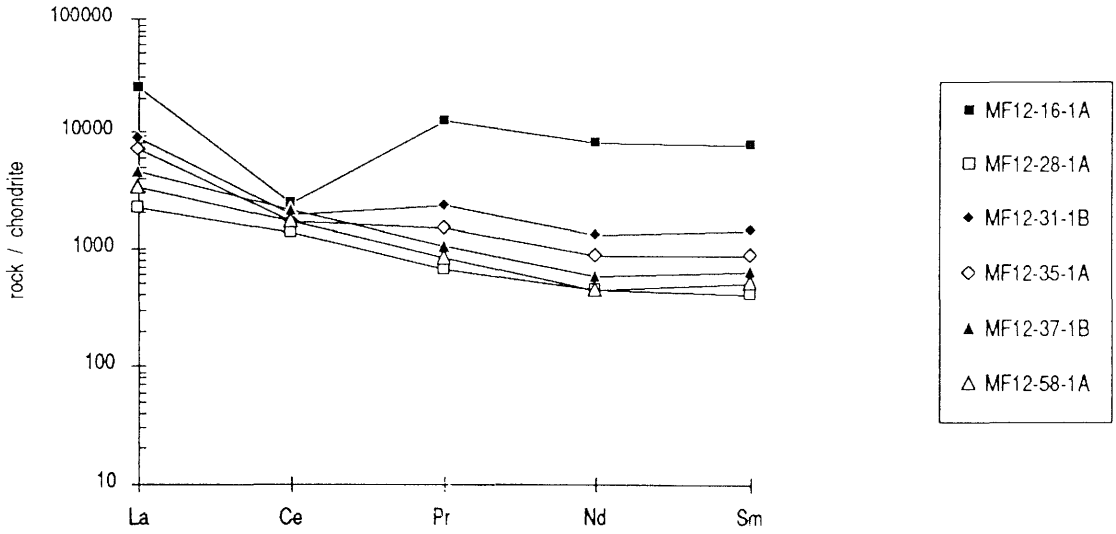

Figure 16. Borehole MF12: LREE normalized to ordinary chondrite (analysis by ICPOES; for normalization factors, see Table IV).

Laterite: sample 16-1A,
Oxidized leucocratic phonolite: samples 28-1A to 35-1A,
Reduced tephri-phonolite: sample 58-1A,
Reduced leucocratic phonolite: sample 37-1B.

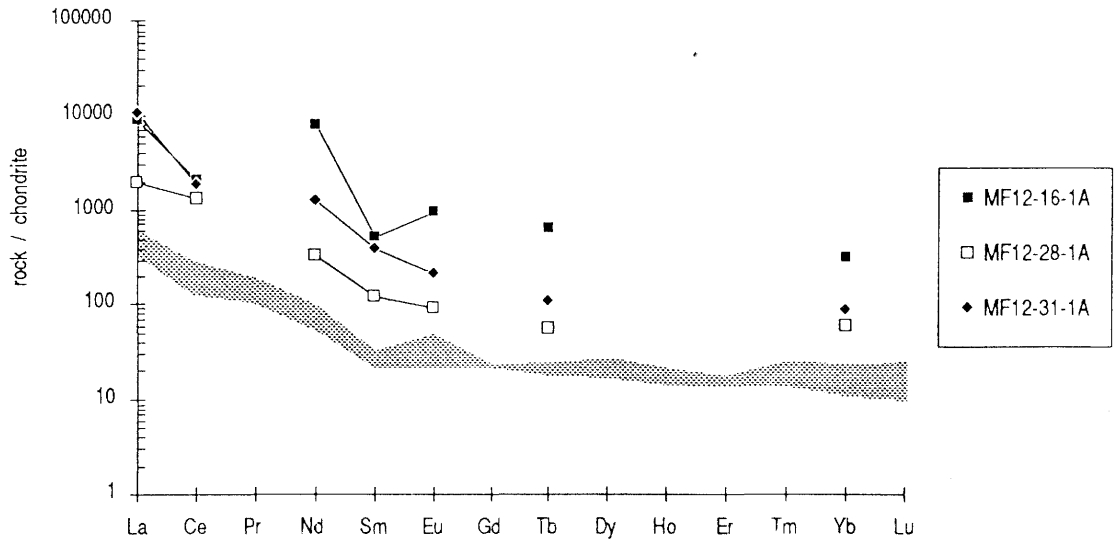

Figure 17. Borehole MF12: REE normalized to ordinary chondrite compared to oxidized, hydrothermally altered phonolites of the Osamu Utsumi mine (shaded area; data from Waber et al., this report series; Rep. 2; analysis by neutron activation and ICPOES; for normalization factors, see Table IV).

Laterite: sample 16-1A,
Oxidized leucocratic phonolite: samples 28-1A and 31-1A.

chondrite. The reduced phonolite samples MF12-37-1A and MF12-58-1A show very similar patterns, with the sample higher in U and Th (MF12-58-1A) displaying a slight tendency towards a positive Ce anomaly. The oxidized samples MF12-28-1A to MF12-35-1A display a modest negative Ce anomaly, with the exception of the sample from the transition zone laterite – oxidized phonolite (MF12-28-1A). This sample also displays the lowest absolute LREE contents. The lateritic sample MF12-16-1A, which is very high in absolute total REEs (Fig. 17), Th and U compared to the other laterite samples, displays a very strong negative Ce anomaly similar to that observed from the weathered carbonatitic host rock (section 7.1.3.3). The distinctly higher contents of REEs, Th and U can be explained by the fact that this sample is a former magnetite vein derived from the carbonatitic host rock.

In the reduced phonolites the LREEs, La, Ce and Nd exhibit a very good interelement correlation, best pronounced between La and Ce ($r = 0.99$; $n = 8$; XRF-data), followed by Ce and Nd ($r = 0.96$; $n = 8$) and finally La and Nd ($r = 0.96$; $n = 8$; Figs. 18a and b). This indicates mineralogical control of the LREEs by the same mineral phases. Certain affinities between LREEs and CO_2 ($r = 0.75$ to 0.82; $n = 8$) and Th ($r = 0.75$ to 0.77; $n = 8$; Fig. 18c) might further indicate the existence of LREE-carbonates (bastnaesite) and Th-LREE phases (cheralite).

In contrast, there is no longer any correlation between Ce, La and Nd in the weathering zone (Figs. 18a and b). La displays a good correlation with Nd ($r = 1$; $n = 5$) and with Y ($r = 0.95$; $n = 5$). Ce behaves completely different ($r_{La\text{-}Ce} = 0.44$, $r_{Nd\text{-}Ce} = 0.43$; $n = 8$) and correlates much better with the residually enriched Zr ($r = 0.96$; $n = 5$).

Compared to both the unaltered regional rocks (Schorscher and Shea, this report series; Rep. 1) and the hydrothermally altered leucocratic phonolites of the Osamu Utsumi mine (Waber *et al.*, this report series; Rep. 2), the Morro do Ferro country rocks generally display higher concentrations of LREEs and exhibit a less steep decline in LREEs from La to Sm. The chondrite normalized La : Sm ratio for the Morro do Ferro country rocks is 3 : 8, compared to 15 : 17 in the oxidized phonolites of the Osamu Utsumi mine.

In three samples (from the laterite and oxidized phonolite), Tb and Yb have also been analyzed by neutron activation (Fig. 17). The absolute abundance of these heavy rare-earth elements (HREEs) is much higher in the Morro do Ferro country rocks than in the oxidized phonolites of the Osamu Utsumi mine. The much stronger enrichment in LREEs compared to HREEs is observed in the chondrite normalized La : Yb ratio of 27 : 119 for the Morro do Ferro country rock as compared to 18 : 19 for the mine phonolites.

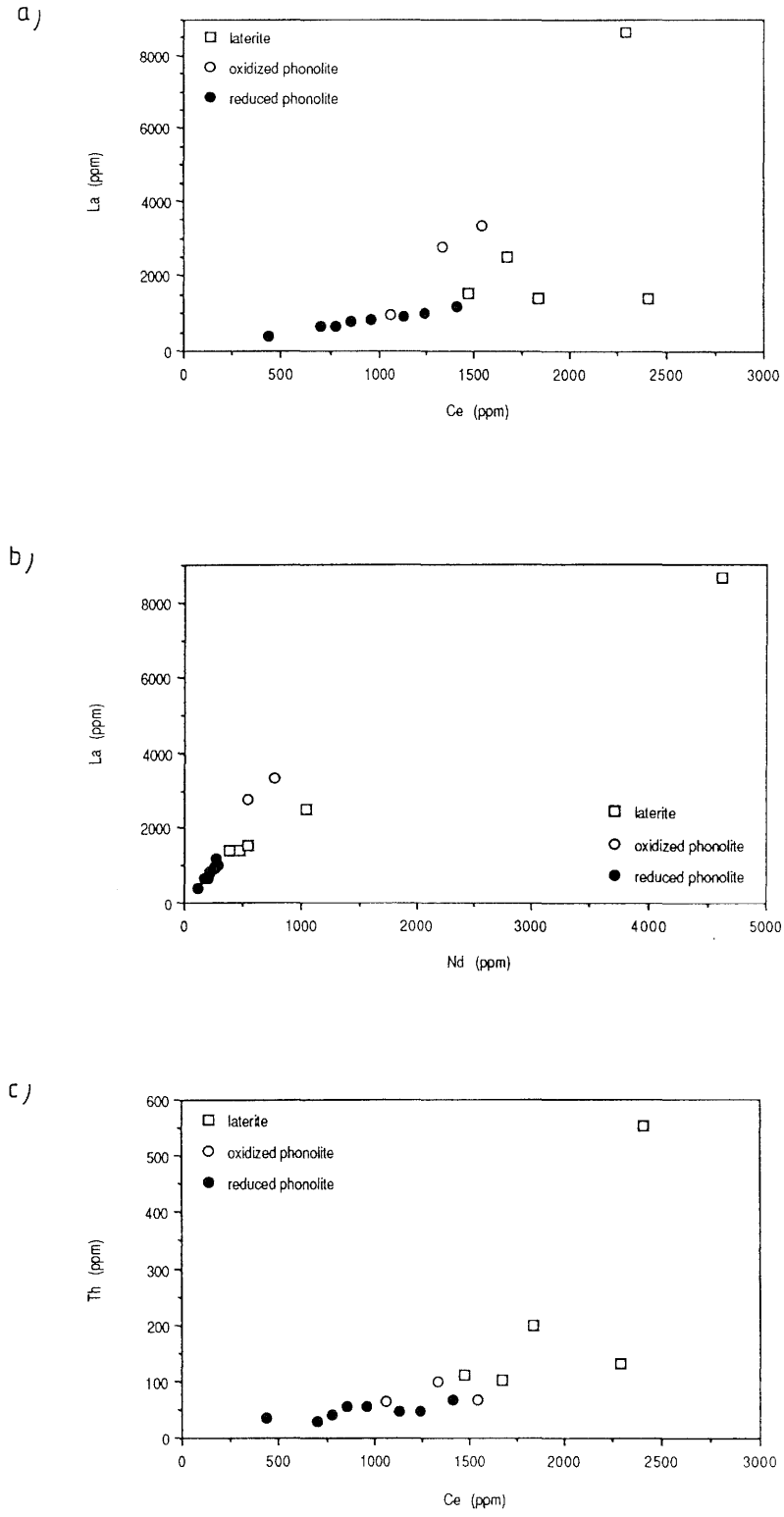

Figure 18. Borehole MF12: binary plot of:
a) lanthanum versus cerium,
b) lanthanum versus neodymium, and
c) thorium versus cerium,

for the different rock units (analysis by XRF).

In four samples of different grain size fractions, La, Ce, Sm, Eu, Tb and Yb were analyzed by the Inductively Coupled Plasma (ICP) method (M-T. Ménager, CEA, Paris; Table V). Unfortunately, whole-rock analyses performed with the same analytical method are not yet available. In the weathered cover, the total abundance of REEs is positively correlated with increasing grain size. The reduced phonolitic samples show exactly the opposite trend, with the tephri-phonolite (MF12-42-1A) displaying higher contents than the leucocratic phonolite (MF12-70-1B). This indicates the very fine-grained, disseminated nature of the REE impregnation during the hydrothermal alteration and the subsequent decomposition/recrystallization of these primary phases into secondary, coarser-grained REE minerals during weathering. Moreover, the HREEs show somewhat higher concentrations in the leucocratic phonolite. Both phonolites have less REEs when compared to the lateritic samples (MF12-11-1A, MF12-16-1A).

Summarizing, the phonolitic country rock of Morro do Ferro is enriched in REEs compared to regional rocks and the hydrothermally altered rocks of the Osamu Utsumi mine. The enrichment is stronger in the LREEs from La to Sm, compared with the few HREE data available. The LREEs display a positive correlation among each other in the reduced rock, but Ce behaves differently in the oxidized rock and the weathering zone due to the oxidation of trivalent Ce to the tetravalent, less soluble Ce^{4+}. Oxidized country rock is characterized by a moderate to strong negative Ce anomaly and by its higher REE concentrations when compared to the reduced country rock. In the weathered zone, REE concentration increases with increasing grain size, whereas in the reduced country rock the $<2\mu$ fraction displays the highest concentrations.

6.2. Lateritic weathering cover

6.2.1. Petrography

A lateritic weathering cover was encountered in the MF12 borehole down to a depth of 27.52 m. The transition between this and the massive oxidized country rock is sharp, to within a few centimetres.

The first 0.68 m of the core consists of friable brown soil material rich in organics. Further down, the core consists of yellowish-red clay/silt material with intercalated red-brown ferricretes in the first 5 m. Down to the weathering cover/country rock transition, the clay/silt material is predominantly yellowish-white in colour. At four locations, intercalated dark red-brown zones of several cm to dm in thickness occur

TABLE V

Borehole MF12: REE analysis of different grain size fractions in laterite and hydrothermally altered phonolitic rocks.

Sample	Rock type	Grain size fraction	La ppm	Ce ppm	Sm ppm	Eu ppm	Tb ppm	Yb ppm
MF12-11-1A	laterite	<2μ	1664	1521	49	12.9	3.91	29.5
MF12-11-1A	laterite	2–6.3μ	1098	1273	55.5	14.4	3.97	21.1
MF12-11-1A	laterite	6.3–20μ	2278	2187	126	30.9	8.01	25.9
MF12-11-1A	laterite	whole-rock (XRF)	2486	1673				
MF12-16-1A	laterite	<2μ	499	537	22.9	6.3	2.1	25.4
MF12-16-1A	laterite	2–6.3μ	7230	2107	520	113.1	18.5	34.8
MF12-16-1A	laterite	6.3–20μ	7976	2188	521	119.6	21.5	36.9
MF12-16-1A	laterite	whole-rock (XRF)	8649	2288				
MF12-42-1A	red. tephri-phon.	<2μ	1398	1937	5	13.4	3.66	9
MF12-42-1A	red. tephri-phon.	2–6.3μ	983	1455	38.25	10.3	3.07	9.6
MF12-42-1A	red. tephri-phon.	6.3–20μ	1004	1433	36.6	10.1	2.97	8.6
MF12-42-1A	red. tephri-phon.	whole-rock (XRF)	1017	1244				
MF12-70-1B	red. leuc. phon.	<2μ	978	1586	34	12.1	4.95	29.8
MF12-70-1B	red. leuc. phon.	2–6.3μ	747	1085	31	8.4	3.24	18.9
MF12-70-1B	red. leuc. phon.	6.3–20μ	851	1235	38	10.3	3.63	17.2
MF12-70-1B	red. leuc. phon.	whole-rock (XRF)	796	854				

Analysis of different grain size fractions by ICP; CEA, Fontenay-aux-Roses, France and whole-rock samples by XRF, University of Bern, Switzerland.

(15.9 m, 22.9 m, 24.8 m and 26.1 m). These zones all contain moderately to strongly oxidized magnetite nodules of several mm to cm in thickness, and represent relicts from the Morro do Ferro ore body. There is no doubt that these zones represent magnetite veins that had originally intruded the unweathered country rock.

Relict, dissolving K-feldspars already occur at a depth of 6 m, and it is not until around 24 m that a strong increase in K-feldspars occur. From there down to the oxidized phonolite, the original rock texture becomes more and more visible and, in the last metre before the transition, the original rock texture is fully preserved (saprolite).

6.2.1.1. Modal content

A qualitative compilation of the mineralogical composition in the weathering zone is given in Table I. The modal abundance of single minerals, as far as this can be defined, and the relative abundance of the clay minerals in the $<2\mu$ fraction are shown in Table II. Figure 6 shows the mineralogical variation with depth in the MF12 borehole. From this it becomes obvious that kaolinite is the most abundant mineral in the weathering zone. The kaolinite : illite ratio is about 9:1 in the first 6 m of the core, decreasing to 4:1 down to 24 m, and is close to 1:1 at the boundary between the weathered zone/oxidized country rock. Gibbsite is most abundant in the first 6 m of the core, reaching slightly more than 10% of the total laterite, and decreases to less than 2% content at 16 m. Assuming that the majority of the iron present is incorporated in Fe-oxyhydroxides, the abundance of these phases can be calculated from the chemical analyses. A high abundance of Fe-minerals (7 – 14%) is present in the first 6 m of the core, before decreasing down to a uniform 4%, with the exception of the thin ferricrete layers and magnetite veins where the Fe-minerals easily comprise 10 to 15% of the laterite. Down to 6 m no K-feldspars are present; down to 24 m their relict abundance constitute less than 10% of the laterite. A marked change occurs between 24 and 28 m, where the K-feldspar contents increase from about 30% to more than 60% of the rock.

6.2.1.2. Rock physical properties

The porosity of the weathered zone, which generally varies between 45–50%, is 10% more porous when compared to the oxidized phonolite sample most adjacent to the laterite junction, or more than 40% porous when compared to the reduced phonolitic

rocks (Fig. 7). This strong increase in porosity within the weathered zone reflects the dissolution of the more stable minerals, mainly K-feldspars. Bulk density decreases down to values below 1.5 g/cm^3, compared to an average of 2.4 g/cm^3 for the hydrothermally altered, reduced phonolites. Grain density displays similar values over the whole core, but increases in zones with accumulated Fe-oxides/hydroxides.

6.2.2. Mineralogy

The mineralogy of the lateritic weathering zones is dominated by very fine-grained minerals representing a $<2\mu$ grain size fraction. Coarser components ($>100\mu$) mainly include iron and manganese concretions (e.g. in the ferricretes or randomly distributed in the clay matrix), newly formed gibbsite, and relict preserved minerals of the hydrothermally altered phonolite such as kaolinite and illite. Hydrothermally produced illite and kaolinite are not expected to be stable in the upper horizons of the weathered cover. Their relict preservation in these horizons is discussed in more detail by Waber (1990). Secondary REE-Th phases formed by decomposition of the hydrothermal REE-Th minerals are always present in trace amounts, sometimes reaching minor contents in certain zones.

Kaolinite

Kaolinite is the most abundant silicate mineral phase formed during weathering. However, a quantification of the newly formed kaolinite is difficult due to the heterogeneous abundance of kaolinite in the hydrothermally altered rocks. A rough estimate indicates that the newly formed kaolinite represents about 70 to 80% of the total abundance. SEM investigations show that secondary weathering kaolinite tends to form more "sparry" aggregates with somewhat less well-defined crystals than in the bedrock. Densely packed kaolinite "booklets" typical for the hydrothermally altered country rock disappear completely in the uppermost 10 m of the profile. In a few samples from this zone, the transformation of kaolinite to gibbsite and, less frequently, to halloysite, occurs. In iron-rich layers kaolinite is often coated with a thin film of iron-hydroxides.

Illite/sericite

Relicts of illite/sericite are mainly preserved in nepheline pseudomorphs intimately intergrown with kaolinite. Only in samples most adjacent to the oxidized country rock (24 to 27 m below surface) does illite occur intimately intergrown with K-feldspars, suggesting growth at the expense of the latter. Further up the vertical profile, illite/sericite becomes altered to kaolinite and its content decreases drastically. Illite/smectite mixed-layers are no longer present in the weathering zone, and neither is chlorite.

Gibbsite

Gibbsite is present in samples down to 16 m below the surface. Its major abundance, however, is in the first 10 m of the core. Textural relationships point to gibbsite formation mainly from the alteration of kaolinite. Subordinate gibbsite forms at the expense of illite and, in some cases, of K-feldspars. An intimate intergrowth between gibbsite crystals and an amorphous gel material can be frequently observed, indicating its formation from amorphous Al-gel.

K-feldspar

K-feldspars are no longer stable under weathering conditions, although the coarser-grained varieties may be preserved in relicts up to 6 m below the surface. Textural relationships indicate a transformation of K-feldspars to kaolinite, illite and gibbsite. Crystallographically orientated etch pits on the surface clearly give evidence of the dissolution of K-feldspars.

Fe-oxides/hydroxides

In contrast to the oxidized country rocks, the Fe-hydroxides are no longer dispersed over the whole rock but tend to be much more concentrated in specific zones and layers (ferricretes). Amorphous to poorly crystalline Fe-hydroxides are the most abundant iron phases in the uppermost 6 m of the core; ferrihydrate, goethite and subordinate hematite are predominant further down the weathering profile. Textural relationships point to ageing of poorly defined Fe-hydroxides to goethite in zones that are no longer accessible to water due to mm-thick coatings of kaolinite. In such zones, goethite and hematite

pseudomorphs after pyrite may be observed. A few centimetres further into more porous conducting zones the dissolution of goethite and hematite may be observed.

In one particular sample from a former magnetite vein (MF12-16-1A), relict magnetite is preserved in the centre of originally cm-sized magnetite nodules.

Mn-oxyhydroxides such as pyrolusite and nsutite are often associated with Fe-hydroxides.

U-Th-REE phases

In common with the reduced country rock, all these minerals are difficult to identify, mainly due to their rather low abundance and their normally very small grain size. In the weathered zone, thin coatings of Fe-hydroxides cause additional problems.

No major U-bearing minerals could be identified; uranium probably occurs mainly incorporated in Th-minerals or adsorbed on Fe-hydroxides. Thorianite $(Th,U)O_2$ and thorogummite $ThAl_3(PO_4)_2(OH)_5$ were detected in several samples and are probably the most important Th-minerals of secondary origin. Relict zircon and bastnaesite $(Ce,Y,La)(F,CO_3)$, as potential Th- (and U-)bearing minerals, were sporadically observed.

Florencite $CeAl_3(PO_4)_2(OH)_6$ occurs in nearly all the investigated samples and is one of the most important Ce-minerals. Furthermore, cerianite $(Ce,Th)O_2$, crandallite group minerals (e.g. goyazite $Sr(REE)Al_3(PO_4)_2(OH)_5$), together with relict (?) monazite $Ce,La,Nd(PO_4)$ and bastnaesite, are the most important REE-bearing minerals.

Trace components

The most important trace components in the weathering zone are alunite and jarosite, both occurring sporadically in close association with Fe-hydroxides and in pyrite pseudomorphs.

6.2.3. Geochemistry

The geochemical variation for selected elements in the weathering zone down to the reduced country rock is shown in Figure 19; the geochemical analyses are given in Appendix 3.

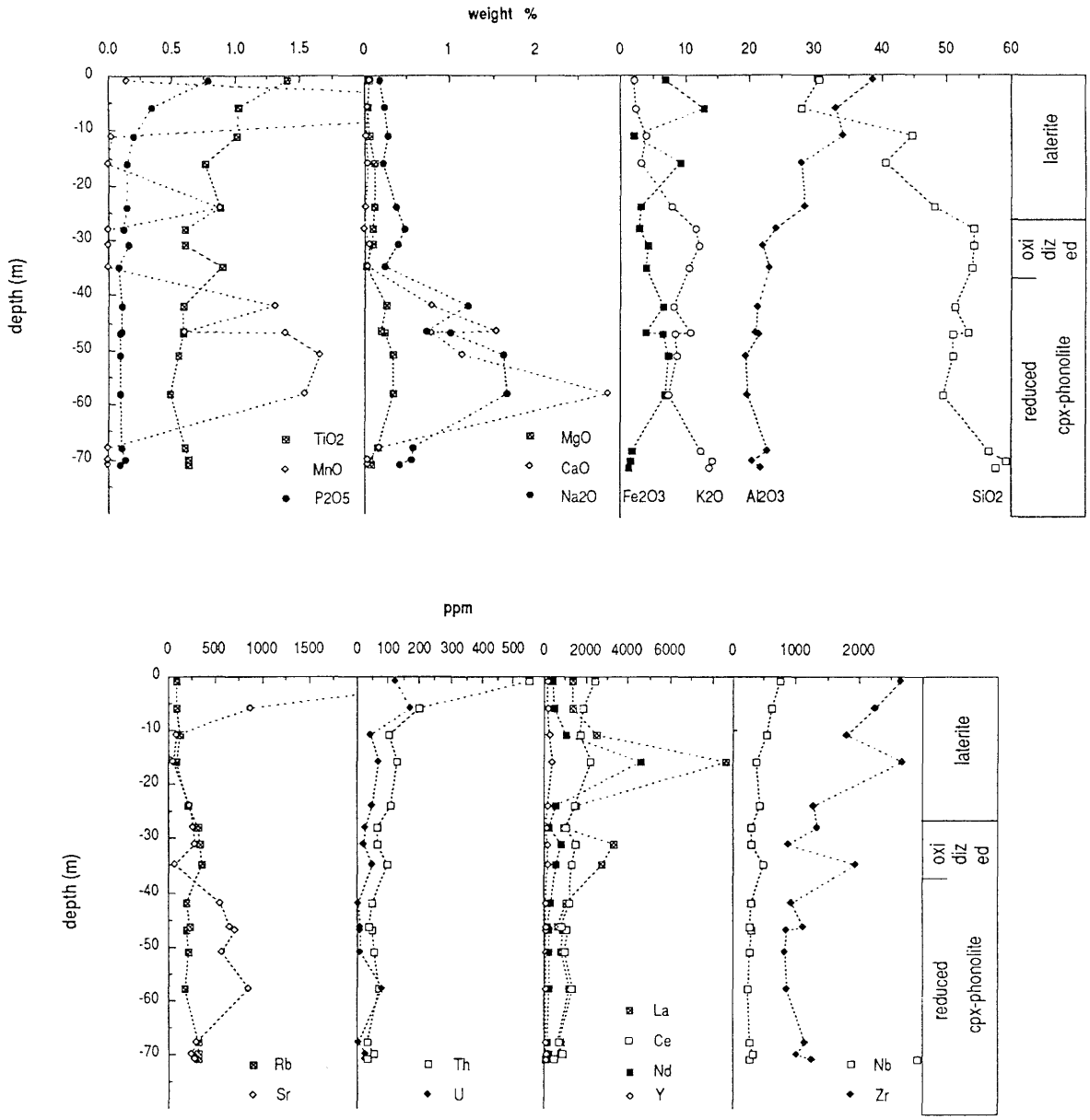

Figure 19. Borehole MF12: geochemical variation with depth for selected major and trace elements (analysis by XRF).

6.2.3.1. Major elements

Characteristic for the major element evolution in the vertical profile of the weathering zone is the controversial evolution of SiO_2 and Al_2O_3, the latter increasing towards the surface. K_2O and SiO_2 are strongly depleted towards the surface. This reflects the overall kaolinization and, in the uppermost part where the Al_2O_3 content becomes greater than the SiO_2 content, the formation of gibbsite. Fe_2O_3 shows an irregular distribution, as does MnO, in response to the concentration of Fe-hydroxides in certain zones. MgO, CaO and Na_2O are further depleted in the weathering zone, whereas TiO_2 and P_2O_5 display an increase towards the surface, reflecting a residual enrichment of refractory minerals.

6.2.3.2. Trace elements

Rb becomes depleted towards the surface and its excellent correlation with K_2O ($r = 0.98$, $n = 5$) shows that it is mainly incorporated in K-feldspars. Sr is depleted in the lower part of the weathering zone but shows a strong increase in the uppermost 6 m of the profile.

Similar trends can be seen with Pb and Th, both showing a close correlation with Sr ($r_{Sr\text{-}Pb} = 1$; $r_{Sr\text{-}Th} = 0.99$; $n = 5$) and P_2O_5 ($r_{P_2O_5\text{-}Pb} = 0.99$; $r_{P_2O_5\text{-}Th} = 0.98$; $n = 5$). All these features reflect the formation of secondary Sr-Pb-Th-phosphates of the crandallite group (goyazite, plumbogummite, thorogummite). V displays similar behaviour but is even better correlated with Nb and TiO_2, which are both residually enriched towards the surface. All these elements are mainly present in association with the hydrothermal alteration products of mafic minerals (leucoxene) which are more resistant to weathering.

Zr shows an irregular distribution with highest contents occurring in the weathered magnetite vein sample (MF12-16-1A). Towards the surface, Zr is residually enriched. It correlates closely with Hf and, surprisingly, with Ce ($r = 0.96$; $n = 5$). A possible explanation for this might be the residual enrichment of zircon and cerianite in the same horizons. U displays a very similar distribution over the weathering profile to Th, with the exception of the very first sample below the surface where U decreases. The average content of U is much higher in the weathering zone (average 92 ppm; $n = 5$) than in the oxidized (average 33 ppm; $n = 3$) and reduced country rock (average 15 ppm; $n = 8$). There are no well-established correlations between U and other elements in the weathering zone. The best affinity for U is shown by Fe_{tot} ($r = 0.85$; $n = 5$), Co ($r = 0.87$;

n = 5), Mn (r = 0.77; n = 5) and crystalline water (r = 0.86), indicating the absorption of U on Fe-hydroxides.

F, Ba and S are all depleted towards the surface, with Ba displaying the most heterogeneous distribution. High Ba concentrations occur in samples with elevated MnO contents and Ba is incorporated in the Mn-hydroxide psilomelane.

The behaviour of REEs in the weathering zone has already been described in section 6.1.4.4.

6.3. Fracture fillings

The entire country rock intercepted by borehole MF12 is intensely fractured. Two major fracture systems occur, one dipping 75–85° to the horizontal plane, the other with an inclination between 50–60° to the horizontal plane. No correlation could be established between inclination, relative age and infilling of the single fractures. All the investigated fractures are potentially water-bearing and their fillings are controlled by the present groundwater system. For this reason, one representative fracture has been selected from the most conductive zone of the MF12 borehole and has been systematically investigated in more detail (MF12-68-1A to C).

All the fractures are characterized by Fe-hydroxide coatings, often exhibiting rhythmic layering, and the investigated fracture fillings are dominated by clay minerals (Table VI). In the oxidized zone, kaolinite is by far the most dominant component. Gibbsite was detected in one of the fractures.

In the tephri-phonolite down to 68 m, illite and kaolinite are the predominant fillings, invariably accompanied by smectite; chlorite was detected in two fractures at a depth of about 50 m. Hydrothermal K-feldspar is sporadically present on fracture planes, usually displaying etch pits on the surface indicating dissolution. The first fluorite occurs only 2 m below the redox front where it exhibits idiomorphic crystals, slightly corroded at the surface, indicating the initiation of dissolution. Pyrite, though oxidized at its surface, was first detected at 47 m (about 12 m below the redox front). Pyrite totally devoid of surface oxidation does not occur until a depth of 65 m. Fe-hydroxides are observed in the core down to 62 m. Between 58 and 65 m there is a zone where abundant illite-smectite mixed-layers are present besides kaolinite, and where calcite also occurs.

In the fractures within the leucocratic phonolite, kaolinite is again the predominant filling below 68 m. Pyrite, here devoid of surface oxidation, fluorite and calcite are often present in such fractures. An open fracture (MF12-68-1A to C) from the conductive

TABLE VI

Borehole MF12: qualitative mineralogical composition of fracture fillings in the hydrothermally altered phonolites; sample numbers refer to depth in metres.

Sample	ill	kao	sme	chl	ML	gib	kf	flu	cc	py	HFO	rut
31-1A		XXX				X					X	
34-1A	X	XXX									X	
37-1A	XX	XX	X					XX			X	
42-1B	XX	X	XX	X			XX				X	
48-1B	XXX	X	X	X			X	X		X		
53-1A-1		XXX	X				XX			X	X	
53-1A-3	X	XXX	X					X		X		X
59-1A	XXX	XX	X		X					X		
62-1B-1	XXX	X	X		X						X	
62-1B-2		X			XXX		XX			XX		
65-1B		X			XXX			X	X	X		
68-1A-1		XXX			X			X	X			X
71-1A-1		XXX										
71-1A-2		XXX										
Conductive fracture MF12-68-1A:												
68-1A-A	XX	XX			X		XXX	XX		X		
68-1A-B	X	XX			X		XXX	X		X		
68-1A-C		X			XXX		X			(X)		

Abbreviations:

ill – illite
kao – kaolinite
sme – smectite
chl – chlorite
ML – ill/sme mixed-layers
gib – gibbsite
kf – K-feldspar
flu – fluorite
cc – calcite
py – pyrite
HFO – hydrous ferric oxides
rut – rutile

zone at a depth of 67.2 m was investigated in more detail in order to study the behaviour of the natural decay series. The selected fracture cuts the drillcore nearly vertically and is between 5 and 7 mm wide (Fig. 20). It is filled with clay minerals (mainly mixed-layers and kaolinite), pyrite, fluorite and K-feldspar by more than 80% (Table VI, subsample C). Pyrite is oxidized at its surface. Subsample B consists of the small leaching zone around the fracture and is characterized by its abundant K-feldspars and the lower amount of mixed-layers. Subsample A was taken 4 cm away from the fracture and mineralogically it resembles subsample B (Table VI). The geochemical composition of these samples is given in Table VII.

In contrast to the fracture fillings observed in the Osamu Utsumi mine (Waber *et al.*, this report series; Rep. 2), no uranium and thorium minerals were found on the fracture

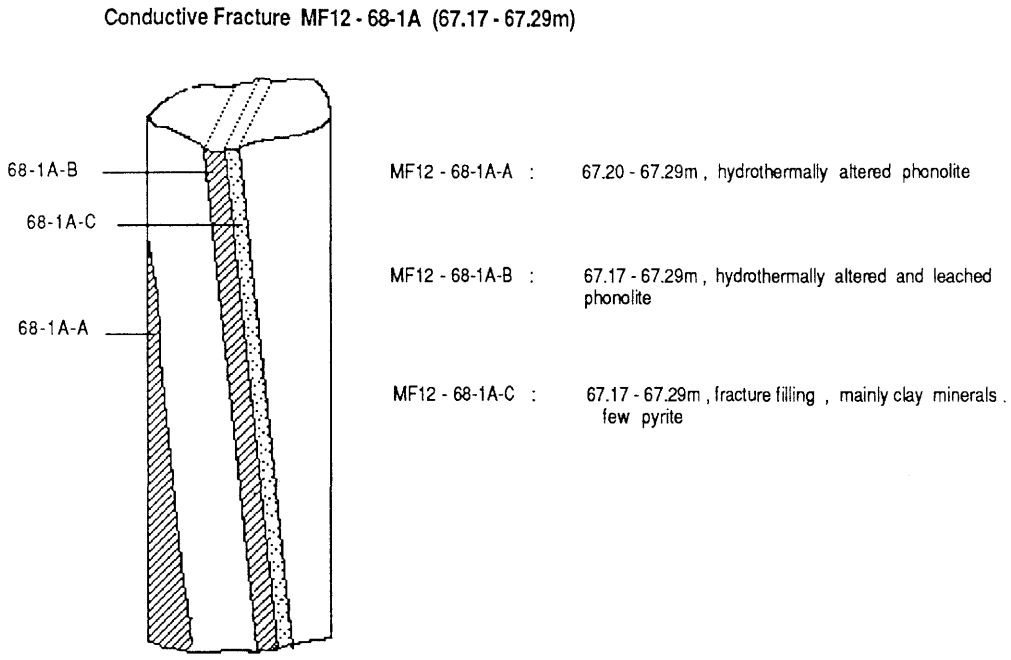

Figure 20. Borehole MF12: location of subsamples of the conductive fracture MF12-68-1A.

TABLE VII

Borehole MF12: chemical composition of three subsamples from the conductive fracture MF12-68-1A.

Sample		68-1A-A	68-1A-B	68-1A-C
Depth in metres		67.23	67.28	67.29
Rock type		Red. l ph	Red. l ph	Frac. fill.
SiO_2	wt.%	57.82	57.63	54.46
TiO_2		0.58	0.66	0.42
Al_2O_3		21.85	22.45	26.11
Fe_{tot}		2.06	2.56	4.11
MnO		0.00	0.02	0.12
MgO		0.15	0.21	0.39
CaO		0.35	0.58	1.88
Na_2O		0.42	0.36	0.43
K_2O		12.70	10.68	4.02
P_2O_5		0.12	0.06	0.03
LOI		2.98	3.95	8.17
Total	wt.%	99.03	99.16	100.14
F	ppm	2888	2549	n.a.
Ba		182	169	n.a.
Rb		315	235	n.a.
Sr		286	260	n.a.
Pb		16	17	n.a.
Th		25	40	n.a.
U		6	b.d.	n.a.
Nb		277	301	n.a.
La		697	358	n.a.
Ce		746	387	n.a.
Nd		208	112	n.a.
Y		82	83	n.a.
Zr		795	1307	n.a.
V		137	113	n.a.
Cr		b.d.	b.d.	n.a.
Ni		b.d.	b.d.	n.a.
Co		b.d.	b.d.	n.a.
Cu		b.d.	b.d.	n.a.
Zn		291	137	n.a.
Hf		9	14	n.a.
Sc		4	5	n.a.
S		5866	4380	n.a.

Rock type abbreviations:

Red. l ph = reduced leucocratic phonolite
Frac. fill. = fracture filling
LOI = Lost On Ignition
b.d. = below detection limit
n.a. = not analyzed
Total iron as Fe_2O_3

Analysis by XRF, University of Bern

planes in the Morro do Ferro country rock. Similarly, no potassium and/or iron sulphates, barite or alunite were observed.

In general, the observed fracture fillings are in very good agreement with the mineral stabilities calculated from the groundwater composition (see Nordstrom *et al.*, this report series; Rep. 14).

7. Supergene Th-REE mineralization

7.1. Host rock

The term "host rock" here applies to the completely weathered material below the Th-REE ore body of Morro do Ferro. Such host rock was encountered in all the boreholes drilled at Morro do Ferro and its lower boundary is still not clearly defined. In some respects the host rock resembles the weathering zone produced on top of the hydrothermally altered country rocks. There are, however, important differences in the mineralogical and geochemical composition that cannot be explained by weathering of the same parent rock. It is proposed that the original host rock at Morro do Ferro was a carbonatite, the weathering of which led to the present supergene Th-REE deposit. The existence of a primary carbonatitic host rock at Morro do Ferro is supported by:

a) the favourable geological environment of the Poços de Caldas plateau, consisting of a suite of more or less differentiated alkaline rocks (M. Ulbrich, 1983; H. Ulbrich, 1984; Schorscher and Shea, this report series; Rep. 1) which may often have associated carbonatites, for example as in other alkaline complexes in Brazil (Heinrich, 1966; H. Ulbrich and Gomes, 1981; Woolley, 1989 and literature cited therein);

b) the primary and secondary mineral paragenesis typical for unweathered and weathered carbonatites (Lottermoser, 1988; Eby, 1975; Reedman, 1984; Jaffe and Selchow, 1960, among others);

c) chemical mass balance calculations, that include chemical, physical and mechanical changes during weathering, from the estimated original overburden (Ulbrich, 1984) and the erosion rate (Holmes *et al.*, this report series; Rep. 5) reveal a geologically meaningful thickness only for rocks with average Th contents of more than 250 ppm (Waber, 1990). Such high Th contents are only reported from two chibinite samples (Rocha *et al.*, 1984; IPT-Report, 1984) and four volcanic breccia samples with vein

mineralizations from the Osamu Utsumi mine (Waber *et al.*, this report series; Rep. 2). Average values for these rocks are, however, much lower; carbonatites, especially ferro-carbonatites, may easily have had even higher Th concentrations (average 276 ppm; n=13; Woolley and Kempe, 1989);

d) the occurrence of magnetite veins; "Highly characteristic of nearly all carbonatites are accessory to locally essential amounts of magnetite. The magnetite tends to occur as disseminated euhedra, not uncommonly in flow bands" (Heinrich, 1966, p. 182). Magnetite ores are well known from many carbonatite occurrences, e.g. Ipanema and Jacupiranga, São Paulo, Brazil (Derby, 1981), Bukusu, Uganda (Taylor, 1955), Kaiserstuhl, Germany (van Wambeke *et al.*, 1964);

e) the much deeper weathering of the Morro do Ferro host rock compared to the surrounding hydrothermally altered country rocks; the susceptibility of a carbonatite to weathering is much greater than for the silicate country rocks due to the high carbonate content of the former. This subsequently led to its complete alteration and allowed the formation of the present supergene Th-REE mineralization;

f) the occurrence of secondary gypsum as fracture fillings in the hydrothermally altered rocks below the completely weathered host rock (Camargo dos Santos, 1984); gypsum was observed nowhere else and is thought to have been precipitated from waters dissolving calcite and sulphides from the original overburden;

g) the occurrence of ultramafic dykes at the Osamu Utsumi mine having carbonatitic affiliations (Waber *et al.*, this report series; Rep. 2).

7.1.1. Petrography

The non-mineralized, weathered carbonatitic host rock was encountered in borehole MF10 from 22 to 75 m, in MF11 from 20 to 40 m, and in MF13 from 5 to 60 m.

The weathered carbonatitic host rock is characterized by its very fine grain size, with 35–55% of the whole rock being less than 20μ. It is yellowish-brown to reddish-brown in colour, lighter than the material of the ore body but darker than the laterite overlying the country rock. A well developed horizontal layering is present throughout the host rock, which contrasts with the more sparry texture of the laterite.

Accumulations of partly to completely oxidized magnetite nodules occur randomly distributed in the host rock; these zones are always dark-brown in colour. Such magnetite layers range from less than a centimetre in width, with nodules of several millimetres in

diameter, to layers of several centimetres in width with cm-sized nodules. Nodules of manganese-oxides are always associated with the magnetite. Due to the large differences in density, the magnetite and manganese nodules "sink" into the underlying clay-silt material, distorting the horizontal layering.

7.1.1.2. Modal composition

A quantitative modal abundance of the minerals present is impossible to determine due to the very fine grain size of most of the host rock and the high variability of the mineralogical composition, including an abundance of normally very rare minerals. A qualitative compilation of the mineralogical composition of the host rock and the ore body (samples 1-1A to 19-1A) derived from XRD, microscopic and SEM investigations is given in Table VIII. The XRD results for different grain sizes (<2μ, 2–6.3μ, 6.3–20μ) are shown in Table IX.

7.1.1.3. Rock physical properties

The average porosity is the same for the host rock and the ore body (41%). The variation of porosity, bulk and grain density with depth in the MF10 borehole is shown in Figure 20. In the host rock, total porosity varies between approximately 37 to 48% of the rock volume, with a zone of somewhat lower porosity between 49 and 56 m, and then increased porosity again at the bottom of the borehole. In the ore body (down to 22 m; Fig. 21), the variation of porosity is greater by up to 20 to 52% of the rock volume.

The bulk density of the host rock is 15% higher compared to the laterite overlying the country rock, but only about 8% lower than that of the ore body. The variation with depth is much less in the host rock when compared to the ore body.

Grain density is about 15% higher in the ore body than in the host rock samples devoid of magnetite nodules. Compared to the laterite, the grain density is about 5% higher. The variation of grain density is high in both host rock and ore body and mainly reflects the abundance of magnetite nodules.

TABLE VIII

Borehole MF10: Qualitative mineralogical composition.

Sample description	Sample	ill/ser	kaol	Ratio ill/kaol	gibb	alun	jaro	flor	bast	mon	pych	cher	thor	ceria	thoria	lanth	hem	goe	HFO	MnOx	lipho
Homog. red-brown clay	1-1A	XXX	XXX	66/34	XX	X			XX					XX	XX		X		XX		
Homog. red-brown clay	1-1B	XX	X	80/20	XXX			X	XXX	X	X?	X	X	XX	XX	X	X	XX	XX		
Red-brown clay, magnetite	1-1C	XX	X	88/12	XXX	XX		X	XX	X	X	XX		X			X		XX	X	
Red+white clay, magnetite	3-1A	XX	XX	58/42	XXX	X			XX	X	X?						X	XX	X		XX
Red clay, magnetite	4-1A	X	XXX	25/75	XX	X	X	X	XX	X	X	X	XX	X			X	XX	XX	X	
White clay + HFO, red layers	6-1A	XX	XX	55/45	X		X	X	X			X		X	X	X		X	X	X	
Dark red clay, magnetite	10-1A	XX	X	84/16	XXX			X	XX	X		X					XX	X	XX		
Homog. white clay	12-1B	XX	XX	43/57	X	X	X		XX	X		XX	X			X	X	X	X		
White clay, red layers	18-1A	XXX	XXX	48/52	X				X	X	X?	XX	X	X	X		X	X	XX	X	
White+red clay, magnetite, HFO	19-1A	XX	X	62/38	XX	X			X	X		X	X				X	XX	X	X	
Light brown clay	25-1A	XX	X	86/14	X	XX		X	XX		X?	X		X	X		XX		X	X	
White clay, red layers	36-1A	XX	XXX	34/66	X	X			X	X						X		X	X	X	
White clay	49-1A-A	XXX	XXX	50/50	X				X	X								X			
Alteration zone around fracture	49-1A-B	XXX	XXX	55/45		X	X		X	X								X	X		
White clay, magnetite layer	54-1A	X	XXX	30/70	X			X			X?			X			X	X	X	X	
White+brown clay	56-1A	XX	XX	42/58	X	X		X	X							X	XX	XX	X	X	X
White clay, magnetite	64-1A	XXX	XXX	55/45		X		X	X	X						X		X	XX	X	
White clay with HFO	73-1A	XXX	XXX	44/56					X	X	X?	X				X			X		

Mineral occurrence: XXX – dominant; XX – major; X – minor

Abbreviation:

ill	– illite	bast	– bastnaesite	lanth	– Nd-lanthanite
ser	– sericite	mon	– monazite	hem	– hematite
kaol	– kaolinite	pych	– pyrochlore	goe	– goethite
gibb	– gibbsite	cher	– cheralite	HFO	– hydrous ferric oxides
alun	– alunite group	thor	– thorite	MnOx	– Mn-oxyhydroxides
jaro	– jarosite group	ceria	– cerianite	lipho	– lithiophorite
flor	– florencite	thoria	– thorianite		

Weight portion of the different grain size fractions (in g)

Sample	<2μ	2-6.3μ	6.3-20μ	>20μ	Total
4-1A	0.51	0.23	0.92	8.34	10.00
12-1B	0.05	0.25	5.27	4.42	10.00
18-1A	0.10	2.15	1.98	5.77	10.00
36-1A	0.15	1.82	2.86	5.17	10.00
49-1A-A	0.05	0.22	0.25	6.77	7.30
49-1A-B	0.07	2.72	2.54	4.68	10.00
64-1A	0.04	0.27	0.47	9.22	10.00
73-1A	0.20	3.06	0.22	6.52	10.00

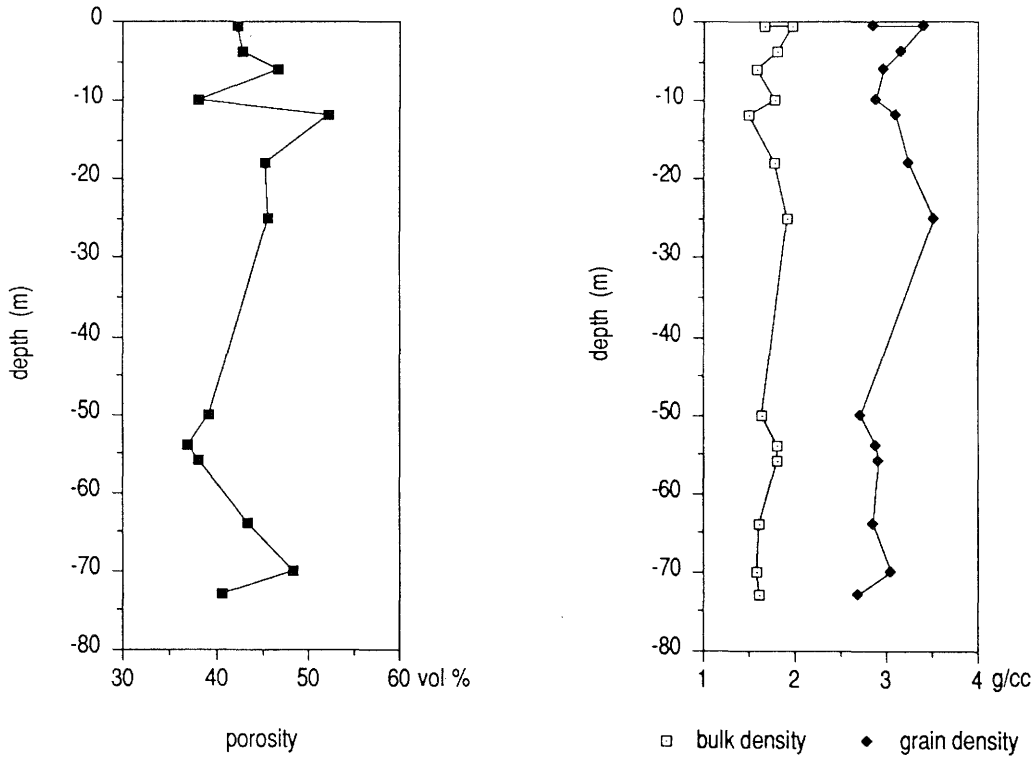

Figure 21. Borehole MF10: variation of porosity, bulk and grain density with depth.

TABLE IX

Borehole MF10: Qualitative mineralogical composition of different grain size fractions.

Fraction <2μ

Sample description	Sample	ill/ser	kaol	Ratio ill/kaol	gibb	alun	jaro	flor	bast	mon	pych	cher	thor	ceria	thoria	lanth	hem	goe	HFO	MnOx	liphy
Homog. red-brown clay	1-1A	XXX	XXX	66/34	XX	X			XX								X		XX		
Homog. red-brown clay	1-1B	X	X	80/20	XXX				XXX	X						X	X	XX	XX		
Red-brown clay, magnetite	1-1C	X	X	88/12	XXX			X	XX								X		XX	X	
Red+white clay, magnetite	3-1A	XX	XX	58/42	XXX	X			XX	X	X?						X	XX	X		XX
Red clay, magnetite	4-1A	X	XX	25/75	XX	X			XX								X	XX	X	X	
White clay+HFO, red layers	6-1A	XX	XX	55/45	X			X	X							X	X	XX	XX	X	
Dark red clay, magnetite	10-1A	XX	X	84/16	XXX			X	XX	X							XX	X			
Homog. white clay	12-1B	XX	XX	43/57	X	X			XX	X						X	X	X			
White clay, red layers	18-1A	XXX	XXX	48/52													X	X	X	X	
White+red clay, magnetite, HFO	19-1A	XX	X	62/38	XX	X			X	X				X	X		X	XX	X	X	
Light brown clay	25-1A	XX	X	86/14	X	XX			XX		X?						XX			X	
White clay, red layers	36-1A	XX	XXX	34/66	X	X			X									X	X	X	
White clay	49-1A-A	XXX	XXX	50/50	X					X								X	X		
Alteration zone around fracture	49-1A-B	XXX	XXX	55/45	X	X				X								X	X		
White clay, magnetite layer	54-1A	X	XXX	30/70	X						X?						X		X	X	
White+brown clay	56-1A	XX	XX	42/58	X	X		X	X							X	XX	XX	X	X	X
White clay, magnetite	64-1A	XXX	XXX	55/45		X			X	X						X		X	XX	X	
White clay with HFO	73-1A	XXX	XXX	44/56	X					X									XX		

Mineral occurrence: XXX – dominant XX – major X – minor

Abbreviation:

ill – illite
ser – sericite
kaol – kaolinite
gibb – gibbsite
alun – alunite group
jaro – jarosite group
flor – florencite
bast – bastnaesite
mon – monazite
pych – pyrochlore
cher – cheralite
thor – thorite
ceria – cerianite
thoria – thorianite
lanth – Nd-lanthanite
hem – hematite
goe – goethite
HFO – hydrous ferric oxides
MnOx – Mn-oxyhydroxides
liphy – lithiophyllite

TABLE IX (contd.)
Borehole MF10: Qualitative mineralogical composition of different grain size fractions.

Fraction 2-6.3μ

Sample description	Sample	ill/ser	kaol	Ratio ill/kaol	gibb	alun	jaro	flor	bast	mon	pych	cher	thor	ceria	thoria	lanth	hem	goe	HFO	MnOx	liphy
Homog. red-brown clay	1-1A																				
Homog. red-brown clay	1-1B																	XX			
Red-brown clay, magnetite	1-1C																				
Red+white clay, magnetite	3-1A																				
Red clay, magnetite	4-1A	XX	XX	50/50	XXX				XX									XX	X	X	
White clay+HFO, red layers	6-1A																				
Dark red clay, magnetite	10-1A																				
Homog. white clay	12-1B	XXX	XXX	40/60					XX	X								X			
White clay, red layers	18-1A	XXX	XXX	33/67																X	
White+red clay, magnetite, HFO	19-1A																				
Light brown clay	25-1A																				
White clay, red layers	36-1A	XX	XXX	25/75					X		X?					X	X	X			
White clay	49-1A-A	XXX	XXX	50/50					X	X							X	X			
Alteration zone around fracture	49-1A-B	XXX	XXX	45/55					X	X							X	X			
White clay, magnetite layer	54-1A																				
White+brown clay	56-1A																				
White clay, magnetite	64-1A	XXX	XXX	50/50						X						X	X	X			X
White clay with HFO	73-1A	XXX	XXX	50/50					X	X							X	X	X		

Mineral occurrence: XXX – dominant; XX – major; X – minor

Abbreviation:

ill	–	illite	cher	–	cheralite
ser	–	sericite	thor	–	thorite
kaol	–	kaolinite	ceria	–	cerianite
gibb	–	gibbsite	thoria	–	thorianite
alun	–	alunite group	lanth	–	Nd-lanthanite
jaro	–	jarosite group	hem	–	hematite
flor	–	florencite	goe	–	goethite
bast	–	bastnaesite	HFO	–	hydrous ferric oxides
mon	–	monazite	MnOx	–	Mn-oxyhydroxides
pych	–	pyrochlore	liphy	–	lithiophyllite

TABLE IX (contd.)

Borehole MF10: Qualitative mineralogical composition of different grain size fractions.

Fraction 6.3-20$_\mu$

Sample description	Sample	ill/ser	kaol	Ratio ill/kaol	gibb	alun	jaro	flor	bast	mon	pych	cher	thor	ceria	thoria	lanth	hem	goe	HFO	MnOx	liphy
Homog. red-brown clay	1-1A																				
Homog. red-brown clay	1-1B																				
Red-brown clay, magnetite	1-1C	XXX	X	97/3	XXX	XX		X	XX		X	X	X	X	X		XX	XX			
Red+white clay, magnetite	3-1A																				
Red clay, magnetite	4-1A	XX	XX	68/32	XXX	X	X	X	X	X				X			XX	X	X	X	
White clay+HFO, red layers	6-1A	XXX	XXX	65/45	XX	X	X					X			X	X	XX	XX			
Dark red clay, magnetite	10-1A	XXX	XX	75/25	XX							X		X			X	XX	X		
Homog. white clay	12-1B	XXX	XXX	28/72	X	XX	X		XX		X?					X	X	X			
White clay, red layers	18-1A	XXX	XXX	50/50	X				X	X	X?			X			X	X			X
White+red clay, magnetite, HFO	19-1A																				
Light brown clay	25-1A	XXX	XX	78/22	XX			X				X		X	X		XX	X			
White clay, red layers	36-1A	XX	XXX	43/57					XX	X						X	X	X			
White clay	49-1A-A	XXX	XXX	60/40					X								X	X			
Alteration zone around fracture	49-1A-B	XXX	XXX	60/40					XX								X	X			
White clay, magnetite layer	54-1A	XXX	XXX	60/40		X		X			X?			X			X	XX			
White+brown clay	56-1A																				
White clay, magnetite	64-1A	XXX	XXX	53/47					X		X?					X	X	X			X
White clay with HFO	73-1A	XXX	XXX	50/50					XX		X?					X	X	XX	X		

Mineral occurrence: XXX – dominant XX – major X – minor

Abbreviation:

ill	–	illite	cher	–	cheralite
ser	–	sericite	thor	–	thorite
kaol	–	kaolinite	ceria	–	cerianite
gibb	–	gibbsite	thoria	–	thorianite
alun	–	alunite group	lanth	–	Nd-lanthanite
jaro	–	jarosite group	hem	–	hematite
flor	–	florencite	goe	–	goethite
bast	–	bastnaesite	HFO	–	hydrous ferric oxides
mon	–	monazite	MnOx	–	Mn-oxyhydroxides
pych	–	pyrochlore	liphy	–	lithiophyllite

7.1.2. Mineralogy

The mineralogical composition of the host rock major components is rather simple, contrasting with the extremely complicated and variable distribution of its minor and trace components. The small grain sizes and the strong iron-oxyhydroxide staining further complicate the mineralogical and mineral-chemical analytical work.

Kaolinite and illite/sericite

Together with the Fe-oxyhydroxides, kaolinite and illite/sericite are by far the most abundant minerals in the host rock, occurring in nearly equal amounts over the whole MF10 profile (average illite:kaolinite ratio 49:51; $<2\mu$ fraction). In the presence of partly oxidized magnetite nodules, kaolinite is more abundant than illite. Otherwise, there exists no obvious relationship between the amount of kaolinite and illite/sericite and any other mineral or textural feature of the host rock. With few exceptions, kaolinite and illite are always coated with a thin film of iron-oxyhydroxides.

Fe-oxides/hydroxides

Among the iron-oxides and -hydroxides, the whole range from magnetite, hematite, goethite, lepidocrocite and ferryhydrite to amorphous iron gel occurs in the host rock. They are all very heterogeneously distributed and may even be absent in certain zones, whilst being the predominant minerals only a few centimetres away. Goethite, ferrihydrite and amorphous iron gel are the most abundant among these minerals; lepidocrocite only occurs in trace amounts in the $<2\mu$ fraction.

Primary magnetite is restricted to certain zones where it is partly preserved. It is always strongly oxidized to hematite, goethite and low crystalline Fe-hydroxides (from core to rim), displaying dissolution. Magnetite is preserved as central relicts only in nodules with a diameter greater than approx. 1 cm. An intimate intergrowth with rhythmically layered Mn-hydroxides precipitated under weathering conditions is often observed in the oxidized part of magnetite nodules. Inclusions in magnetite are abundant and mainly consist of Th-REE phases. Bastnaesite (up to 0.2mm), cheralite, monazite, thorite, zircon and pyrochlore occur as more or less idiomorphic inclusions, with bastnaesite, monazite and zircon being the most coarse-grained. All these inclusions are considered to be of primary origin.

Hematite is far less abundant than the iron-hydroxides and forms through oxidation of magnetite which it replaces pseudomorphically. However, it only seems to be stable in certain zones where it is isolated from water. In such zones, it may also be formed by in situ dehydration of iron-hydroxides.

Goethite and ferrihydrite are the most abundant iron phases in the host rock and they are often in very close association with amorphous or lower crystalline iron-hydroxides. They always constitute the outermost rim around magnetite nodules, occur as concretions in open pore spaces, and are also finely disseminated throughout the host rock. Textural relationships suggest, on the one hand, the formation of goethite and ferrihydrite from low crystalline phases and, on the other hand, alteration to such phases, often only a few centimetres apart, most probably related to fluctuations in the water input (dry – wet season changes).

Amorphous iron gel may partly form large nodules (0.5 cm), often in close association with amorphous Al-gel.

The crystalline to amorphous iron-hydroxides display a very complex behaviour of formation, dissolution and recrystallization, all changing over very short distances. Such behaviour is well known from laterites all over the world and the processes taking place are still not fully understood (Boulangé, 1984; Tardy and Nahon, 1985; Schwertmann, 1985; Muller, 1988; Boudeulle and Muller, 1988).

Mn-oxides/hydroxides

Nodules of cryptomelane ($K_xMn^{4+}_{8-x}Mn^{3+}_xO_{16}$) are always associated with magnetite nodules but are much less abundant; sporadically, psilomelane ($Ba_xMn^{4+}_{8-x}Mn^{3+}_xO_{16}$) occurs. Cryptomelane is often rimmed by Mn-hydroxides such as nsutite ($Mn_{1-y}^{4+}Mn_y^{3+}O_{2-y}(OH)_y$) and birnessite ($Mn_5^{4+}Mn_2^{3+}O_{13} \cdot 5H_2O$) and pyrolusite ($Mn^{4+}O_2$). The manganese-oxides /hydroxides display a similar complex behaviour to the iron phases. Similar inclusions to those found in magnetite could not be observed in cryptomelane, although idiomorphic florencite, thorianite and cerianite do occur. Lithiophorite ($(Al_2Mn_3^{4+}O_9) \cdot H_2O$) and lithiophyllite ($(Li,Mn)(PO_4)$) occur in trace amounts.

Gibbsite and amorphous Al-hydroxides

Gibbsite occurs throughout the host rock mainly in the $<2\mu$ fraction. It is often found as pore infillings and is normally coated with iron-hydroxides; coarser-grained gibbsite is sporadically present and somewhat more abundant in the upper part of the host rock.

Low crystalline Al-hydroxides and amorphous Al-phases are frequently distributed throughout the host rock. In several places, the formation of gibbsite from Al-gels has been observed.

Alunite and jarosite

Alunite $[(K,Na)Al_3(SO_4)(OH)_6]$ and jarosite $[(K,Na)Fe_3(SO_4)(OH)_6]$ both occur throughout the host rock, with alunite being somewhat more abundant. Both these minerals are indicators of a highly acid environment and may have formed through oxidation of primary sulphides, e.g. pyrite.

Th-REE minerals

A large variety of Th-REE minerals have been detected in the host rock and the list given in section 7.2.2. is probably far from being complete. Nevertheless, the most abundant are included. Difficulties arise when distinguishing between minerals of primary (magmatic or hydrothermal) and secondary origin. Because most of these minerals are still poorly or not at all defined with respect to their thermodynamic stability, textural relationships are virtually the only indications to go by (and these are often poorly developed). The only indicator of value is the occurrence of a mineral as inclusions in the unoxidized magnetite. However, several of the minerals occur as idiomorphic inclusions in the hematite rim of magnetite nodules (e.g. florencite), and as different shapes in the matrix compared to the inclusions (e.g. monazite). Such minerals are difficult to define as primary or secondary in origin and might even represent both types, as in the case of monazite. Among the primary Th-REE minerals, bastnaesite is by far the most abundant in the host rock, followed by monazite. Both these minerals occur in all the different grain size fractions (Table VIII). Cheralite and zircon occur in minor amounts in the $>6.3\mu$ fraction in samples with abundant magnetite nodules (e.g. samples MF10-54-1A, MF10-64-1A, MF10-73-1A). Similarly, relicts of pyrochlore were detected in the same samples; their existence, however, requires further confirmation.

Barretto and Fujimori (1986) reported the same primary Th-REE minerals (monazite, cheralite, pyrochlore, zircon) from a deep-seated, hydrothermally altered potassic rock (most probably the sample came from the 463 m-deep borehole drilled by Urânio do Brasil; see section 2.), where they occur together with magnetite, pyrite and rutile or anatase. Similar parageneses are found as vein infillings in the phonolitic country rocks in the MF12 borehole (section 6.1.2.2.).

To the author's knowledge, it is the first time that the crandallite group minerals florencite, gorceixite and goyazite, secondary monazite and the REE-carbonate Nd-lanthanite have been detected in the Morro do Ferro host rock and ore body. Abundant tiny euhedral crystals of Nd-lanthanite occur as infillings in open pore spaces and are certainly of secondary origin. All the investigated Nd-lanthanites are free of Ce and the formation of these minerals might therefore help to explain the negative Ce anomalies observed in most of the host rock samples (see section 7.1.3.3).

Secondary Th-REE minerals are more abundant in the host rock than in the ore body, especially the hydroxyphosphates of the crandallite group (florencite, gorceixite, goyazite) and Nd-lanthanite. Oxidic secondary minerals like cerianite and thorianite sporadically occur in the uppermost part of the host rock and in samples containing abundant magnetite.

7.1.3. Geochemistry

The geochemical variation with depth along borehole MF10, which penetrates through the ore body and down into the weathered host rock, is shown in Figure 22 for selected elements. The geochemical analyses, carried out by routine XRF for the single samples, are given in Appendix 2. The very high contents of Th, total REEs and total iron result in high mass absorption and therefore the standard correction procedures are no longer applicable for such extreme rock compositions. This in turn produces less accurate values for the light major elements evidenced by the low totals of the major element sums. Trace element compositions are, however, in fair agreement with results obtained by ICPOES (LREE) and alpha-spectrometry (U, Th).

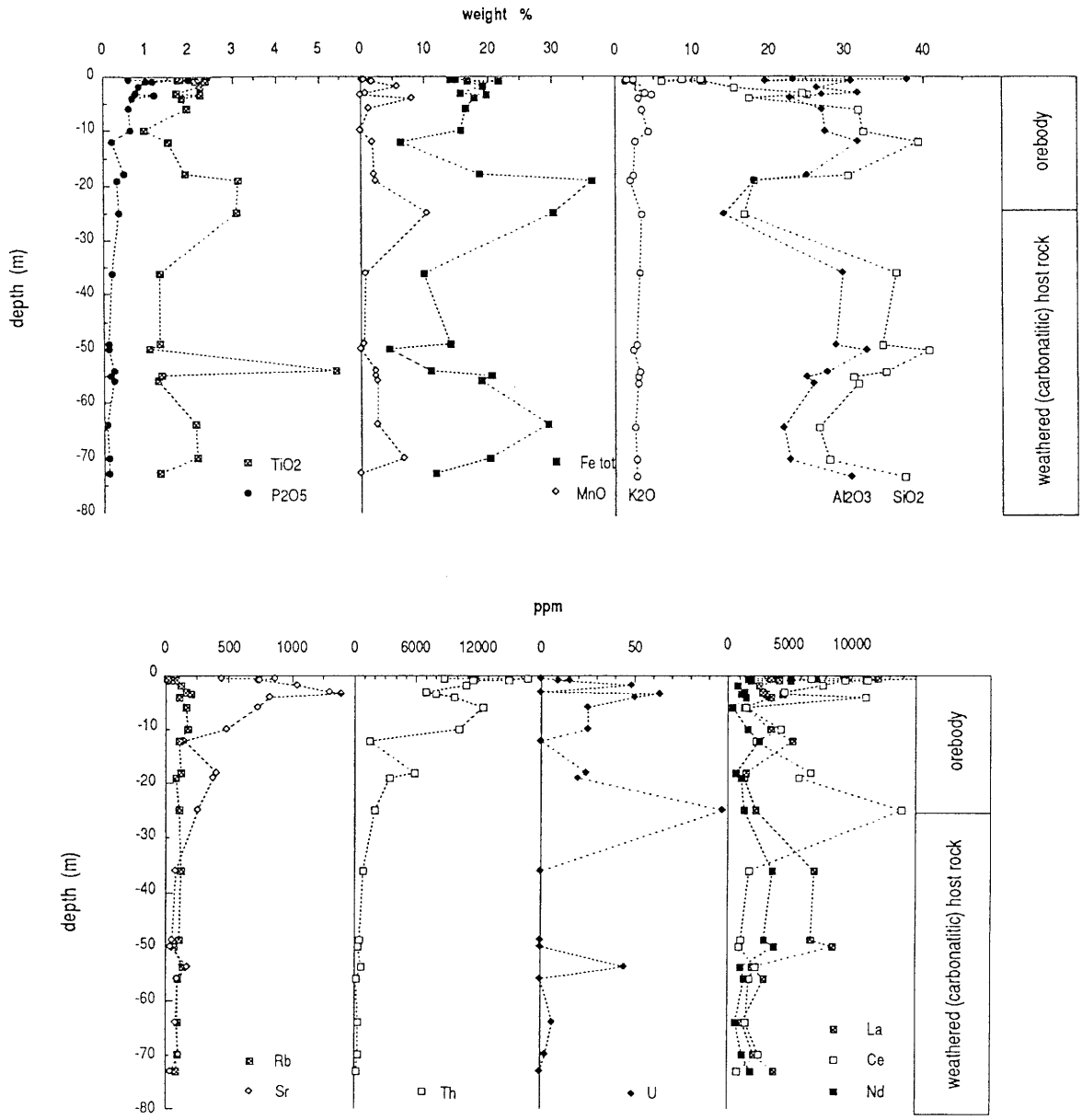

Figure 22. Borehole MF10: geochemical variation with depth for selected major and trace elements (analysis by XRF).

7.1.3.1. Major elements

The most striking feature in the major element composition of the host rock is the extremely good correlation between SiO_2 and Al_2O_3 (r = 1.0) over the whole profile, whereas K_2O remains almost stable over the same distance (Fig. 22). This is in strong contrast to all the investigated weathering profiles overlying the hydrothermally altered rocks (cf. Fig. 19, Figs. 42–45 in Waber *et al.*, this report series; Rep. 2).

Fe_{tot}, MnO and TiO_2 display a rather heterogeneous distribution, reflecting the alternating occurrence of ferrricretes and magnetite veins, both of which are much higher in their average contents in the host rock as compared to the other weathering profiles. Fe_{tot} is normally three times higher, and MnO and TiO_2 more than two times higher, in the host rock than in the weathered zone overlying the MF12 phonolites (Table III). Only a very weak correlation is observed between Fe_{tot} and MnO (r = 0.75); TiO_2 shows a completely different distribution.

MgO, CaO and Na_2O are all present in very low concentrations similar to those found in the weathering zone (Table III; Appendix 3).

7.1.3.2. Trace elements

One of the major characteristics of the trace element composition in the host rock are the higher concentrations of Th, REE, Nb, V, Cr, Co and Zn, when compared to the weathered zone of the country rock. On the other hand, Sr, Pb and U concentrations are all slightly decreased (Fig. 22; Appendix 3). Th displays a rather homogeneous distribution in the lowest 20 m of the core, varying between 160 and 290 ppm. Further up towards the ore body, the concentration generally increases and strong variations in Th content occur. The highest concentrations are always found in samples associated with magnetite veins. The average concentration of Th in the host rock is 408 ppm (XRF data; n = 8) and 487 ppm (ICP data; n = 7), respectively. Th is fairly well correlated with Ce (r = 0.92; n = 8), supporting the presence of Th-Ce minerals. Moreover, Th is correlated with Sr (r = 0.94; n = 8) and U (r = 0.90; n = 8).

Nb is increased by a factor of 2 – 6 in the host rock compared to the weathered zone of the country rock. Nb correlates closely with TiO_2 (r = 0.95; n = 8), Zr (r = 0.98; n = 8) and Hf (r = 0.93; n = 8). Highest Nb contents are recorded in samples with abundant magnetite. The same applies for V which can be enriched by a factor of 6 in such samples compared to the country rock weathering zone. In magnetite-free samples, the contents are enriched by a factor of about 1.5 to 2 (300 ppm). A certain relationship between V

and TiO_2 (r = 0.82; n = 8), MnO (r = 0.80; n = 8), Sr (r = 0.86; n = 8) and U (r = 0.81; n = 8) seems to exist.

Cr and Co contents are both considerably higher in the host rock than in the country rock weathering zone. Whereas Co is mainly bound in magnetite-rich samples, Cr contents are increased in all samples.

U displays a similar distribution to Th. The concentrations are comparatively low, around the detection limit, with the exception of a magnetite-rich sample where U reaches 45 ppm (Fig. 22).

Sr and Pb occur in concentrations similar to those in the lower part of the country rock weathering zone. They both show only minor variation with depth, Sr tending to be enhanced in samples with abundant magnetite. Sr is best correlated with P_2O_5 (r = 0.86; n = 8) and Ba (r = 0.86; n = 8), indicating the presence of goyazite. For Pb no such relationship has been observed.

7.1.3.3. Rare-earth elements

Similarily to Th, the light rare-earth (LREE) contents are at their lowest within the last 20 m of the core, occurring in concentrations comparable to those in the weathered zone of the phonolites (borehole MF12). However, further up in the remaining 30 m of the host rock, La and Nd are strongly increased (by a factor 3 to 4 and 2 to 3, respectively), whereas Ce displays a decrease in some samples and an increase in others. In Figure 23, the LREEs from La to Sm analyzed by ICPOES (MacKenzie *et al.*, this report series; Rep. 7) are normalized to chondrite. Four samples show a pronounced negative Ce anomaly, one sample has a moderate negative Ce anomaly (MF10-56-1A) and two samples (MF10-64-1A, MF10-70-1A) do not display any anomaly. Samples with a negative Ce anomaly also have higher total abundances of all the LREEs other than Ce, but lower Ce contents if compared to the samples without any Ce anomaly. The different behaviour of Ce compared to the other LREEs is also expressed in the excellent correlation of Ce with Ba (r = 0.96; n = 8; XRF data), F (r = 0.93; n = 8), U and Th (for both r = 0.92; n = 8), Cr (r = 0.96; n = 8) and the fairly good correlation with Sr (r = 0.87; n = 8), MnO (r = 0.87; n = 8) and P_2O_5 (r = 0.81; n = 8). In contrast, La and Nd correlate perfectly with one other (r = 0.99; n = 8) and display a rather good correlation with Y (r = 0.85 and r = 0.90, respectively; n = 8).

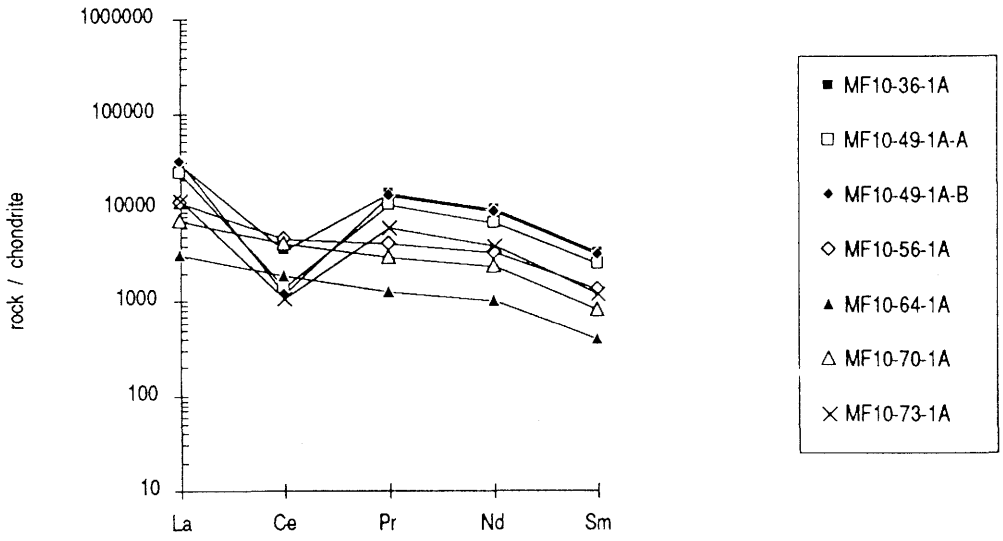

Figure 23. Borehole MF10: LREEs of the weathered carbonatite normalized to ordinary chondrite (analysis by ICPOES: for normalization factors, see Table X).

TABLE X

Borehole MF10: LREE analysis of the ore body and the weathered carbonatitic host rock.

Sample	Rock-type	La ppm	Ce ppm	Pr ppm	Nd ppm	Sm ppm
MF10-1-1B	ore body	41170	54682	6800	23624	3031
MF10-3-1A	ore body	3151	7545	159	637	100
MF10-4-1A	ore body	4162	18050	251	1206	169
MF10-6-1A	ore body	1125	1599	77	150	12
MF10-12-1A	ore body	5243	2891	789	1771	135
MF10-18-1A	ore body	1448	8226	143	444	32
MF10-25-1A	ore body	2151	14246	213	594	45
MF10-36-1A	host rock	8744	2679	1623	5520	624
MF10-49-1A-A	host rock	7025	1117	1173	3989	473
MF10-49-1A-B	host rock	9287	941	1519	5192	591
MF10-56-1A	host rock	3430	3515	466	1915	255
MF10-64-1A	host rock	945	1440	146	588	73
MF10-70-1A	host rock	2108	3174	341	1331	154
MF10-73-1A	host rock	3556	848	677	2215	231
Chondrite normalized (normalizing factors):		0.2974	0.7643	0.1129	0.5732	0.1864
MF10-1-1B	ore body	138433	71545	60230	41214	16261
MF10-3-1A	ore body	10595	9872	1408	1111	536
MF10-4-1A	ore body	13995	23616	2223	2104	907
MF10-6-1A	ore body	3783	2092	682	262	64
MF10-12-1A	ore body	17629	3783	6988	3090	724
MF10-18-1A	ore body	4869	10763	1267	775	172
MF10-25-1A	ore body	7233	18639	1887	1036	241
MF10-36-1A	host rock	29401	3505	14376	9630	3348
MF10-49-1A-A	host rock	23621	1461	10390	6959	2538
MF10-49-1A-B	host rock	31227	1231	13454	9058	3171
MF10-56-1A	host rock	11533	4599	4128	3341	1368
MF10-64-1A	host rock	3178	1884	1293	1026	392
MF10-70-1A	host rock	7088	4153	3020	2322	826
MF10-73-1A	host rock	11957	1110	5996	3864	1239

Analysis by ICPOES; New York University Medical Center, New York.

7.2. Th-REE ore body

The geographical location of the ore body at Morro do Ferro is shown in Figure 2 and its vertical dimensions in Figure 5.

7.2.1. Petrography

The Th-REE ore body consists of a fine-grained clay-silt matrix similar to the underlying host rock; coarse-grained components are, however, much more abundant. The most obvious feature of the ore body is the abundance of magnetite layers of variable thicknesses which have stabilized the hill from excessive erosion, allowing a residual enrichment of Th- and REE-minerals to accumulate through dissolution of the more soluble mineral phases.

The ore material is mainly dark reddish-brown in colour; magnetite nodules occur loosely arranged in layers and vein-like structures and also more randomly distributed throughout the matrix.

Modal compositions (Table VIII) and the rock physical properties (Fig. 21) of the ore body have been previously described (sections 7.1.1.2. and 7.1.1.3.) in association with the host rock.

7.2.2. Mineralogy

The general mineralogy very much resembles that described for the host rock. Major exceptions include gibbsite, the distribution of illite/sericite and kaolinite, and the Th-REE mineralogy.

Kaolinite and illite/smectite

In the ore body the illite:kaolinite ratio increases from nearly 1:1 at the lower boundary to 4:1 towards the surface. This is in strong contradiction to the weathering profiles overlying the phonolite in borehole MF12, and overlying the hydrothermally altered rocks of the Osamu Utsumi mine (Waber *et al.*, this report series; Rep. 2). Furthermore, this also contrasts markedly with the expected stability of illite compared to kaolinite in a normal lateritic weathering profile. The reason for such behaviour is not yet clearly understood, but two factors may play an important role: firstly, illite/sericite in the ore

body is on average coarser-grained than in the host rock, forming flakes of up to 200μ and, secondly, illite/sericite in the ore body is always coated with an iron-hydroxide film and is very often completely included in iron-hydroxides and/or aluminium-hydroxides. This may protect the illite/sericite from water interaction and, therefore, from complete dissolution.

Gibbsite and amorphous Al-hydroxide

Gibbsite occurs in all the different grain size fractions and, compared to the host rock, is much more abundant in the first 10 m below the surface. These dense concretions of gibbsite and amorphous Al-hydroxide may reach up to 1 cm in diameter. Such concretions enclose different types of minerals such as sericite, oxidized magnetite nodules, and primary and secondary Th-REE minerals. Well crystallized gibbsite is always associated with poorly crystalline varieties and completely amorphous Al-gel (Al-plasma).

Fe-oxides/hydroxides

Magnetite nodules occur much more frequently in the ore body, their size varying between several millimetres and several decimetres. In the small grain size ranges, the nodules are completely oxidized, while in coarser-grained nodules the magnetite tends to be well preserved in the central parts, where all the primary Th-REE phases are found.

Otherwise, the iron phases occur in the same manner as described for the host rock, with the exception that Fe-hydroxides and amorphous iron gel are finely distributed throughout the ore material.

Th-REE minerals

The Th-REE minerals can be subdivided into minerals of primary and secondary origin according to textural relationships. Th-REE minerals found as inclusions in unoxidized magnetite are of primary origin, whereas euhedral Th-REE minerals found as overgrowth and pore infillings are of secondary weathering origin. The latter group is commonly much more fine-grained (0.01–10μ). The list of Th-REE minerals given below is not complete but comprises the most abundant phases.

- *Th-REE minerals of primary origin*

bastnaesite	$(Ce,La)(CO_3)F$
cheralite	$(Ce,Th)(PO_4)$
monazite	$REE(PO_4)$
thorite	$Th(SiO_4)$
zircon	$(Zr,Th,U)(SiO_4)$
pyrochlore	$(Th,Ca,REE)_2Nb_2O_6(OH,F)$

- *Th-REE minerals of secondary origin*

monazite	$REE(PO_4)$
florencite	$CeAl_3(PO_4)(OH)_6$
cerianite	$(Ce,Th)O_2$
thorianite	$(Th,U)O_2$
goyazite	$(Sr,REE)Al_3(PO_4)(OH)_5$
gorceixite	$(Ba,REE)Al_3(PO_4)(OH)_5$
thorogummite	$(Th,Al_3)(PO_4)(OH)_5$
Nd-lanthanite	$(La, Nd)_2(CO_3)_3 \cdot 8\ H_2O$

Additional data have contributed to a better understanding of the primary or secondary origin of some of these minerals compared to previous investigations (e.g. Barretto and Fujimori, 1986). For example, bastnaesite and thorbastnaesite have been found as inclusions in magnetite and are therefore considered to be of primary origin. In the rock matrix these minerals always have strongly corroded crystal surfaces and become altered to cerianite and crandallite group minerals. Furthermore, monazite is of primary as well as of secondary origin, the former (found in magnetite) being much coarser-grained than the secondary monazite, which occurs as tiny euhedral crystals (1-10μ) forming matrix aggregates. These features are similar to the secondary monazite known from the lateritic covers of the Mt. Weld carbonatite, Australia (Lottermoser, 1988), and at Araxá and Catalão I, Brazil (Mariano, 1989).

Cheralite alters mainly to cerianite, and thorite (and possible huttonite) to thorianite and thorogummite. Pyrochlore occurs as strongly metamict and corroded grains. Florencite pseudomorphically replaces pyrochlore, similarly to the processes described from the Mt. Weld carbonatite (Lottermoser and England, 1988). Zircon occurs as euhedral, slightly corroded crystals displaying variable concentrations of Th and U.

In the ore body, Nd-lanthanite was only observed in samples MF10-1-1B, MF10-6-1A and MF10-12-1A (Fig. 24), all of them displaying either a negative Ce anomaly or none at all. As in the host rock, Nd-lanthanite does not occur as a clearly defined alteration product of a primary phase, but seems to have been precipitated from solution.

Among the secondary Th-REE minerals, the oxidic ones are more abundant than the hydroxyphosphates. This is of special importance because cerianite exclusively incorporates Ce^{4+} but not the trivalent REEs.

a)

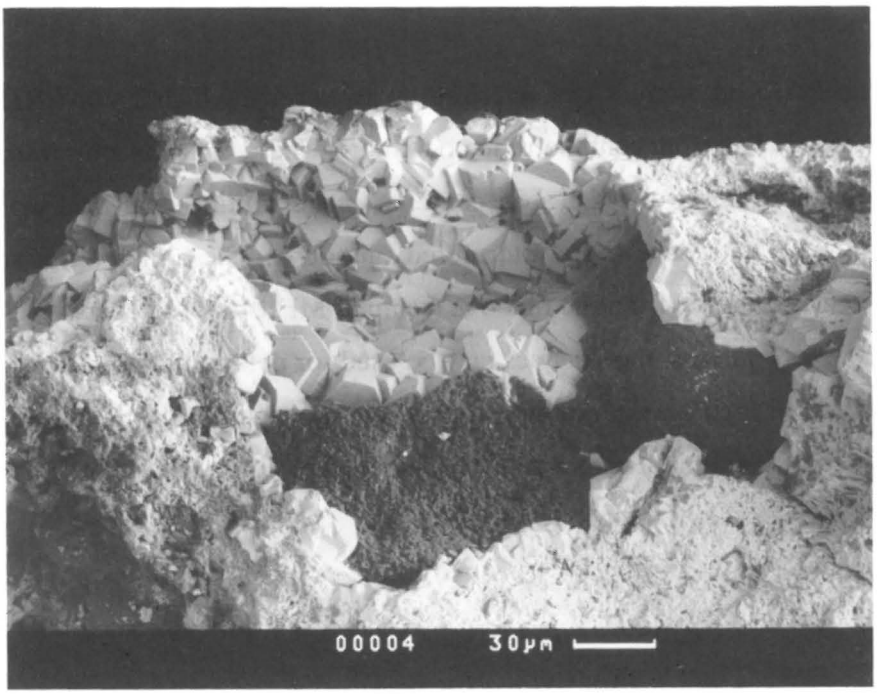

b)

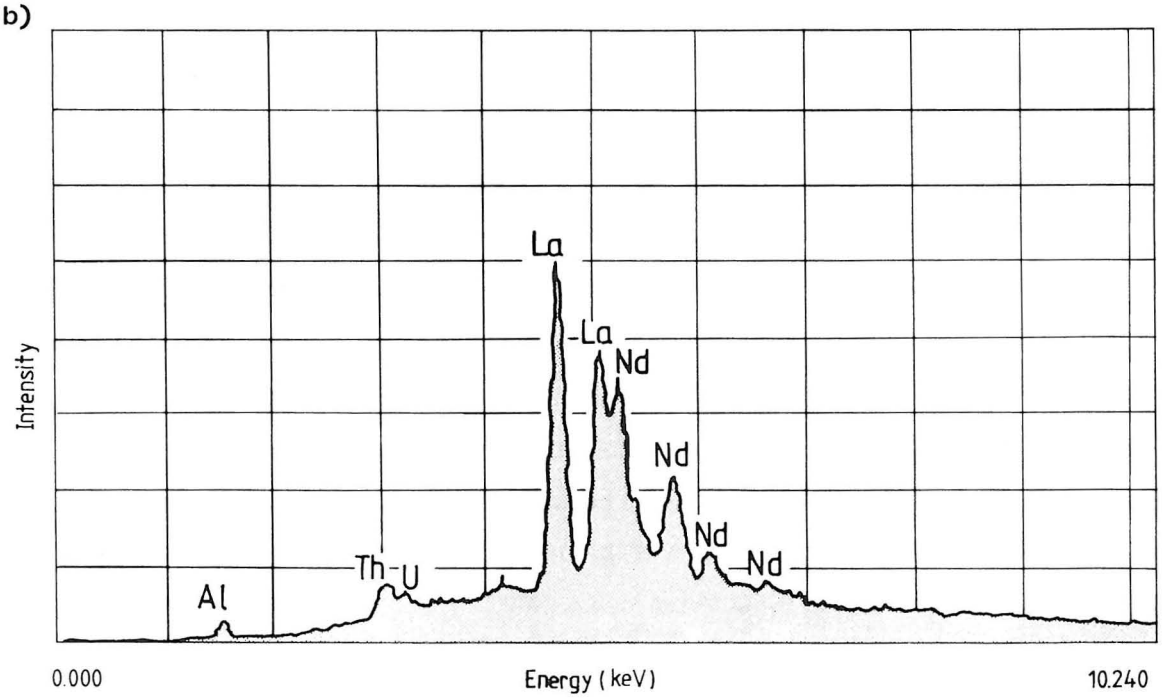

Figure 24.
a) Back-scattered scanning electron image of secondary lanthanite idiomorphically formed in a pore space.

b) Energy dispersive spectra (EDS) of a single crystal selected from the left-hand side of the pore.
(Sample: MF10-12-1A).

7.2.3. Geochemistry

The Morro do Ferro ore body is characterized by its extremely high Th and REE concentrations, which vary from centimetre to centimetre. These high concentrations, together with the invariably very high iron contents, make routine analytical work difficult and the XRF data have to be interpreted cautiously. These difficulties are particularly evident in samples from the first 6 m (samples MF10-1-1A to MF10-6-1A; see Appendix 3). Nevertheless, the analyses may be used for determining the general geochemical trends. Much more accurate results with respect to the absolute concentrations of Th, U and the REEs have been obtained by alpha-spectrometry and ICPOES (MacKenzie *et al.*, this report series; Rep. 7).

7.2.3.1. Major elements

In the lower part of the ore body, SiO_2 and Al_2O_3, in common with the host rock, are positively correlated (Fig. 25); towards the surface SiO_2 drastically decreases whereas Al_2O_3 increases, reflecting the formation of gibbsite. K_2O, with values similar to those from the weathered carbonatitic host rock, only shows minor fluctuations up to the uppermost metre in the ore body, where it then becomes depleted.

Fe_2O_3 is abundant throughout the ore body, with concentrations ranging between about 15 and 20 wt.%. MnO displays a very heterogeneous distribution from zero in some samples to values of up to 8 wt.% in other samples only a few decimetres apart. No relationship between iron and manganese is observed.

P_2O_5 is residually enriched towards the surface, reaching concentrations of 2 wt.%. Throughout the ore body, P_2O_5 concentration is much higher than in the host rock, i.e. by a factor of about 3 to 8, reflecting the much higher abundance of REE phosphates.

TiO_2 contents are low in the lower part of the ore body; in the uppermost 6 m the range of values is similar to that for the host rock.

7.2.3.2. Trace elements

Apart from Th and REEs, strong enrichments of Sr, F and Pb, in comparison to the weathered carbonatitic host rock, occur in the ore body; U is also higher in overall abundance. All the other trace elements are present in similar concentrations and display

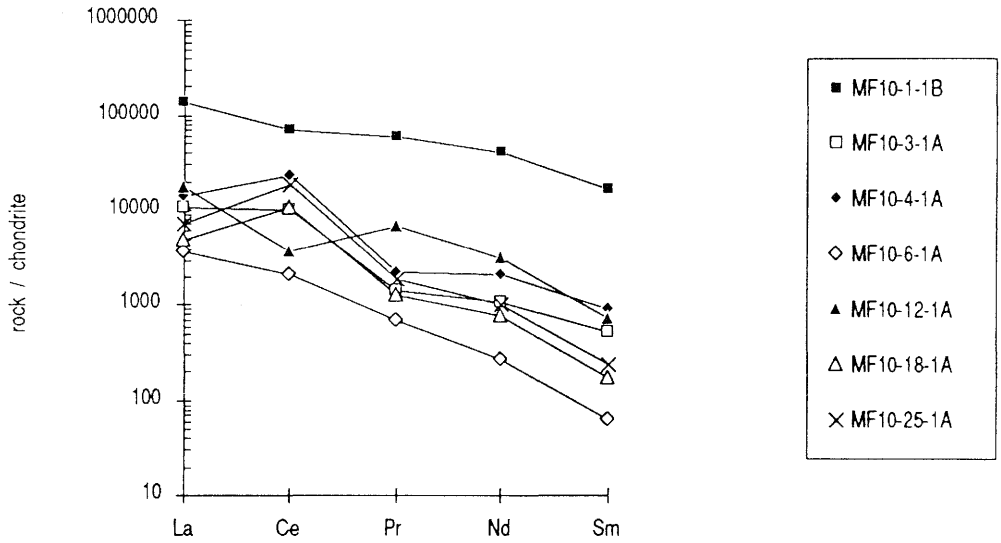

Figure 25. Borehole MF10: LREEs of ore body normalized to ordinary chondrite (analysis by ICPOES: for normalization factors, see Table X).

the same variations as shown in the host rock, with the exception of Ba which is depleted in the ore body (Fig. 25; Appendix 2).

Th is strongly enriched in the first 10 m of the ore body, then decreases slowly with depth to values representative for the host rock. In comparison to the following 2 m, the uppermost soil samples show a low Th content which, however, is still within the average of the first 10 m. Th shows a certain affinity to Ce but not to the other LREEs, which becomes even more obvious in the data obtained by alpha-spectrometry and ICPOES (MacKenzie *et al.*, this report series; Rep. 7). Moreover, Th shows an affinity with samples rich in iron-oxyhydroxides. In contrast, white coloured samples that consist mainly of illite and kaolinite are comparably low in Th (e.g. sample MF10-12-1A).

U displays a higher total abundance in the ore body than in the host rock, but is also extremely variable (Fig. 22). In common with Th, samples nearly free of iron-oxyhydroxides are also free of U. Autoradiographs of thin and polished sections show a finely disseminated distribution of radiation intensity in the fine-grained, iron-stained zones of the ore material. Strong intensity is recorded where highly birefringent minerals are observed in the matrix, along the oxidized rims of magnetite nodules, and around their primary inclusions. White-coloured ore samples display only very weak or negligible radiation intensities.

In comparison to the host rock, Sr is strongly enriched in the ore body by a factor of up to 10; the enrichment is highest from a depth of 1.5 to 6m. At the surface, the Sr concentrations decrease once again. Similar behaviour can be observed for F, except that F displays a more heterogeneous distribution. Compared to the host rock, F is enhanced by a factor of 2 to 3.

Good interelement correlations between trace elements in the ore body are rare. Affinities exist between U-Sr, Rb-V-K_2O, Th-Ce and F-Ce; the best correlation exists between La and Nd.

7.2.3.3. Rare-earth elements

The behaviour of the LREEs differs markedly between the ore body and the host rock. La and Nd occur in equal or lower amounts in the ore body, whereas Ce is increased (Fig. 22). Ce shows no correlation with the other LREEs (Fig. 26a). La and Nd show a good correlation throughout the ore body ($r = 0.99$; $n = 7$; Fig. 25b) whereas Ce shows a weak trend with Th ($r = 0.9$; $n = 7$; Fig. 25c).

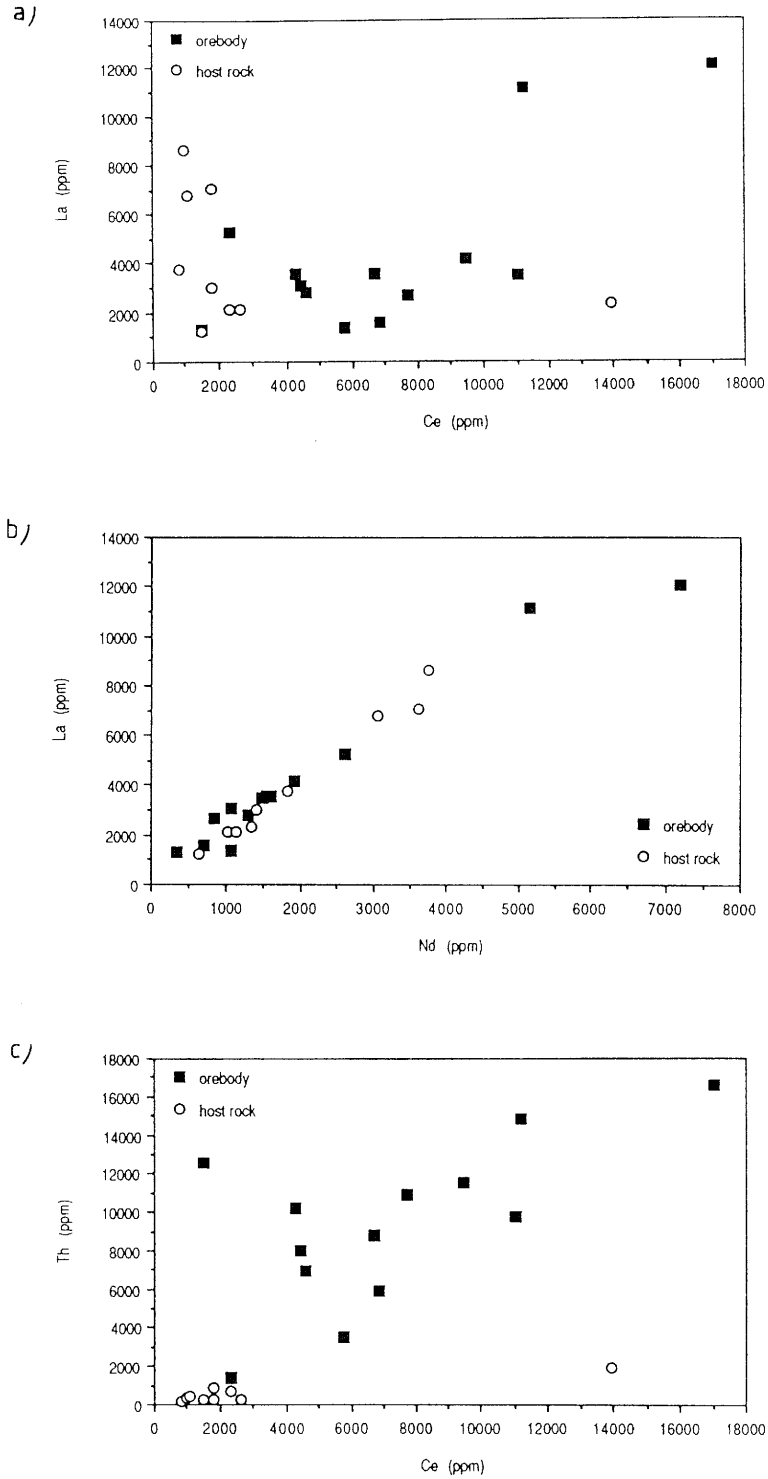

Figure 26. Borehole MF10: binary plot of:

a) lanthanum versus cerium,
b) lanthanum versus neodymium, and
c) thorium versus cerium.

The chondrite normalized LREE patterns from La to Sm (ICPOES data from MacKenzie *et al.*, this report series; Rep. 7) show a modest to strong positive Ce anomaly for all samples except three (Fig. 25). Two of these exceptions are samples MF10-6-1A and MF10-12-1A, which display a modest to strong negative Ce anomaly as observed in most samples of the host rock. Similarly, these two samples also display higher concentrations in the other LREEs if compared to most of the overlying samples from the drillcore. Both these samples consist mainly of white-coloured clay material. The third exception is sample MF10-1-1B which comes from just below the surface and displays a considerable enrichment in all LREEs. The positive Ce anomaly reported from the other samples of the ore body is in agreement with the occurrence of cerianite in these samples (Table VIII).

Summarizing, the behaviour of Ce as compared to the other LREEs is observed to be different over the entire drillcore profile through the ore body and weathered carbonatitic host rock. The positive Ce anomalies in the ore body can be explained mineralogically by the slow dissolution of the primary REE minerals, whereby Ce^{3+} is oxidized to Ce^{4+} and incorporated into secondary cerianite. Ce is therefore retained in the ore body, whereas the trivalent LREEs have migrated downwards in the profile, resulting in an apparent positive Ce anomaly. The faster-moving trivalent LREEs subsequently become more readily available for secondary mineral formation (Nd-lanthanite) and/or adsorptive processes, as exemplified by the negative Ce anomalies and the increased total abundance of LREEs (except for Ce) in samples from the host rock. These processes are further controlled by the abundance and type of occurrence (e.g. inclusion) of the primary REE phases and their differing solubilities during weathering. These observations are, at least in part, sustained by the natural decay series data (MacKenzie *et al.*, this report series; Rep. 7).

8. Discussion

Based on the regional geology study by Schorscher and Shea (this report series; Rep. 1), it appears that the Morro do Ferro area underwent a late phase of subvolcanic activity and associated hydrothermal alteration. This event led to the formation of a carbonatite with associated magnetite layers and veins enriched in both Th and REEs, compared to the regional country rocks. Related to this event were the brecciation and hydrothermal alteration of the surrounding phonolitic country rocks. Xenolithic evidence of breccia veins in the phonolites indicates that brecciation and alteration took

place subsequent to the phonolites being deuterically altered. This deuteric alteration is similar to that generally observed in the rocks of the Poços de Caldas plateau. Clay mineral parageneses, including kaolinite, indicate that the phonolites at Morro do Ferro had cooled down substantially before the hydrothermal alteration occurred. The recurrence of magmatic activity was dual in terms of the emplacement of the carbonatitic host rock and in the nearly contemporaneous intrusion of yet a second phase of minor phonolitic plugs and dykes.

Subsequent weathering of the carbonatite has been so complete that no relicts now survive; the only primary feature preserved is a resistant stockwork of partially oxidized magnetite layers and veins which cap the deposit. This stockwork has probably stabilized the underlying 130 m thickness of highly altered rock from greater erosion.

The existence of a primary carbonatite at Morro do Ferro is inferred from the primary and secondary mineral parageneses (bastnaesite, cheralite, monazite, thorite, pyrochlore and florencite, goyazite, cerianite, thorianite, respectively), from the geochemical mass balance calculations, and from the type of country rock alteration (fenitization). Furthermore, the identification of a carbonatite is supported by the occurrence of ultramafic dykes at the Osamu Utsumi mine with carbonatitic affiliations (Waber *et al.*, this report series; Rep. 2), and by the fact that the Poços de Caldas plateau consists of alkaline rocks. Elsewhere in Brazil, alkaline complexes of similar age usually contain associated carbonatites.

There is clear evidence that the hydrothermal alteration induced by the emplacement of the carbonatite was polyphase. It consisted mainly of an early potassium metasomatism with associated disseminated pyritization, followed by a vein-type thorium-REE mineralization with associated fluorite, pyrite, carbonate and zircon. During the second phase of magmatic activity, phonolitic plugs and dykes were apparently emplaced shortly after the carbonatitic magmatic activity and were not subjected to the same intensive hydrothermal alkali-exchange alteration as the primary phonolites of identical composition.

The hydrothermal alteration of the early phonolites at Morro do Ferro is generally very similar to that observed in the Osamu Utsumi uranium mine (Waber *et al.*, op. cit.). It includes a strong enrichment of K, S, Th, U, Pb and Rb and a depletion in Sr compared to the regional rocks. In addition, the Morro do Ferro phonolites are strongly enriched in REEs, especially in the LREEs and in Y, but depleted in Ba. Compared to the hydrothermally altered rocks of the Osamu Utsumi uranium mine, the phonolites show an enrichment in Th, REEs, Y, Pb, F, P and CO_2 and a depletion in U, S and Ba.

The carbonatite, which by definition has a carbonate content in excess of 50 vol.%, is much more susceptible to weathering than the silicate country rocks. Subsequent lateritic weathering has therefore completely destroyed the carbonatite and led to the supergene enrichment of Th and REEs. In contrast, weathering of the phonolite country rocks formed a lateritic cover around 30 m thick, including a saprolite horizon and an oxidation zone about 10–50 m in thickness. The weathering zone on top of the phonolites is mineralogically and geochemically very similar to that in the Osamu Utsumi uranium mine. It is characterized by the dissolution of sulphides, fluorite, carbonates and K-feldspar, by the formation of kaolinite, gibbsite and secondary REE-phases, and by the residual enrichment of P, Ti, Th, Ce, Sr, and Zr towards the surface.

The conclusion that the primary rock hosting the Th-REE mineralization was carbonatitic in composition is also of importance to the long-term study of the mobility of Th and REEs. Initial weathering of the carbonatite (i.e. dominated by carbonate and phosphate removal) created a chemical environment that may have appreciably buffered the dissolution and mobility of the primary Th-REE phases. With time, when oxidizing conditions had become established throughout the bedrock to considerable depth, a redistribution of Th and REEs gradually occurred, resulting in present-day profiles.

The strong enrichment of Th and Ce in the ore body, and the enrichment of the other LREEs in the host rock below, can be explained by mineralogical controls. Thus, the formation of thorite has fixed Th, and the oxidation of trivalent Ce^{3+} to the less soluble tetravalent Ce^{4+} has given rise to cerianite. In contrast, the trivalent LREEs were not retained and have migrated further down the weathering column. Hence, their higher concentrations at depth have resulted in the formation of secondary minerals such as Nd-lanthanite and REE-hydroxyphosphates, and their adsorbtion on poorly crystalline iron- and aluminium-hydroxides. This results in the observed enrichment of trivalent LREEs in the lower samples of the ore body and the weathered carbonatitic host rock. Seasonally controlled fluctuations of the water input into the weathering column may explain the observed repetition of Ce-enriched zones underlain by trivalent LREE enriched zones.

9. Acknowledgements

This study would not have been possible without the field support, helpful discussions and hospitality of Ruy Frayha, Luiz Barroso Magno Jr., Norbert Miekeley and Hans Schorscher. Considerable thanks are due to Dagmar Riesen for geochemical sample

preparation, Heidi Haas for porosity measurements, Jürg Megert for preparing excellent thin and polished sections of the strongly weathered soil and rock material, Karl Ramseyer for support in the cathodoluminescence analytical work, Alfred Zweili for the SEM analytical work, and Beda Hofmann, Paul Linsalata and Tjerk Peters for stimulating discussions. The rare-earth element analyses were carried out under the supervision of Marie-Thérese Ménager (CEA, Paris), R. Krähenbühl (Chemisches Institut, Universität Bern) and Paul Linsalata (New York University Medical Center). Thanks are also due to Lina Bobade for typing the various versions of the manuscript.

10. References

Almeida Filho, R. and Paradella, W.R., 1977. Estudo do maciço alcalino de Poços de Caldas através de imagens Landsat com ênfase em mineralizações radioativas. São José dos Campos, *INPE* (11/2 – TPT/065).

Bailey, D.K., 1966. In: Carbonatites, O.F. Tuttle and J. Gittins (Editors), Carbonatite volcanoes and shallow intrusions in Zambia. *John Wiley*, New York, 127-154.

Barretto, P.M.C. and Fujimori, K., 1986. Natural analogue studies: geology and mineralogy of Morro do Ferro, Brazil. *Chem. Geol.*, 55, 297-312.

Boudeulle, M. and Muller, J.-P., 1988. Structural characteristics of hematite and goethite and their relationships with kaolinite in a laterite from Cameroon. A TEM study. *Bull. Minéral.*, 111, 149-166.

Boulangé, B., 1984. Les formations bauxitiques latéritiques de Côtes d'Ivoire. Les faciès, leur distribution et l'évolution du modelé. *Trav. et Docum.*, ORSTOM, 175, 363 pp.

Brown, P.E., 1964. The Songwe scarp carbonatite and associated feldspathization in the Mbeya Range, Tanganyika. *Q. J. Geol. Soc.*, 120, 223-240.

Camargo dos Santos, R., 1984. Descrição lithologica do furo SC:38-01. In: Instituto de Pesquisas Tecnológicas (IPT) do Estado de São Paulo, 1984. Revisão da bibliografia sobre o Morro do Ferro, Poços de Caldas, Minas Gerais. Relatório no. 20993, Vol. 2, 25-35.

Derby, O.A., 1981. Magnetite ore districts of Jacupiranga and Ipanema, São Paulo, Brazil, *Am. J. Sci.*, 41, 311-321.

Drew, R.T. and Eisenbud, M., 1966. The natural radiation dose to indigenous rodents on the Morro do Ferro, Brazil. *Health Phys.*,12, 1267.

Eby, G.N., 1975. Abundance and distribution of the rare earth elements and yttrium in the rocks and minerals of the Oka carbonatite complex, Quebec. *Geochim. Cosmochim. Acta*, 39, 597-620.

Eisenbud. M., 1979. The thorium deposit of Morro do Ferro in Minas Gerais as an analogue for modeling the transport of plutonium over geological time. *Inst. Environ. Med.*, New York Univ., New York, (Intern. Report).

Eisenbud. M., 1980. The mobility of thorium and other elements from the Morro do Ferro. *Com. Nac. Energia Nucl.*, Rio de Janeiro. (Intern. Report)

Eisenbud. M., Lei, W., Ballad, R., Krauskopf, K., Penna Franca, E., Cullen, T.L. and Freeborn, P., 1982. Mobility of thorium from the Morro do Ferro. In: Environmental Migration of Long-lived Radionuclides. *Int. At. Energy Agency*, Vienna, IAEA-SM-257/49, 739-755.

Ellert, R.,1959. Contribuição à geologica do maciço alcalino de Poços de Caldas. *Bol. Fac. Fil. Ciênc. Letras, Univ. São Paulo*, 237, Geol. 18, São Paulo, 5-63.

Frayha, R., 1962. Urânio e tório no planalto de Poços de Caldas. *Dep. Nac. Prod. Min., Bull.*, 116, 75 pp.

Frayha, R., 1966. Região de Poços de Caldas, MG. In: Oliveira, G. M. A., Relatório da Diretoria, 1965, *DNPM, Div. Fom. Prod. Miner., Bol.*, 93, 117-124.

Frayha, R., 1967. Região de Poços de Caldas, MG. In: Oliveira, G. M. A., Relatório da Diretoria, 1966, *DNPM, Div. Fom. Prod. Miner., Bol.*, 130, 1103-114.

Frondel, C. and Marvin, U.B., 1959. Cerianite, CeO_2, from Poços de Caldas, Brazil. *Am. Mineral.*, 44, 882-884.

Fujimori, K., 1974. Minerais radioativos do Campo Agostinho, Poços de Caldas (MG). *Livre-Docência Thesis*, Inst. Geociênc., Univ. São Paulo, 161 pp.

Fujimori, K., 1982. Silicato do terras raras (Ce,La,Nd,Ca,Th)SiO_4 e cheralite (Th,Ca,Ce,La)(P,SiO4) minerais responsáveis pela anomalia do Morro do Ferro, Poços de Caldas. *Ann. 32nd Braz. Geol. Congr.*, Salvador, Bahia, 2, 669-671.

Fujimori, K.,1983. Migração de tório e outros elementos no Morro do Ferro. *Relatório de Pesquisa*, Rio de Janeiro, Convênio 37/82, 37 pp.

Fujimori, S., 1967. Rochas alcalinas do Sul do Estado da Bahia. *DNPM, Div. Fom. Prod. Miner.* – Notas Preliminares e Estudos, Brasília, 141, 1-11.

Heinrich, E.W., 1966. The geology of carbonatites. *Rand McNally*, Chicago, Illinois.

Instituto de Pesquisas Tecnológicas (IPT) do Estado de São Paulo, 1984. Revisão da bibliografia sobre o Morro do Ferro, Poços de Caldas, Minas Gerais. *Relatório no. 20993*, Vol. 1, 153 pp, and Vol. 2, 36 pp.

Jaffe, H.W. and Selchow, D.H., 1960. Mineralogy of the Araxá Columbium deposit. Union Carbide Ore Company Research Report, 4. Research Center, Tuxedo, N.Y.

Kubler, B., 1968. Evaluation quantitative du métamorphisme par la crystallinité de l'illite. *Bull. Centre Rech. Pau-SNPA*, 2, 385-397.

Lei, W., 1984. Thorium mobilization in a terrestrial environment. *PhD Thesis*, New York University, New York, N.Y., 414 pp.

Lei, W., Linsalata, P., Penna Franca, E. and Eisenbud, M., 1986. Distribution and mobilization of cerium, lanthanum and neodymium in the Morro do Ferro Basin, Brazil. *Chem. Geol.*, 55, 312-322.

Lottermoser, B.G.,1988. Supergene, secondary monazite from the Mt. Weld carbonatite laterite, Western Australia. *N. Jb. Miner. Mh.*, H. 2, 67-70.

Lottermoser, B.G. and England, B.M., 1988. Compositional variation in pyrochlores from the Mt. Weld carbonatite laterite, Western Australia. *Min. Petrol.*, 38, 37-51.

Mariano, A.N., 1989. Economic Geology of Rare Earth Minerals. In: B.R. Lipin and G.A. McKay, (Editors), Geochemistry and Mineralogy of Rare Earth Elements, *Min. Soc. Amer., Reviews in Mineralogy*, 21, 309-348.

Marshall, D.J., 1988. Cathodoluminescence of Geological Materials. *Unwin Hyman Ltd*, London, 146 pp.

Miekeley, N., Vale, M.G.R., Tavares, T.M. and Lei, W., 1982. Some aspects of the influence of surface and groundwater chemistry on the mobility of thorium in the "Morro do Ferro" environment. Scientific Basis for Nuclear Waste Management, V. *Mat. Res. Soc. Proc.*, 11, 725-733.

Miekeley, N., Dotto, R.M., Kuechler, I.L. and Linsalata, P., 1985. The importance of organic compounds on the mobilization and bioassimilation of thorium in the Morro do Ferro environment. Scientific Basis for Nuclear Waste Management, VIII. *Mat. Res. Soc. Proc.* 44, 591-597.

Miekeley, N. and Kuechler, I.L., 1987. Interactions between thorium and humic compounds in surface waters. *Inorg. Chim. Acta*, 140, 315-319.

Muller, J.-P., 1988. Analyse pétrologique d'une formation latéritique meuble du Cameroon. *Trav. et Docum., ORSTOM*, 50, 188 pp.

Nisbet, E.G., Dietrich, V.J. and Eisenwein, A., 1979. Routine trace element determination in silicate minerals and rocks by X-ray fluorescence, *Fortschr. Miner.*, 57/2, 264-279.

Penna Franca, E., Almeida, J.C., Becker, J., Emmerich, M., Roser, F.X., Kegel, G., Hainsberger, L., Cullen, T., Petrow, H., Drew, R.T. and Eisenbud, M., 1965. Status of investigations in the Brazilian areas of high natural radioactivity. *Health Phys.*, 11; 699-712.

Ramseyer, K., Fischer, J., Matter, A., Eberhardt, P. and Geiss, J., 1989. A cathodoluminescence microscope for low intensity luminescence. *Res. Methods Pap.*, 619-622.

Reedman, J.H., 1984. Resources of phosphate, niobium, iron and other elements in residual soils over the Sukulu carbonatite complex, southeastern Uganda. *Econ. Geol.*, 79, 716-724.

Reusser, E., 1986. Das XRF-System Version 86: Softwarepaket mit unpubl. Manual, ETH-Zürich.

Rocha, E.B., Fujimori, K. and Ulbrich H.H.G.J., 1984. Determinação de urânio et tório em rochas de macico alcalino de Poços de Caldas (MG-SP), por meio de ativação neutronica. XXXIII *Congr. Brasil. Geol.*, Rio de Janeiro, Resumo e Breves Comunicações, 80-81.

Schwertmann, U., 1985. Occurrence and formation of iron oxides in various pedeoenvironments. In: J.W. Stucki, B.A. Goodman and U. Schwertmann, (Editors), Iron in soils and clay minerals. NATO ASI Series, Series C Mathematical and Physical Science, no. 217, D. *Reidel Publ. Co.*, Dordrecht, Holland, 267-308.

Sommerauer, J., 1981. COMIC-ED Manual, Version 2.EXT, Institut für Kristallographie und Petrographie, *ETHZ*, Zürich, Switzerland.

Środoń, J., 1980. Precise identification of illite/smectite interstratifications by X-ray powder diffraction. *Clays and Clay Miner.*, 28, 401-411.

Środoń, J., 1984. X-ray powder diffraction identification of illitic material. *Clays and Clay Miner.*, 32, 337-349.

Sutherland, D.S., 1967. A note on the occurrence of potassium-rich trachytes in the Kaiserstuhl carbonatite complex, West Germany. *Min. Mag.*, 36, 334-341.

Tardy, Y. and Nahon, D., 1985. Geochemistry of laterites, stability of Al-goethite, Al-hematite, and Fe^{3+}-kaolinite in bauxites and ferricretes: an approach to the mechanism of concretion formation. *Am. J. Sci.*, 285, 865-903.

Taylor, R., 1955. The magnetite-vermiculite occurrences of Bukusu, Mbale District. *Bull. Surv. Uganda Rec.*, 59-64.

Tolbert, G.E., 1958a. Preliminary report on the uraniferous zirconium deposits of the Poços de Caldas Plateau, Brazil. Part I. *Eng. Min. Metal.*, 27(161), 265-269.

Tolbert, G.E., 1958b. Preliminary report on the uraniferous zirconium deposits of the Poços de Caldas Plateau, Brazil. Part II. *Eng. Min. Metal. 27(162),* 353-360.

Tolbert, G.E., 1966. The uraniferous zirconium deposits of the Poços de Caldas Plateau, Brazil. *USGS, Bull.*, 1185-C, 28 pp.

Ulbrich, H.H.G.J., 1984. A petrografia, e estrutura e o quimismo de nefelina sienitos do Maciço Alcalino de Poços de Caldas, MG-SP. *Tese de Livre Docência*, Instituto de Geosciências da Universidade de São Paulo, 2 Vol.

Ulbrich, H.H.G.J. and Gomes, C.B., 1981. Alkaline rocks from continental Brazil. *Earth Sci. Rev.*, 17, 135-154.

Ulbrich, M.N.C., 1983. Aspectos mineralógicos et petrólogicos de nephelina sienitos de Poços de Caldas, MG-SP. *Tese de Doutoramento*, Instituto de Geosciências da Universidade de São Paulo, 369 pp.

Waber, N., 1990. Hydrothermal and supergene evolution of the Osamu Utsumi uranium deposit and the Morro do Ferro thorium – rare earth deposit, Minas Gerais, Brazil, *PhD-Thesis*, Universität Bern, 179 pp.

van Wambeke, L., Brink, J.W., Deutzmann, W., Gonfiantini, R., Hubeaux, A., Metais, D., Omenetto, P., Tongiorgi, E., Verfaillie, G., Weber, K. and Wimmenauer, W., 1964. Les roches alkalines et les carbonatites du Kaiserstuhl. *Euratom*, 1827.

Wedow, Jr. H., 1967. The Morro do Ferro thorium and rare earth ore deposits, Poços de Caldas District, Brazil. *U.S. Geol. Surv., Bull.*, 1185-D, Washington, 34 pp.

Woolley, A.R., 1989. The spatial and temporal distribution of carbonatites. In: K. Bell (Editor), Carbonatites: Genesis and Evolution. *Unwin Hyman Ltd*, London, 15-37.

Woolley, A.R. and Kempe, D.R.C., 1989. Carbonatites: nomenclature, average chemical compositions, and element distribution. In: K. Bell (Editor), Carbonatites: Genesis and Evolution. *Unwin Hyman Ltd*, London, 1-14.

11. PLATES 1 – 5

PLATE 1. *Borehole MF10;*
typical core section of the Th-REE ore body with magnetite nodules.

PLATE 2. *Borehole MF10;*
typical core section of the carbonatitic host rock (completely weathered) below the ore body.

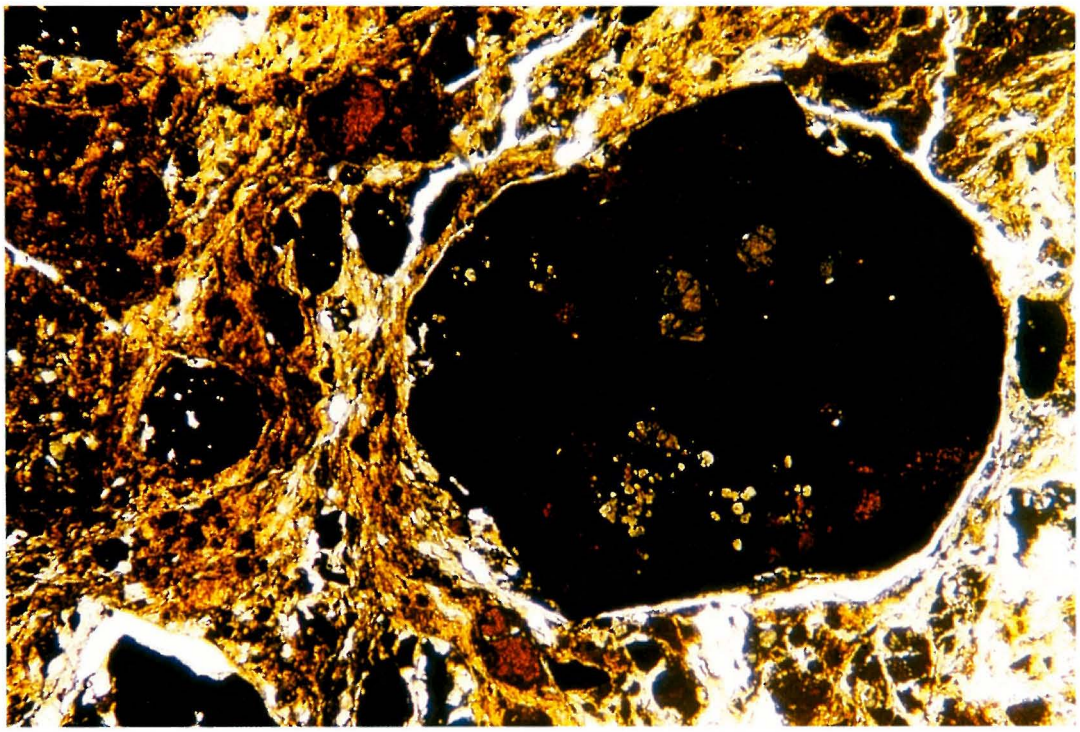

PLATE 3. Borehole MF10 (sample MF10-1-12); representative photomicrograph of the Th-REE ore consisting of magnetite nodules oxidized to variable degrees and embedded in a fine-grained matrix. Inclusions of primary bastnaesite occur in the large magnetite nodule (mag. 25x).

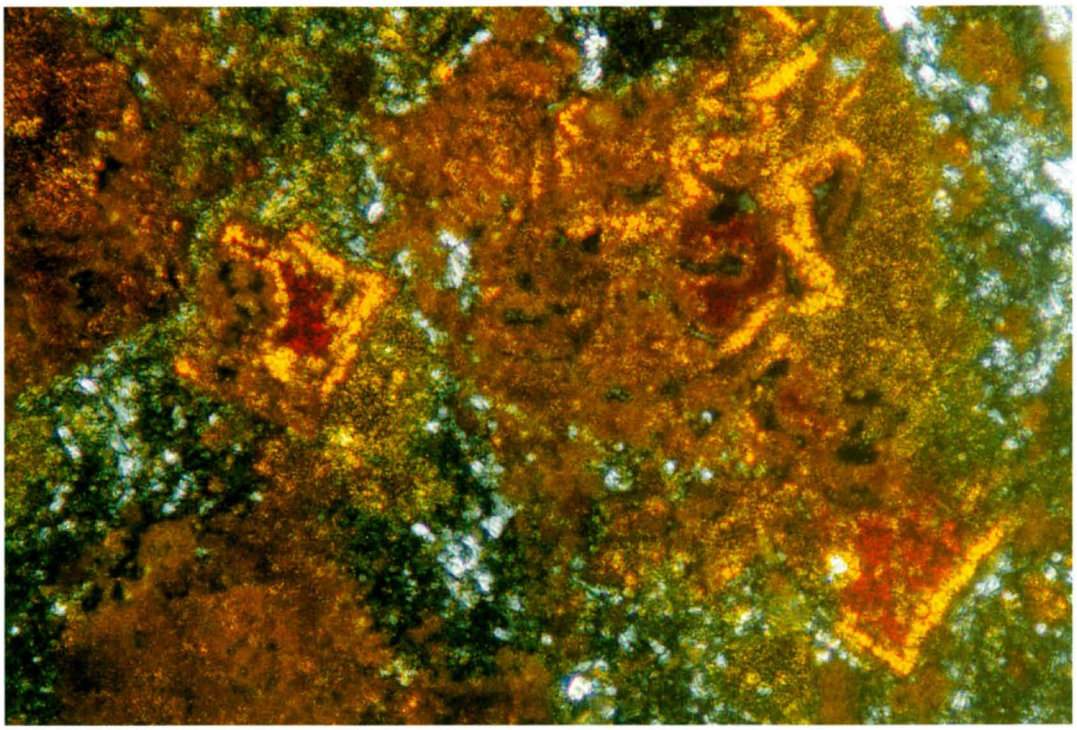

PLATE 4. Borehole MF10 (sample MF10-4-1A); photomicrograph showing hematite (red), goethite (yellow) and poorly crystalline ferric oxides in close association, replacing idiomorphic magnetite. Matrix consists of kaolinite and gibbsite (mag. 25x).

PLATE 5. *Borehole MF12;*
typical core section of the weathering zone overlying the hydrothermally altered phonolites.

Appendix 1

Lithological and scintillometric logs from borehole MF10.

BOREHOLE MF 10 , MORRO DO FERRO

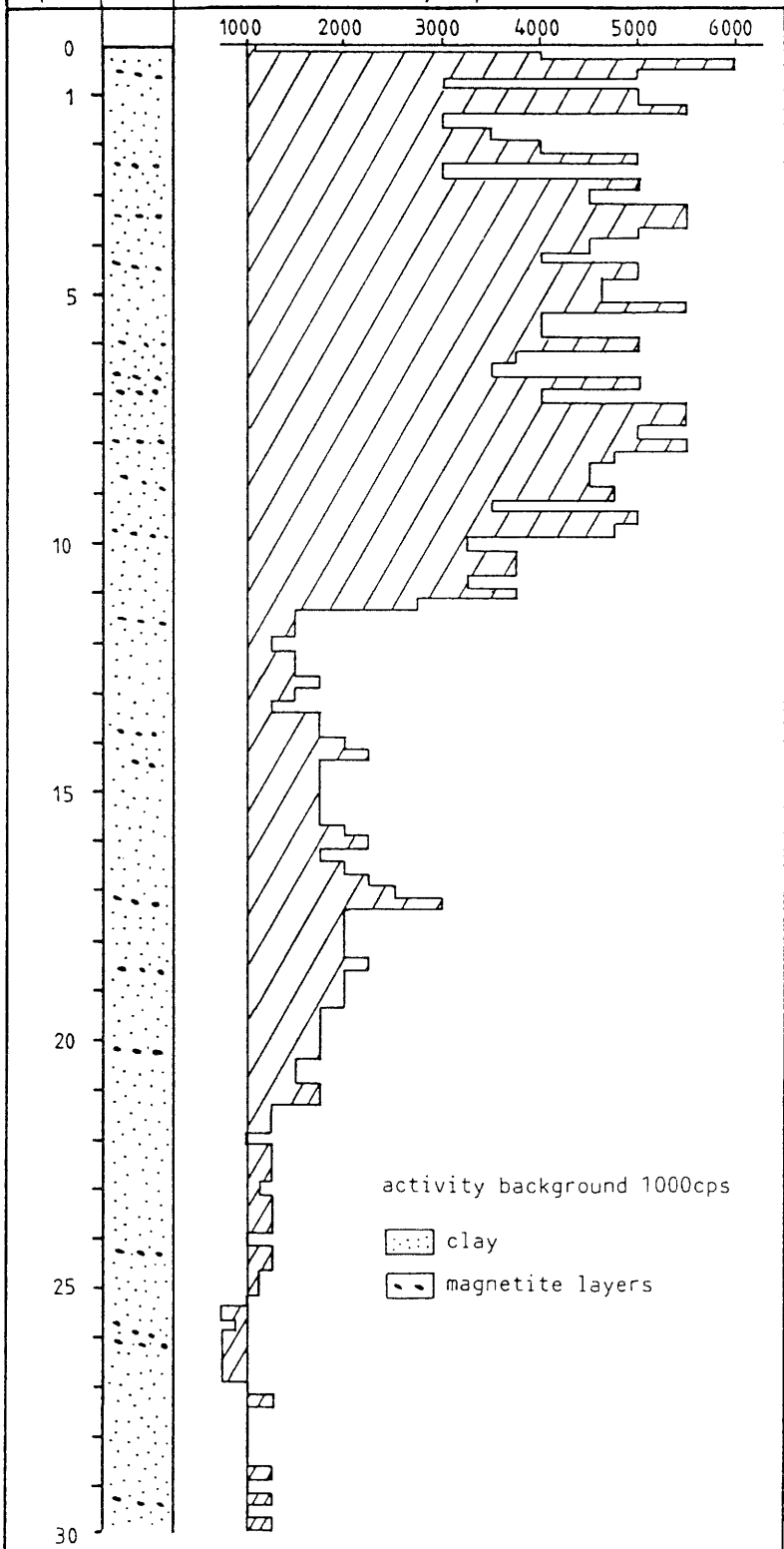

Notes

red-brown clay, magnetite
white clay, Fe-oxides
red-brown clay
white clay, magnetite
bright red + white clay

red brown clay, magnetite

white clay, magnetite
red-brown clay

white clay, Fe-oxides
red clay with white layers
magnetite-breccia

red-brown clay, magnetite

red-brown clay with small white layers, several thin magnetite layers

white clay, homogeneous, Fe-oxides, some violet coloured layers (Mn?)

red-brown clay-layer

alternating white and brown layers

red-brown clay-layer

alternating brown, red-brown and white clay layers with magnetite and Fe-oxides

magnetite-breccia

alternating bright brown and white clay layers, few red-brown layers

16.10.86 N.Waber

Appendix 2

Lithological, hydrogeological, geophysical and scintillometric logs from borehole MF12.

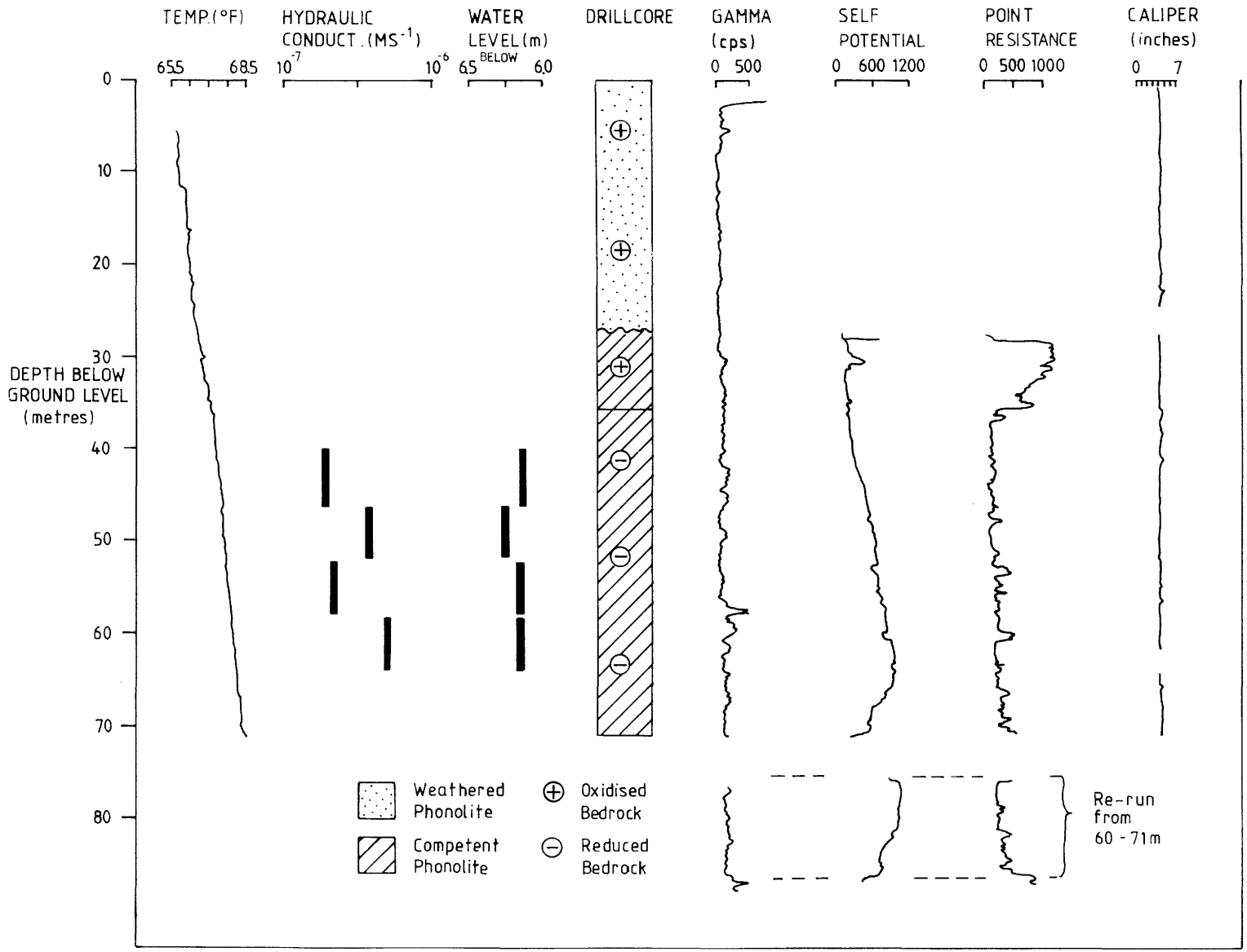
TEMP.(°F)
65.5
68.5
HYDRAULIC CONDUCT.(MS^{-1})
10^{-7}
10^{-6}
WATER LEVEL(m) BELOW
6.5
6.0
DRILLCORE
GAMMA (cps)
0 500
SELF POTENTIAL
0 600 1200
POINT RESISTANCE
0 500 1000
CALIPER (inches)
0 7
DEPTH BELOW GROUND LEVEL (metres)
0
10
20
30
40
50
60
70
80
Weathered Phonolite
Competent Phonolite
Oxidised Bedrock
Reduced Bedrock
Re-run from 60 - 71m

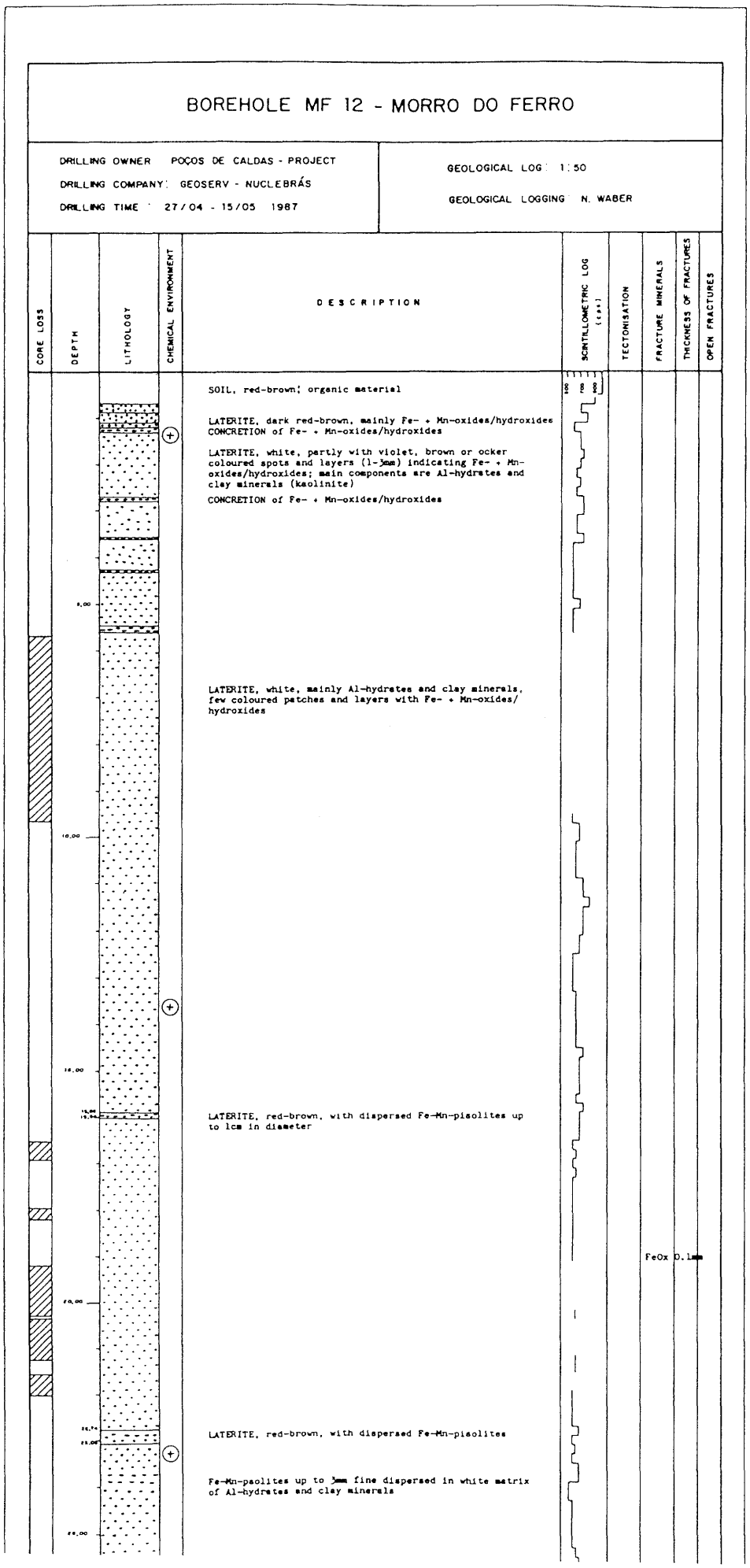
BOREHOLE MF 12 - MORRO DO FERRO
DRILLING OWNER POÇOS DE CALDAS - PROJECT
DRILLING COMPANY GEOSERV - NUCLEBRÁS
DRILLING TIME 27/04 - 15/05 1987
GEOLOGICAL LOG 1:50
GEOLOGICAL LOGGING N. WABER
CORE LOSS
DEPTH
LITHOLOGY
CHEMICAL ENVIRONMENT
DESCRIPTION
SCINTILLOMETRIC LOG (cps)
TECTONISATION
FRACTURE MINERALS
THICKNESS OF FRACTURES
OPEN FRACTURES
SOIL, red-brown; organic material
LATERITE, dark red-brown, mainly Fe- + Mn-oxides/hydroxides CONCRETION of Fe- + Mn-oxides/hydroxides
LATERITE, white, partly with violet, brown or ocker coloured spots and layers (1-3mm) indicating Fe- + Mn-oxides/hydroxides; main components are Al-hydrates and clay minerals (kaolinite)
CONCRETION of Fe- + Mn-oxides/hydroxides
8,00
LATERITE, white, mainly Al-hydrates and clay minerals, few coloured patches and layers with Fe- + Mn-oxides/hydroxides
10,00
15,00
LATERITE, red-brown, with dispersed Fe-Mn-pisolites up to 1cm in diameter
FeOx
0.1mm
20,00
LATERITE, red-brown, with dispersed Fe-Mn-pisolites
Fe-Mn-psolites up to 3mm fine dispersed in white matrix of Al-hydrates and clay minerals
25,00

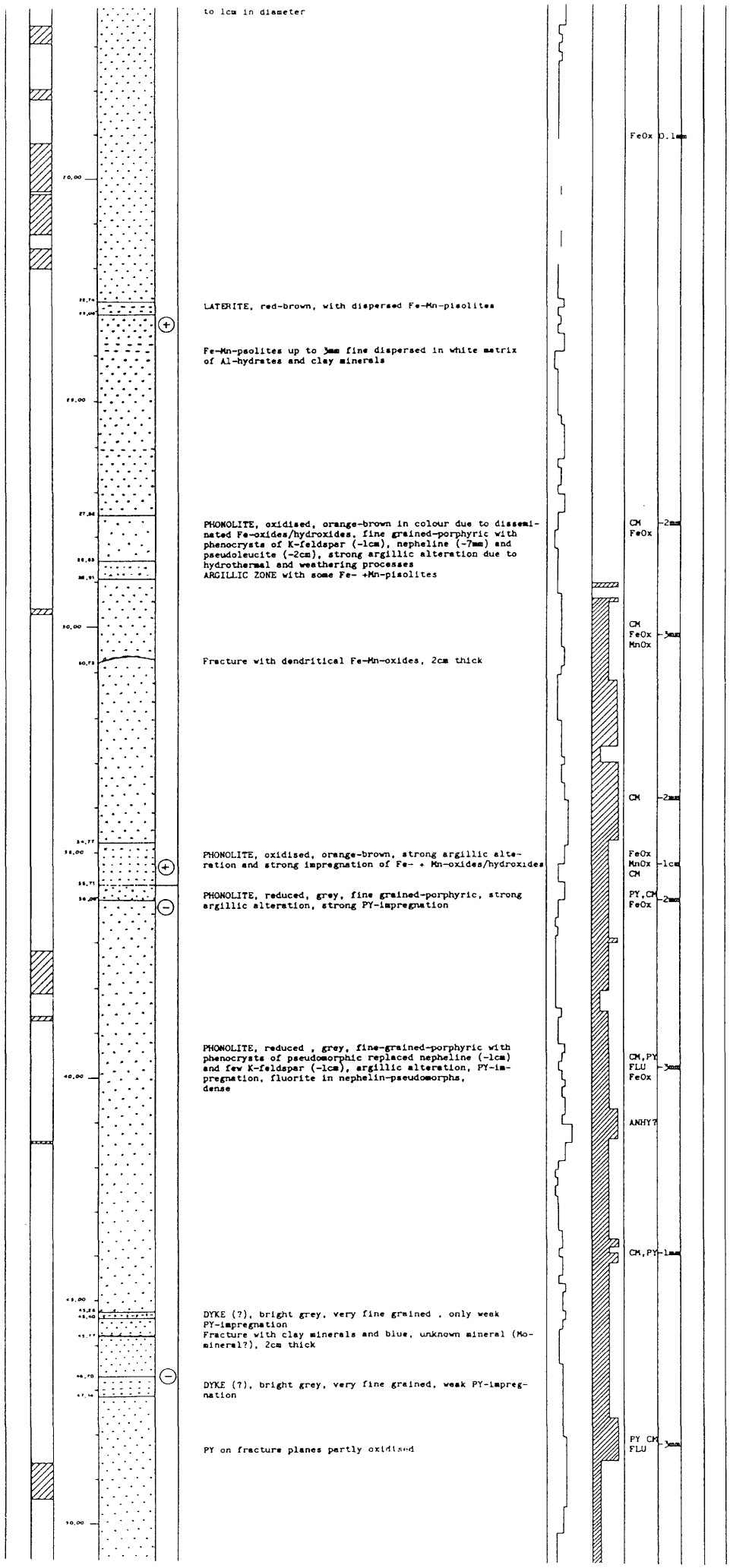
to 1cm in diameter
LATERITE, red-brown, with dispersed Fe-Mn-pisolites
Fe-Mn-psolites up to 3mm fine dispersed in white matrix of Al-hydrates and clay minerals
PHONOLITE, oxidised, orange-brown in colour due to disseminated Fe-oxides/hydroxides, fine grained-porphyric with phenocrysts of K-feldspar (-1cm), nepheline (-7mm) and pseudoleucite (-2cm), strong argillic alteration due to hydrothermal and weathering processes
ARGILLIC ZONE with some Fe- +Mn-pisolites
Fracture with dendritical Fe-Mn-oxides, 2cm thick
PHONOLITE, oxidised, orange-brown, strong argillic alteration and strong impregnation of Fe- + Mn-oxides/hydroxides
PHONOLITE, reduced, grey, fine grained-porphyric, strong argillic alteration, strong PY-impregnation
PHONOLITE, reduced , grey, fine-grained-porphyric with phenocrysts of pseudomorphic replaced nepheline (-1cm) and few K-feldspar (-1cm), argillic alteration, PY-impregnation, fluorite in nephelin-pseudomorphs, dense
DYKE (?), bright grey, very fine grained , only weak PY-impregnation
Fracture with clay minerals and blue, unknown mineral (Mo-mineral?), 2cm thick
DYKE (?), bright grey, very fine grained, weak PY-impregnation
PY on fracture planes partly oxidised
FeOx 0.1mm
CM FeOx 2mm
CM FeOx MnOx 3mm
CM 2mm
FeOx MnOx CM 1cm
PY,CM FeOx 2mm
CM,PY FLU FeOx 3mm
ANHY?
CM,PY 1mm
PY CM FLU 3mm

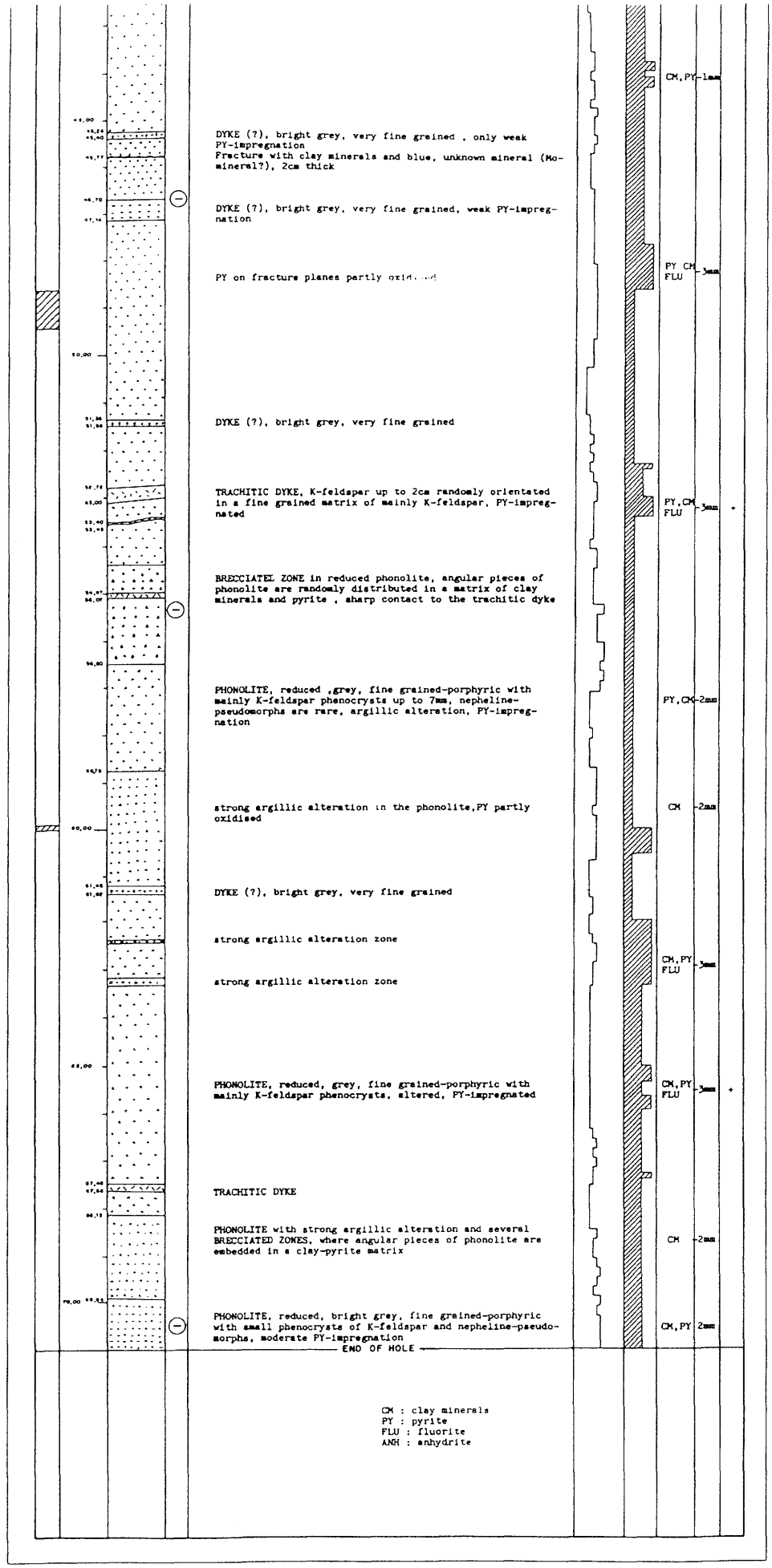
DYKE (?), bright grey, very fine grained , only weak PY-impregnation
Fracture with clay minerals and blue, unknown mineral (Mo-mineral?), 2cm thick
DYKE (?), bright grey, very fine grained, weak PY-impregnation
PY on fracture planes partly oxid...d
DYKE (?), bright grey, very fine grained
TRACHITIC DYKE, K-feldspar up to 2cm randomly orientated in a fine grained matrix of mainly K-feldspar, PY-impregnated
BRECCIATEL ZONE in reduced phonolite, angular pieces of phonolite are randomly distributed in a matrix of clay minerals and pyrite , sharp contact to the trachitic dyke
PHONOLITE, reduced ,grey, fine grained-porphyric with mainly K-feldspar phenocrysts up to 7mm, nepheline-pseudomorphs are rare, argillic alteration, PY-impregnation
strong argillic alteration in the phonolite,PY partly oxidised
DYKE (?), bright grey, very fine grained
strong argillic alteration zone
strong argillic alteration zone
PHONOLITE, reduced, grey, fine grained-porphyric with mainly K-feldspar phenocrysts, altered, PY-impregnated
TRACHITIC DYKE
PHONOLITE with strong argillic alteration and several BRECCIATED ZONES, where angular pieces of phonolite are embedded in a clay-pyrite matrix
PHONOLITE, reduced, bright grey, fine grained-porphyric with small phenocrysts of K-feldspar and nepheline-pseudomorphs, moderate PY-impregnation
END OF HOLE
CM, PY 1mm
PY CM FLU 3mm
PY,CM FLU 3mm +
PY,CM 2mm
CM 2mm
CM,PY FLU 3mm
CM,PY FLU 3mm +
CM 2mm
CM,PY 2mm
CM : clay minerals
PY : pyrite
FLU : fluorite
ANH : anhydrite

Appendix 3

Major and trace element whole-rock analysis from boreholes MF10 and MF12.

Borehole MF10: Major and trace element analysis of the ore body.

Sample		1-1A	1-1C	1-1D	2-1A	3-1A	4-1A	6-1A	10-1A	12-1A	18-1A	19-1A	25-1A
Depth in m		0.06	0.6	0.92	1.45	2.42	3.58	5.65	9.48	11.5	17.13	18.57	24.82
Rock type		ore body	ore body	ore body	ore body	ore body	ore body	ore body	ore body	ore body	ore body	ore body	ore body
SiO_2	wt.%	11.05	6.01	11.46	15.54	25.02	17.37	31.71	32.38	39.41	30.31	18.16	16.74
TiO_2		1.78	2.39	2.15	2.28	2.26	1.83	1.96	0.97	1.50	1.91	3.12	3.09
Al_2O_3		38.06	19.55	30.82	26.34	27.09	22.85	27.01	27.44	31.71	25.20	18.14	14.11
Fe_{tot}		15.05	21.84	17.06	19.22	19.88	17.93	16.77	15.99	6.49	18.72	36.21	30.14
MnO		0.48	1.98	1.62	5.81	0.09	8.14	1.22	0.09	1.80	2.25	2.48	10.63
MgO		0.10	0.11	0.15	0.22	0.27	0.19	0.34	0.25	0.37	0.51	0.19	0.13
CaO		0.02	0.05	0.05	0.04	0.04	0.04	0.02	0.04	0.00	0.04	0.00	0.03
Na_2O		0.29	0.20	0.34	0.52	0.39	0.35	0.33	0.29	0.37	0.20	0.55	0.37
K_2O		2.32	1.30	2.44	3.15	4.77	2.97	3.52	4.34	2.71	2.50	2.04	3.43
P_2O_5		0.58	1.14	0.99	0.85	1.19	0.68	0.58	0.64	0.18	0.49	0.31	0.36
LOI		20.43	15.40	17.61	14.46	10.66	13.38	10.91	10.65	11.53	11.50	10.21	9.15
F	ppm	1467	2557	2009	1889	612	2754	665	1226	1600	1423	n.a.	2585
Ba		18	10	117	128	52	165	52	56	334	144	529	504
Rb		85	40	84	127	196	104	168	179	112	127	81	110
Sr		446	735	740	1037	1395	828	733	491	146	409	385	257
Pb		107	253	165	199	99	175	211	103	89	65	120	114
Th		8818	14843	11474	10846	8015	9786	12540	10210	1404	5845	3472	1888
U		b.d.	15	9	49	64	50	25	25	b.d.	24	20	97
Nb		838	776	863	1029	1165	981	1055	1307	1129	731	2206	1532
La		3566	11100	4160	2633	3080	3452	1286	3548	5260	1539	1341	2338
Ce		6704	11184	9487	7723	4419	11029	1516	4285	2295	6824	5782	13962
Nd		1556	5142	1913	847	1069	1479	339	1598	2602	701	1077	1344
Y		416	693	692	354	326	402	259	355	251	200	265	222
Zr		1805	1599	2020	2292	2676	2194	2525	2594	2606	1469	3619	3427
V		325	95	411	531	621	475	633	845	472	436	1156	1409
Cr		35	87	52	47	35	52	17	29	21	42	99	91
Ni		12	33	16	13	11	14	7	12	10	7	40	10
Co		b.d.	b.d.	b.d.	26	b.d.	26	13	5	b.d.	16	58	54
Cu		20	44	28	28	10	27	11	18	b.d.	5	41	22
Zn		553	648	672	924	773	1147	1018	583	135	735	819	1039
Hf		60	70	70	78	56	58	67	74	53	28	n.a.	72
Sc		b.d.	b.d.	3	2	3	2	2	3	b.d.	2	7	2
S		174	106	862	1496	196	1649	84	105	775	273	211	259

Total iron as Fe_2O_3; LOI = Lost On Ignition; b.d. = below detection limit; n.a. = not analyzed
Analysis by XRF, University of Bern

Borehole MF10: Major and trace element analysis of the weathered carbonatitic host rock.

Sample		36-1A	49-1A-A	49-1A-B	54-1A	56-1A	64-1A	70-1A	73-1A
Depth in m		34.99	48.28	48.3	53.49	55.26	63.7	70.08	72.71
Rock type		WCR	WCR	WCR	WCR	WCR	WCR	WCR	WCR
SiO_2	wt.%	36.51	34.63	40.64	35.06	31.58	26.73	27.92	37.64
TiO_2		1.33	1.31	1.09	5.42	1.28	2.13	2.17	1.31
Al_2O_3		29.79	28.82	32.84	27.79	25.90	22.07	22.92	30.89
Fe_{tot}		10.13	14.34	4.50	11.00	18.99	29.44	20.31	12.01
MnO		0.79	0.58	0.00	2.42	2.61	2.77	6.91	0.00
MgO		0.22	0.15	0.11	0.12	0.15	0.07	0.12	0.02
CaO		0.02	0.02	0.01	0.04	0.03	0.02	0.02	0.02
Na_2O		0.18	0.17	0.13	0.21	0.23	0.27	0.14	0.08
K_2O		3.34	2.76	2.48	3.18	3.13	2.70	2.89	2.74
P_2O_5		0.18	0.11	0.12	0.23	0.23	0.06	0.12	0.11
LOI		11.49	12.41	12.70	9.66	11.44	10.72	10.36	11.40
F	ppm	893	534	863	504	880	242	1144	486
Ba		106	70	13	86	163	108	187	30
Rb		123	102	74	136	100	91	97	83
Sr		83	56	39	175	94	78	113	42
Pb		52	85	75	95	29	31	67	9
Th		849	427	323	694	240	289	274	165
U		b.d.	b.d.	b.d.	45	b.d.	6	3	b.d.
Nb		624	1112	866	3144	613	1263	808	504
La		7005	6757	8573	2083	2977	1239	2122	3754
Ce		1807	1100	986	2298	1802	1496	2632	842
Nd		3606	3039	3758	1026	1408	638	1154	1833
Y		581	383	436	256	195	163	193	168
Zr		1517	2514	2164	5253	1553	3001	2082	1473
V		306	446	365	1259	372	897	1029	367
Cr		36	34	27	29	36	41	44	23
Ni		18	13	15	7	b.d.	b.d.	b.d.	b.d.
Co		6	9	b.d.	21	29	31	34	9
Cu		b.d.	b.d.	b.d.	b.d.	b.d.	b.d.	b.d.	b.d.
Zn		448	486	125	182	1531	1836	605	184
Hf		33	44	45	91	23	41	32	21
Sc		b.d.	b.d.	b.d.	3	b.d.	b.d.	b.d.	b.d.
S		344	348	236	119	1044	528	217	196

Total iron as Fe_2O_3; LOI = Lost On Ignition; b.d. = below detection limit; n.a. = not analyzed
Analysis by XRF, University of Bern

WCR = weathered carbonatitic host rock.

Borehole MF12: Major and trace element analysis of the laterite horizon.

Sample		1-1B	6-1A	11-1A	16-1A	24-1A	28-1A	31-1A	35-1A	42-1A	46-1A	46-1B	47-1A
Depth in m		0.075	5.54	10.32	15.95	23.05	28.45	30.16	34.18	41.42	45.22	45.62	46.14
Rock type		Laterite	Laterite	Laterite	Laterite	Laterite	Oxid. l ph	Oxid. l ph	Oxid. l ph	Red. te ph	Red. ph di	Red. te ph	Red. te ph
SiO_2	wt.%	30.68	28.10	44.85	40.66	48.16	54.21	54.32	53.99	51.40	57.55	53.57	51.07
TiO_2		1.41	1.03	1.02	0.77	0.89	0.61	0.61	0.90	0.60	0.61	0.59	0.60
Al_2O_3		38.84	33.18	34.37	28.04	28.59	23.98	21.95	23.06	21.11	22.15	21.00	21.39
Fetot		6.81	12.94	2.11	9.15	3.25	2.79	4.18	4.04	6.59	1.54	4.03	6.68
MnO		0.14	4.11	0.03	0.00	0.89	0.00	0.00	0.00	1.31	0.02	0.61	1.39
MgO		0.05	0.04	0.06	0.12	0.11	0.09	0.09	0.02	0.26	0.15	0.20	0.24
CaO		0.05	0.03	0.01	0.03	0.02	0.00	0.05	0.03	0.79	0.58	1.55	0.80
Na_2O		0.18	0.24	0.28	0.21	0.37	0.47	0.39	0.24	1.21	0.82	0.73	1.02
K_2O		2.10	2.36	4.06	3.17	7.93	11.51	12.14	10.41	8.10	11.86	10.86	8.48
P_2O_5		0.79	0.35	0.20	0.14	0.15	0.12	0.16	0.08	0.10	0.11	0.10	0.09
H_2O		15.19	14.97	10.74	11.07	7.51	3.97	2.96	0.77	3.55	2.73	2.79	3.51
CO_2		1.00	0.35	0.40	0.90	0.45	0.25	0.75	3.95	3.25	0.35	1.70	3.35
total	wt.%	97.24	97.70	98.13	94.26	98.32	98.00	97.60	97.49	98.27	98.47	97.73	98.62
F	ppm	1045	1186	599	1777	1063	1406	2123	1672	3851	3252	7185	3820
Ba		122	367	36	77	360	199	177	66	106	141	137	109
Rb		97	95	126	93	220	322	338	357	193	308	241	203
Sr		3181	888	95	51	238	279	282	72	562	580	675	721
Pb		822	251	43	74	55	33	23	31	34	14	22	44
Th		554	198	103	132	110	63	67	100	48	34	40	48
U		122	173	45	72	50	28	23	49	10	10	10	11
Nb		751	621	533	368	441	299	288	478	292	290	275	286
La		1412	1405	2486	8649	1539	961	3336	2755	1017	786	668	924
Ce		2406	1837	1673	2288	1470	1062	1540	1333	1244	877	777	1132
Nd		387	469	1037	4723	548	257	773	536	288	209	193	257
Y		199	193	233	378	136	105	123	125	93	87	110	88
Zr		2646	2239	1808	2669	1304	1355	903	1949	943	942	1134	868
V		347	256	173	110	214	185	148	76	94	112	110	104
Cr		15	25	8	39	6	b.d.	7	9	10	b.d.	b.d.	7
Ni		8	6	8	19	b.d.	b.d.	b.d.	b.d.	b.d.	b.d.	b.d.	b.d.
Co		10	40	b.d.	12	9	7	9	10	13	4	9	15
Cu		7	8	b.d.	18	b.d.	b.d.	b.d.	b.d.	b.d.	b.d.	b.d.	b.d.
Zn		114	363	60	332	111	65	110	59	606	280	951	446
Hf		51	42	30	50	20	20	11	29	12	10	13	11
Sc		3	2	2	3	4	5	6	5	3	5	3	3
S		110	131	114	72	245	267	88	62	3142	962	5050	1089

Total iron as Fe_2O_3; b.d. = below detection limit
Analysis by XRF, University of Bern

Borehole MF12: Major and trace element analysis of the different rock units.

Sample		51-1A	58-1A	68-1B	70-1B	71-1C
Depth in m		50.26	57.06	67.54	69.74	70.75
Rock type		Red. te ph	Red. te ph	Red. l ph	Red. l ph	Red. l ph
SiO_2	wt.%	50.98	49.54	56.68	59.16	57.77
TiO_2		0.56	0.49	0.61	0.63	0.63
Al_2O_3		19.48	19.78	22.72	20.43	21.69
Fe_{tot}		7.32	6.72	1.82	1.60	1.43
MnO		1.66	1.54	0.00	0.00	0.00
MgO		0.33	0.34	0.16	0.05	0.08
CaO		1.15	2.86	0.18	0.04	0.03
Na_2O		1.62	1.66	0.57	0.55	0.42
K_2O		8.74	7.29	12.37	14.08	13.53
P_2O_5		0.09	0.09	0.10	0.13	0.09
H_2O		5.79	4.09	2.66	1.93	2.26
CO_2		0.50	3.50	0.30	0.25	0.25
total	wt.%	98.22	97.90	98.17	98.85	98.18
F	ppm	4749	10076	2295	1514	1309
Ba		155	245	160	168	146
Rb		216	188	318	333	332
Sr		577	870	298	248	287
Pb		24	30	12	52	19
Th		55	68	30	56	34
U		13	83	10	28	25
Nb		272	246	270	325	277
La		831	1200	668	796	382
Ce		964	1415	707	854	441
Nd		217	267	168	216	121
Y		87	108	71	101	82
Zr		847	871	1171	1015	1258
V		98	80	200	206	156
Cr		11	11	b.d.	b.d.	b.d.
Ni		b.d.	b.d.	b.d.	b.d.	b.d.
Co		17	15	5	5	5
Cu		b.d.	b.d.	b.d.	b.d.	b.d.
Zn		391	417	351	92	45
Hf		9	11	11	9	16
Sc		4	b.d.	5	7	6
S		4064	3949	1580	4851	2988

Total iron as Fe_2O_3; b.d. = below detection limit
Analysis by XRF, University of Bern

Oxid. l ph = oxidized leucocratic phonolite
Red. l ph = reduced leucocratic phonolite
Red. ph di = reduced phonolitic dyke
Red. te ph = reduced tephri-phonolite